The Pennsylvania State University
The Graduate School

PANDORA'S BOX: CAN WE DISTINGUISH GROUNDWATER TRANSPORT HYPOTHESES GIVEN OBSERVATIONAL UNCERTAINTIES?

A Thesis in
Civil Engineering
by
Rachel Lorah Urban

Submitted in Partial Fulfillment
of the Requirements
for the Degree of

Master of Science

May 2013

The thesis of Rachel Lorah Urban was reviewed and approved* by the following:

Patrick M. Reed
Associate Professor of Civil Engineering
Thesis Co-Advisor

Kamini Singha
Associate Professor of Geology and Geologic Engineering
Colorado School of Mines
Thesis Co-Advisor

Michael Gooseff
Associate Professor of Civil Engineering

Peggy A. Johnson
Professor of Civil Engineering, Department Head

*Signatures are on file in the Graduate School.

Abstract

This study explores the difficulties associated with using groundwater transport models to distinguish alternative process hypotheses given observational uncertainties. A well-characterized laboratory sand tank, packed with two sands, serves as the basis for our study. Using time-series breakthrough curves at multi-port wells, we monitor the flow (steady state) and transport of a 1.7-h step-pulse injection of NaCl across nine replicate experiments. The replicate tracer tests show significant variability despite the simplicity and highly controlled nature of the experiments. Local and non-local transport models are shown to be indistinguishable given experimental uncertainty. Moreover, our results demonstrate how physically implausible parameterizations of the more complex non-local transport model lead to improved model performance measures with little basis in the true system transport dynamics. The replicate tracers experiments performed in this study represent a lower bound of problem complexity. The inability to distinguish transport hypotheses as observed in these results would only be exacerbated in higher complexity groundwater systems.

Table of Contents

List of Figures

List of Tables

Acknowledgments

I'd like to thank Michael Gooseff for serving on my committee as well as Patrick Reed and Kamini Singha for serving as my advisors. Their patience and support have been tremendous, especially as my masters degree entered into its third year. Special thanks to the Penn State Water Resources graduate students for being friends and colleagues for the past three years. I am deeply indebted to both Christa Kelleher and Alisha Fernandez for their friendship and ability to keep my sane this past year. Special thanks to Ryan Swanson for being a wealth of information about experimental techniques and electrical resistivity methods. To whoever runs the "What Should We Call Grad School" Tumblr account (`http://whatshouldwecallgradschool.tumblr.com`), your silly animated gifs got me through the worst of graduate school. Finally, I'd like to thank my friends and family for their unending support and love. I am incredibly grateful for everything you all have done for me.

Dedication

Dedicated to my mother and father

Chapter 1

Introduction

Model-based inference and hypothesis testing for groundwater transport processes has long been recognized as being challenging given the dearth of observations, highly uncertain and possibly localized subsurface properties (e.g., hydraulic conductivity), the complexity of the models, and the ill-posed nature of the underlying inverse problems [1; 2; 3]. For example, a number of experimental studies have shown that concentration data are better described by non-Fickian (i.e., diffusion flux is not proportional to concentration gradient) transport [4; 5; 6]. These results have lead to the development of alternative non-local groundwater transport models in an effort to explain these data [7; 8; 9; 10; 11; 12]. However, the necessity of these models is debated in the literature [13; 14; 15; 16]. Understanding whether non-local transport models are valid representations of field-scale processes remains a fundamental scientific challenge. One significant limitation of past experiments, especially at the field scale, is the lack of replicate experimental data to quantify observational uncertainty. This study explores the difficulties associated with inferring transport processes given observational uncertainties using a well-characterized lab experiment and nine replicate solute tracer tests. Observed system variability across experiments (caused by small fluctuations in pumping rates, background fluid conductivity levels, and differential flowpaths) is substantial for our simple, well-controlled system. Consequently, the uncertainty in the underlying observed transport processes strongly limits our ability to distinguish alternative groundwater transport hypotheses.

Chapter 2

Physical Experiment

Figure 2.1 illustrates the physical experiment, constructed with a steel frame and acrylic panels, measuring 71 cm wide by 73 cm long by 70 cm tall. Twenty-five inlet ports are located at the upstream side of the tank. At the downstream side, there are five horizontal outlet ports located at a height of 62.5 cm from the bottom of the tank. Steady flow was established across the tank. No-flow boundaries exist on the sides opposite to the imposed head gradient and bottom of the tank. The tank was fed by a constant-head reservoir at 1.725 m with an outlet elevation of 0.625 m. The resulting hydraulic head gradient across the length of the tank was 0.0179 m/m. The tank was wet-packed with 1.1 mm diameter Accusand (K = 0.005 m/s) with a 20 cm cube of 0.26 mm diameter Accusand (K = 0.00014 m/s) embedded at the center of the tank. Ten fully screened (0.015 cm slots), 1.27 cm diameter PVC wells were installed as shown in Figure 2.1. These wells were instrumented with stainless-steel electrodes on the interior for water conductivity measurements. Each probe was installed halfway down each well at a height of 35 cm. For more details and photographs of construction, see Appendix A.

Using the water and saturated sand resistivity, Archie's law [17] was used to estimate system porosity (0.31 - 0.34):

$$\theta = \left(\frac{\rho_{res,water}}{\rho_{res,rock}} \right)^{1/m} \tag{2.1}$$

where $\rho_{res,rock}$ is saturated rock resistivity (ohm-m), $\rho_{res,water}$ is solution resistivity (ohm-m), and m is the cementation exponent (1.3 for unconsolidated

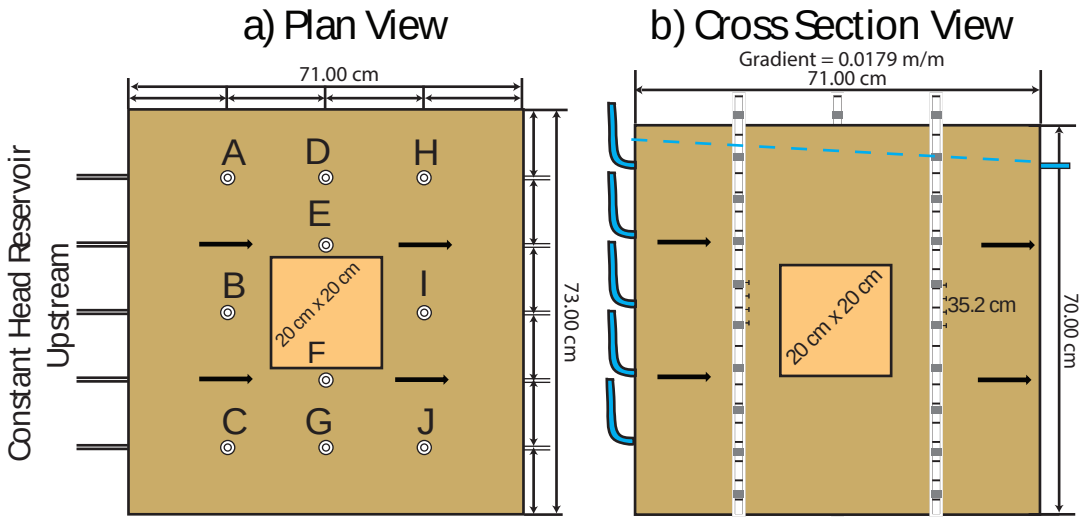

Figure 2.1: Experimental setup of physical experiment

sands). Using the estimated porosity, Kozeny-Carman [18] is then used to estimate hydraulic conductivity:

$$K_{conductivity} = \left(\frac{\rho_{density} g}{\mu}\right)\left[\frac{\theta^3}{(1-\theta)^2}\right]\left(\frac{d^2}{180}\right) \tag{2.2}$$

where $\rho_{density}$ and μ are the density (kg m^{-3}) and dynamic viscosity of water (Pa-s), respectively, g is acceleration due to gravity (m s^{-2}), θ is porosity (-) and d is particle diameter (m). Using this method, hydraulic conductivity varied between 0.0036 - 0.005 m/s, decreasing due to overburden pressure across the depth of the tank. A three-dimensional represenation of the conductivity field is displayed in Figure 2.2.

Nine solute injection experiments were conducted with a well-mixed 0.55 g L^{-1} solution of NaCl (Sigma Aldrich NaCl # 310166 - Reagent grade >98 %, 80 mesh). Tap water was used for both background conditions and solute mixture, and the background conductivity of the tap water was removed from calculations of concentration below. Solute was injected through the twenty-five inlet ports at a bulk rate of 20 mL s^{-1} (72 L hr^{-1}) for 1.7 hours (6000 s), then injection was returned to background (0 g L^{-1} NaCl) conditions. Measurements were collected at all ten wells every five to nine minutes. Additionally, along with these nine replicate experiments with the same experimental variables (0.55 g L^{-1} solution of NaCl,

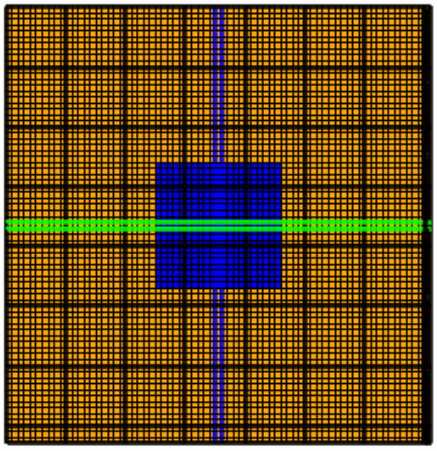

(a) Top view of tank hydraulic conductivity at center layer (Low conductivity cube present) a-a'

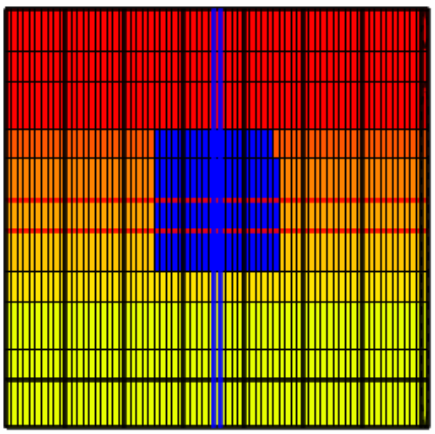

(b) Tank cross section, lateral direction (Low conductivity cube present) b-b'

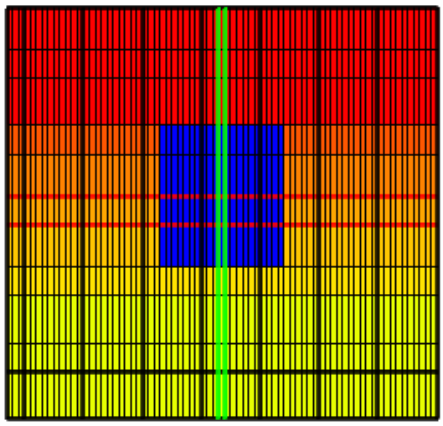

(c) Tank cross section, transverse direction (Low conductivity cube present) c-c'

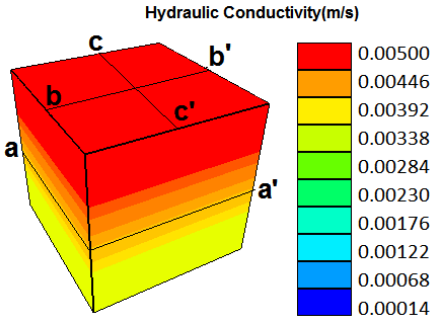

(d) Three dimensional view, with hydraulic conductivity legend

Figure 2.2: Hydraulic conductivity field of tank

injection into 25 inlet ports, and same geophysical measurement frequency), nine other experiments were conducted to explore the effects of (1) varying concentration, (2) varying geophysical measurement frequency, and (3) varying areal extent of injection. These results are documented in Appendix B. These additional tests serve as a preliminary study on how experimental variables affect the ability to infer subsurface properties.

Chapter 3

Methods

3.1 Electrical Resistivity Tomography (ERT)

Electrical resistivity tomography (ERT) was used to collect electrical resistivity data from the solute transport experiments. Electrical resistivity (ohm-m) was used to estimate fluid and bulk electrical conductivity values (μS cm^{-1}), and fluid and bulk solute concentration values (g L^{-1}). Electrical resistivity data was collected using four stainless steel electrodes - two to inject current (I) and two to measure voltage (V). Given Ohm's law and the electrode geometry, these measurements are then used to estimate apparent resistivity, and convert that to fluid concentration using the following three equations:

$$K_{geom} = 2\pi \left[\left(\frac{1}{AM} - \frac{1}{MB} \right) - \left(\frac{1}{AN} - \frac{1}{NB} \right) \right]^{-1} \tag{3.1}$$

$$\rho_{res} = \frac{V}{I} K_{geom} \tag{3.2}$$

$$\sigma = \frac{1}{\rho_{res}} \tag{3.3}$$

Where AM, MB, AN, and NB are the respective distances (m) between the current electrodes (A, B) and the voltage electrodes (M, N), K_{geom} is the geometric factor for an electrode configuration, V is voltage (V), I is current (A), ρ_{res} is resistivity (ohm-m), and σ is electrical conductivity (S/m). Electrical conductivity was

then normalized to values between zero and one to estimate solute concentration, based on the minimum and maximum concentration for a solute test. Appendix A.4.1 documents the process of physically determining these geometric factors.

3.2 Flow and Transport Modeling

3.2.1 Tank Discretization

The tank was discretized into 1 cm x 1 cm cells in the x and y directions, and layers varying between 5 cm and 12 cm in thickness. Layer thickness was determined by tank geometry. If a layer intersected with inlet or outlet ports, it was thinner to capture source loading dynamics and any possible vertical flow near the inlet. Other layer thicknesses were determined by hydraulic conductivity geometry and where conductivity values changed in the tank. Full discretization is displayed in Figure 3.1

3.2.2 Flow Modeling

The experimental flow was modeled using MODFLOW 2005 [19]. Along with the basic MODFLOW packages, the horizontal flow boundary (HFB) package was used to simulate no-flow boundaries of the tank and the well (WEL) package was used to simulate inlet and outlet ports. The strongly implicit package (SIP) was used to solve for steady-state flow.

3.2.2.1 Local Transport - Advection Dispersion

MT3DMS [20] was used for solute transport modeling. Two competing solute transport models were used to model behavior in the tank: the local, non-reactive advection-dispersion equation model (ADE), and a simple non-local model that describes transport by single-rate dual-domain mass transfer (DDMT). The governing equation for the ADE model is shown in 3.4:

$$\frac{\partial C}{\partial t} = \nabla \left(D \nabla C \right) - \nabla \left(\nu C \right) \tag{3.4}$$

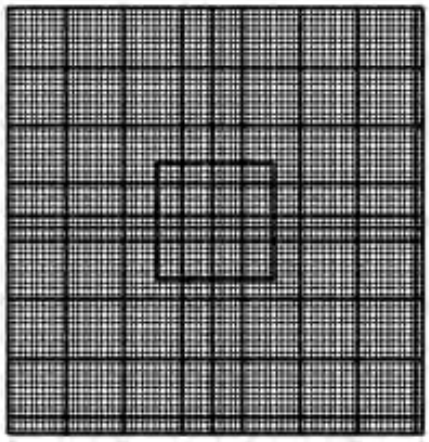

(a) Top view of tank discretization at center layer (Low conductivity cube outlined)

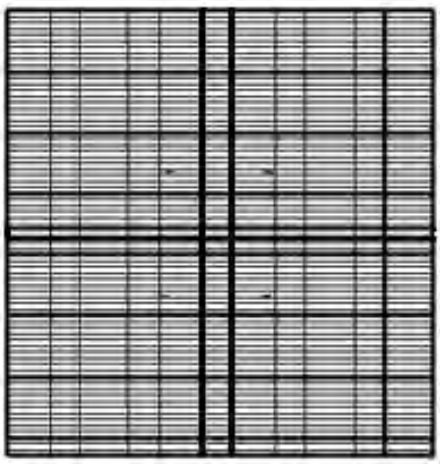

(b) Tank cross section, transverse direction

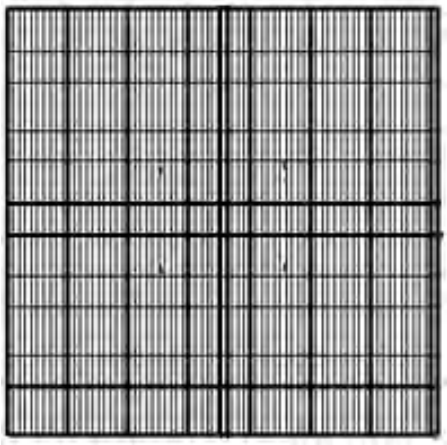

(c) Tank cross section, lateral direction

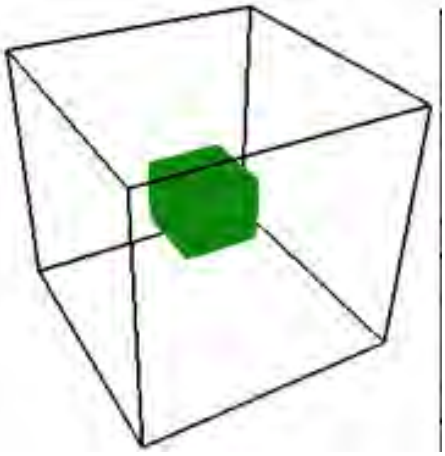

(d) Three dimensional view, with low conductivity cube in green

Figure 3.1: Tank Discretization

where C is concentration (kg m^{-3}); D is the dispersion coefficient (m^2 s^{-1}); and ν is the average linear velocity (m s^{-1}).

3.2.2.2 Nonlocal Transport - Dual Domain Mass Transfer

Equations 3.5 and 3.6 provide the two governing equations for the DDMT model:

$$\theta_m \frac{\partial C_m}{\partial t} + \theta_{im} \frac{\partial C_{im}}{\partial t} = \theta_m \nabla \left(D \nabla C_m \right) - \theta_m \nabla \left(\nu C_m \right) \tag{3.5}$$

$$\theta_{im}\frac{\partial C_{im}}{\partial t} = \alpha\left(C_m - C_{im}\right) \tag{3.6}$$

where θ_m and θ_{im} are the mobile and immobile porosities, respectively; C_m and C_{im} are the mobile and immobile concentrations (kg m^{-3}), respectively; and α is the mass transfer rate coefficient (s^{-1}).

3.2.2.3 Competing Models

Using these two governing models, three MODFLOW/MT3DMS models were created to simulate observed tracer breakthroughs. In our computational experiment, we have parameterized the ADE and a "plausible" case of the DDMT based on our understanding of the materials. These produce similar results, in that limited immobile porosity and mass transfer are expected for a well-sorted, well-rounded, spherical sand. Additionally, an "implausible" DDMT case was fit to improve model performance while not constraining ourselves to being physically meaningful. The specifics of these parameterizations are given below.

1. Advection-Dispersion - dispersion was set equal to one tenth of the system length scale [21] and porosity was constrained using resistivity measurements ($D = 0.075$, $\theta_m = 0.31$ - 0.34)

2. Dual-Domain - Physically Plausible - based on Swanson's [22] column experiments ($D = 0.075$, $\theta_m = 0.30$ - 0.33, $\theta_{im} = 0.01$, $\alpha = 10^{-5}$)

3. Dual-Domain - Physically Implausible - to illustrate fit improvements with unrealistic parameters ($D = 0.075$, $\theta_m = 0.20$ - 0.23, $\theta_{im} = 0.10$, $\alpha = 10^{-2}$)

Dispersivity was not optimized to the observed data. The reasoning behind this is that for such a simple system, an optimation approach to fitting the dispersivity value may overfit the data. A value of one tenth of the system length scale ($D = 0.075$) was chosen based on Gelhar's empirical data [21] and held constant across model runs. Future work may contain a more robust fitting of the dispersivity value.

3.3 Evalation of Model Performance

The Nash Sutcliffe Efficiency (NSE) [23] coefficient was used as a metric to evaluate model performance. NSE was calculated at each of the ten wells, for each of the nine experiments, using the three competing models, giving a total of 270 different NSE values. The formula for NSE is shown in Equation 3.7:

$$NSE = 1 - \frac{\sum_{t=1}^{T} \left(C_{obs}^{t} - C_{mod}^{t}\right)^2}{\sum_{t=1}^{T} \left(C_{obs}^{t} - \overline{C}_{obs}\right)^2} \tag{3.7}$$

where C_{obs}^{t} is the observed concentration, C_{mod}^{t} is the modeled concentration, T is the total time of the experiments, and $\overline{C}_{obs}$ is the mean concentration of an observed breakthrough curve. An NSE value less than zero indicates that the mean observation fits the data better than the model, an NSE value equal to zero means that the model predictions are as accurate as the mean of the data, and an NSE value of one indicates the model perfectly fits the data.

Chapter 4

Results and Discussion

4.1 Data Uncertainty

Despite the simplicity of the laboratory aquifer system, which has strict controls on hydraulic head, well-characterized hydraulic conductivity, and well-known background conditions, the tracer dynamics are difficult to model using either the ADE or DDMT models [24]. A novel aspect of this study is that replicate experiments allow us to consider the uncertainty of concentration observations through time. Figure 4.1 displays the concentration breakthrough dynamics in both linear and log scales, along with the experimental mean and the three modeled breakthrough curves. The experimental ranges in observations are shown in the linear scale breakthroughs with grey shading. We aimed to keep each experiment as similar as possible, but differences in the experimental data still exist, likely due to immeasurable changes in pumping rates and timing, alternative flowpaths, or fluctuations in background fluid conductivity. That said, this test is a best-case scenario, where any variation in experimental procedure is significantly less than would be seen in repeat experiments in a field setting.

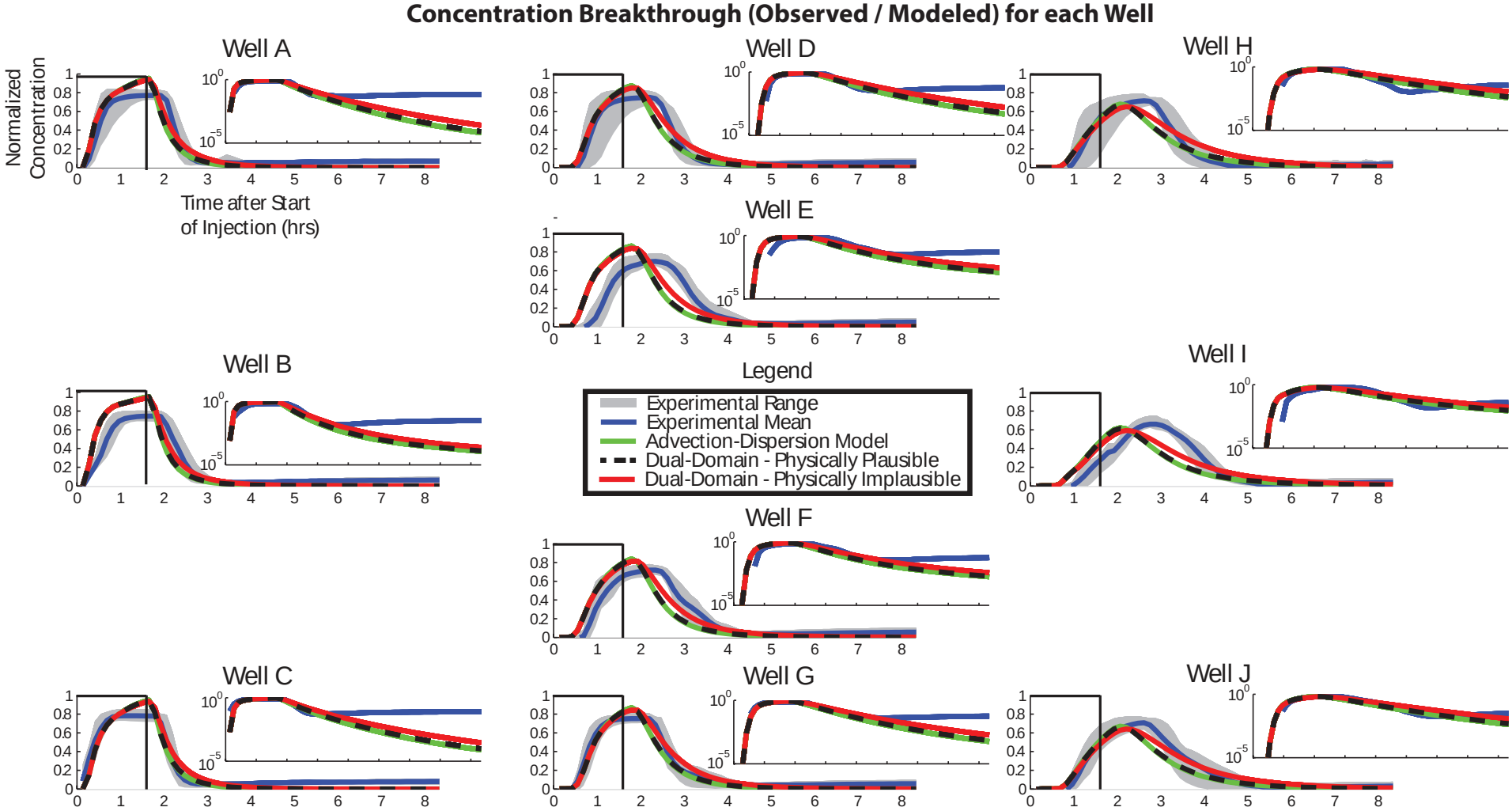

Figure 4.1: Linear and logarithmic breakthrough curves of nine experiments vs. three competing models.

Although it may be tempting to assume that the mean of the observed breakthroughs is the best known reference, the availability of only 9 replicates make it difficult to assume that this statistical moment is fully converged. Consequently, the individual traces are equally plausible observed states. In almost all cases, the models fail to capture the shape, peak, timing, or tail of the nine observed tests past wells A, B, and C. The models differ at upstream wells A, B, and C, but this is visually indistinguishable since the three models roughly fall within the noise of the observables. As far as the spatial and temporal properties of the uncertainty, the uncertainty in upstream wells (Wells A, B, and C) is largest with respect to the breakthrough timing and is not as significant in the tails. Wells adjacent to the fine-sand block (Wells D, E, F, and G) show a similar degree of uncertainty in their breakthrough timing but with increasing variability in the tail of their curves. The tail is less uncertain along the longitudinal axis of the tracer transport path from Well B to Well I through the fine sand lens. The tracer breakthroughs along the transverse axis of the tracer plume (i.e., Wells H and J) have increased uncertainties throughout their extents. The "implausible" DDMT model is the poorest overall in capturing the observed tailing behavior.

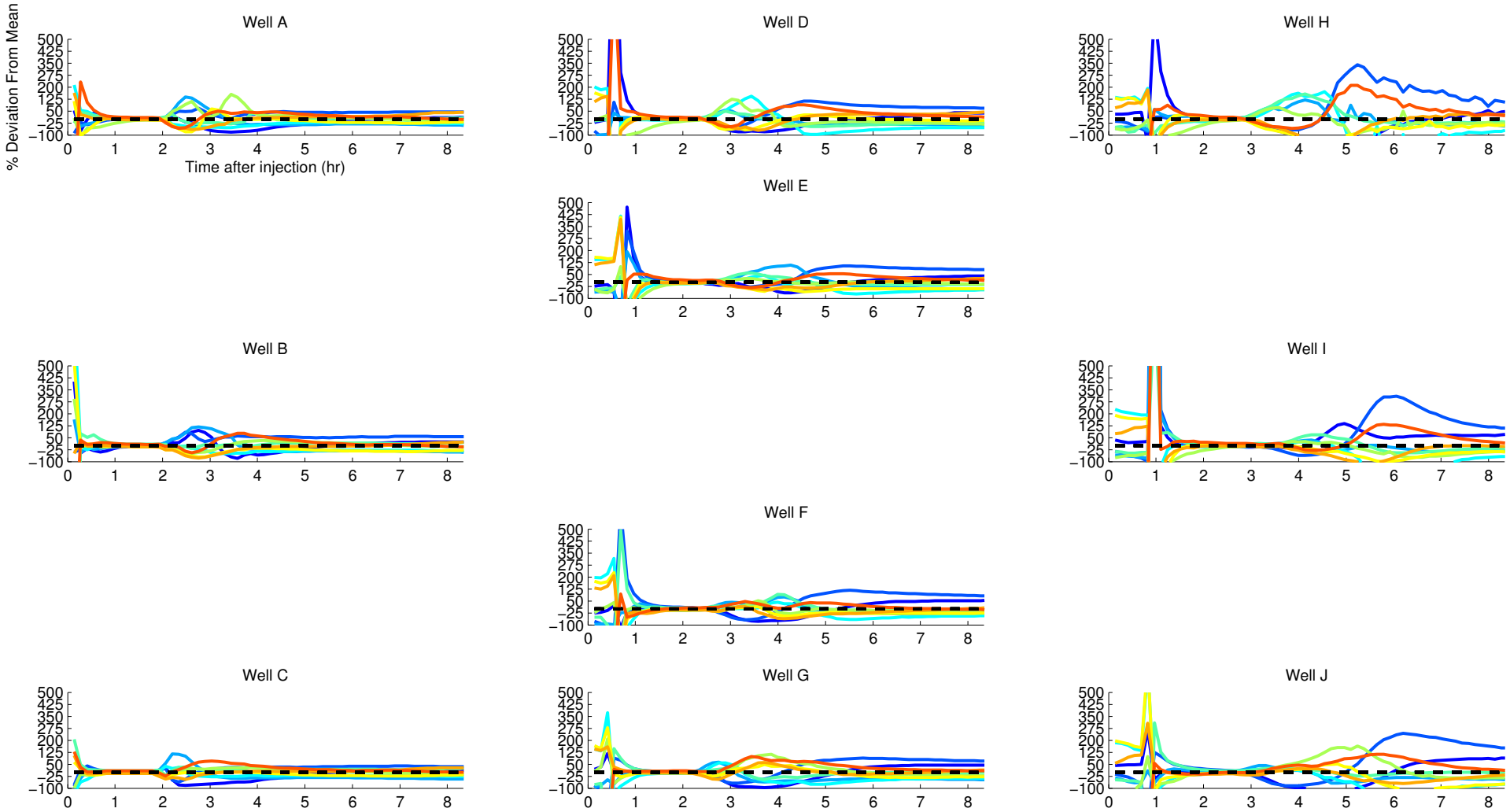

Figure 4.2: Percent deviation from experimental mean for all experiments.

Figure 4.2 describes each experiment's percent deviation from the experimental mean value. Across tests, there is a large range of discrepancies, shown from -100% to 500% deviation from the mean. Wells with the lowest percent discrepancy about the mean (A,B,C) still have a ± 50% discrepancy from the mean. For downstream wells H, I, and J, one test (labeled "Test10" in Appendix Data) has the largest percent discrepancy in the breakthrough test tail. The smallest deviations about the mean occur during the peak of the breakthrough concentration. The large outlying discrepancies come from large percent discrepancies that occur when normalized conductivity values are close to zero. Low percent deviations occur across hours 1 - 3 where the variation across experiments is low. Percent deviation in the tails of the data become larger as you move downstream.

4.2 Nash-Sutcliffe Coefficients

Table 4.1 summarizes the best and worst NSE values for each well across the three different models. These ranges were constructed by calculating the NSE between each of the nine observed breakthrough curves to the three competing models. It would be expected that the DDMT model's increased parametric complexity could bias the NSE value given the potential for overfitting. Note that the best-fit parameters vary between models and are all within close range of each other, making them statistically indistinguishable despite having different mechanistic interpretations. There is a consistent trend that the poorest fits for all of the models occur from the mid-section of the laboratory aquifer (Wells D, E, F, and G) and get worse at the leading edge (Wells H, I, and J). The implausible DDMT model often attains better NSE because the measure is strongly biased by the peak breakthrough errors and less so by errors in the tails of the breakthrough curves. Overall, the key insight is that the models are statistically indistinguishable.

4.3 Error Cumulative Density Function (CDF)

Since there are nine replicate tests, one can compute the error between each of the three models and each of the nine tests, creating twenty seven empirical error CDFs at each well (270 total CDFs). Error was calculated as normalized concentration

	Advection-Dispersion Range		Dual Domain Plausible Range		Dual Domain Implausible Range	
	Min	Max	Min	Max	Min	Max
A	0.75	0.94	0.75	0.94	0.80	0.94
B	0.72	0.91	0.73	0.91	0.78	0.94
C	0.87	0.94	0.87	0.94	0.87	0.94
D	0.56	0.93	0.57	0.93	0.66	0.95
E	0.35	0.73	0.37	0.74	0.51	0.82
F	0.65	0.85	0.66	0.86	0.80	0.91
G	0.87	0.97	0.87	0.97	0.85	0.97
H	0.49	0.84	0.50	0.83	0.64	0.87
I	0.25	0.71	0.27	0.72	0.52	0.83
J	0.65	0.89	0.66	0.90	0.72	0.96

Table 4.1: NSE values for each of the nine experiments compared to each of the three competing models, at each well. Performance is largely indistinguishable across models

of the model minus normalized observed concentration:

$$Error = C_{norm,mod} - C_{norm,obs} \tag{4.1}$$

This means that if an error value is negative, the model is underpredicting the current concentration by a certain percentage of total concentration. For example for an error of -0.3 this means that the model is underpredicting flow by 0.3*(Maximum conductivity measurement). Conversely, positive error values mean that the model is overpredicting concentration. These results are displayed in Figure 4.3. Like Table 4.1, these empirical CDF plots reinforce the idea that the models are highly indistinguishable given that the error across tests and different models are incredibly similar.

It is interesting to note, that in almost all cases (except downstream wells H, I, J), the probability that the model is overpredicting is always greater than 50 %. It is also worth noting that the distributions change as you move from upstream wells to downstream wells. From upstream to downstream, the slope of the empirical CDF decreases, meaning that the error values spread over the total error range. This differs from the upstream wells where error values of the same magnitude create steeper slopes in the empirical CDF curves.

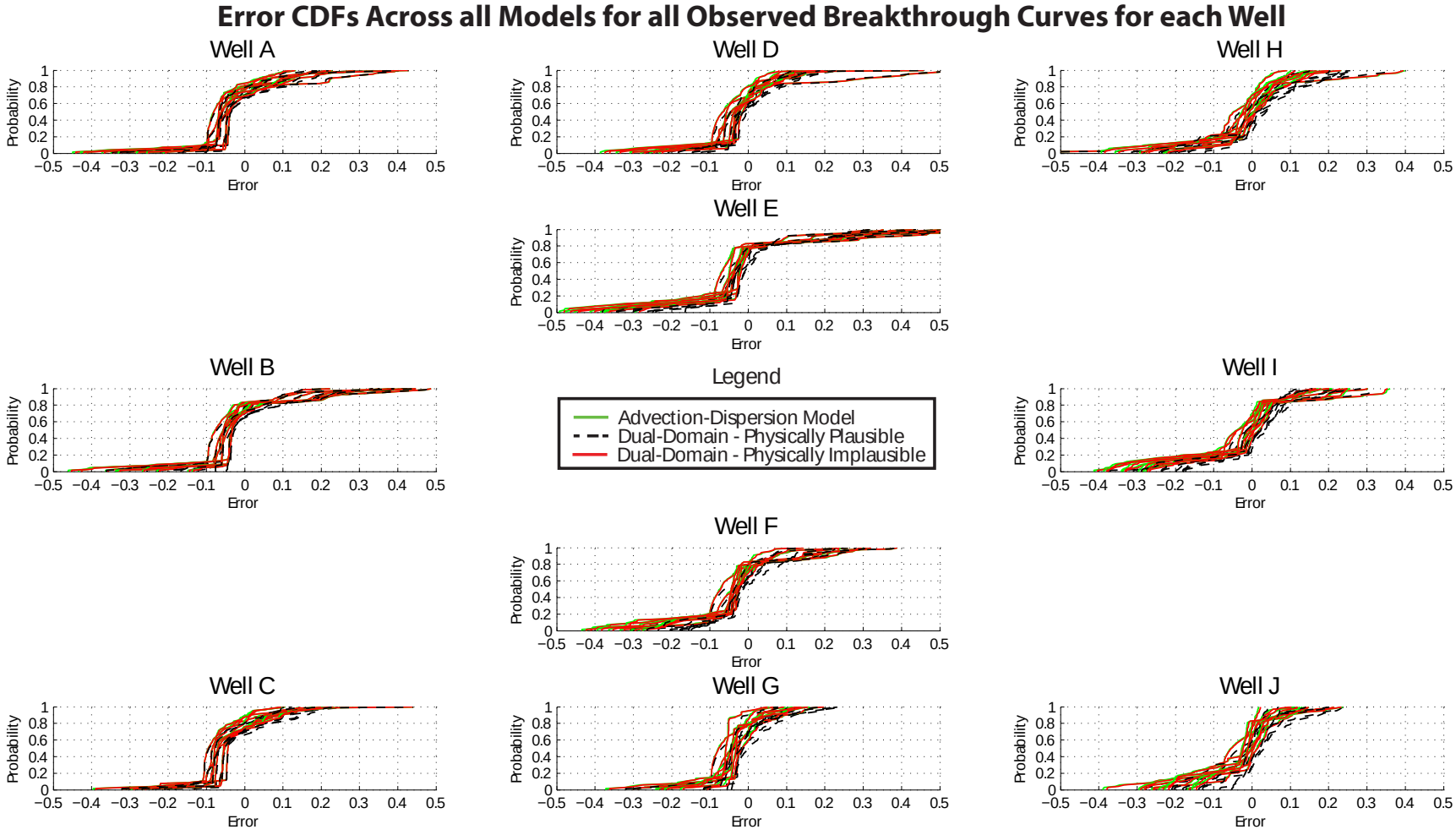

Figure 4.3: Error Empirical CDFs at each well for each model for all nine experiments

Chapter 5

Conclusions

This study's replicate experiments provide an important contribution and troubling result for the groundwater transport community. Our lower-bound complexity laboratory aquifer system shows significant variability across the nine replicate, well-controlled experiments. In field settings there would be no expectation that the initial conditions, boundary conditions, material properties, background conductivities, and tracer dynamics would be as well characterized. Given that our simple system's results make distinguishing transport hypotheses incredibly difficult, this issue should only be expected to be exacerbated with increases in complexity. Dual-domain mass transfer has three fitting parameters (D, θ_{im}, α) while advection dispersion only has one (D), which from a statistical fitting perspective favors the dual-domain model but from the perspective of Occam's Razor, poses a poor scientific inference of non-local mechanisms. Our experiment only explores the most basic of transport questions and does not deal with the complexities of reactive system dynamics. A key concern that arises with our results is "Given the data scarcity constraints and complexity of field-scale hydrogeological systems is model-based scientific inference possible?". This question has profound implications given the growing consensus that the subsurface biogeochemistry has global implications [25; 26; 27].

Chapter 6

Contributions and Future Work

This study provides a unique addition to the literature in that it includes replicate data to explore uncertainty in a small, well-controlled system. A lasting contribution of this work will be to encourage researchers to collect replicate data, no matter how well-controlled and well-characterized they may think their system is. For future work, this data set should continue to be used to explore the intricacies of data uncertainty not covered in this study. While this study only covers one or two parameterizations of two models, it would be beneficial to expand the simulations to include Monte Carlo sampling of model parameters. Using a Monte Carlo framework would add model uncertainty on top of observational uncertainty, and allow for direct comparison of the two uncertainty ranges. This would be useful in attempting to explain why the system uncertainties are occurring.

While this study only looked at fluid conductivity measurements, there is a plethora of bulk (sand and water) conductivity measurements that are not discussed in this study, but are detailed in Appendices A and B. It is possible that the bulk conductivity measurements will provide an insight into the puzzle of distinguishing process. Along with the yet-to-be analyzed bulk conductivity data, there are an additional nine experiments that were documented (see Appendix B), but not included in this study. These include experiments that (1) vary injection concentration, (2) vary areal extent of injection and (3) vary frequency of bulk conductivity data collection. These results were documented in [28], but have not been simulated via Modflow/MT3DMS. These results were collected to consider how changing experimental values affect what is observable over the course

of an experiment (in my case, whether the low conductivity cube is visible or not). These results were collected in triplicate, and may provide additional insight into the problem of distinguishing process, especially if an experimental variables has a strong control on uncertainty.

A final future methodological improvement to this work will be to look at bias-aware ensemble Kalman filtering frameworks to evaluate the biases of the models across observational uncertainty.

Appendix A

Tank Construction and Probe Calibration

A.1 Wells - Bulk, Fluid Probes, Multi-level Samplers

A.1.1 Fluid Conductivity Probes

Fluid conductivity probes were constructed from # 316 stainless steel 1-inch nails connected to 22 AWG, 8 Amp wiring. These probes were installed at 35 cm on each well. Probes were also installed at 16 cm and 54 cm, but they were unused over the course of experiments. Fluid probes are pictured in Figure A.1, and a scale diagram of each well is displayed in Figure A.2.

A.1.2 Bulk Conductivity Probes

Bulk conductivity probes were constructed from # 304 stainless steel 0.002-inch thick foil connected to 22 AWG, 8 Amp wiring. These probes are located approximately every 7.5 cm along the well. They can be seen in detail in the center portion of Figure A.1, and with detailed geometry in Figure A.2.

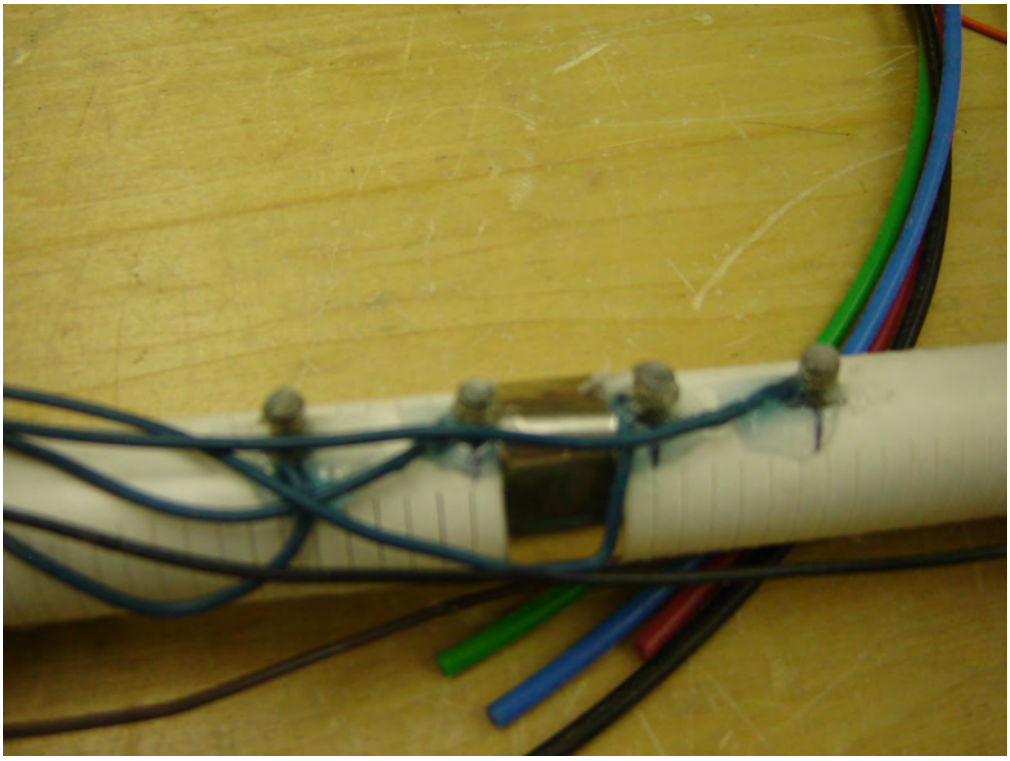

Figure A.1: Conductivity Probes - Fluid probes are the four vertical stainless steel nails puncturing the PVC well, the pictured stainless steel foil is a bulk probe

A.1.3 Multilevel Sampling Ports

Multilevel sampling ports were installed on each well at depths of 5in, 10in, 15in, 20in, and 25in. These ports remained unused over the course of experiments, but were installed should fluid samples need to be extracted from the tank. These ports are documented in Figure A.3. A full shot of each well with all bulk probes and multi-level sampling ports can be seen in Figure A.4.

A.2 Tank - Media Packing

The tank was wet-packed to try and minimize overburden pressure and consolidation of sand (though consolidation still occurred). Sand was thoroughly rinsed to remove any silicate dust that may have been packaged with the uniform sand. To hold wells in place while media was packed, a wooden frame was used to hold wells in place, while the bottom of each well was held vertical by plumber's putty.

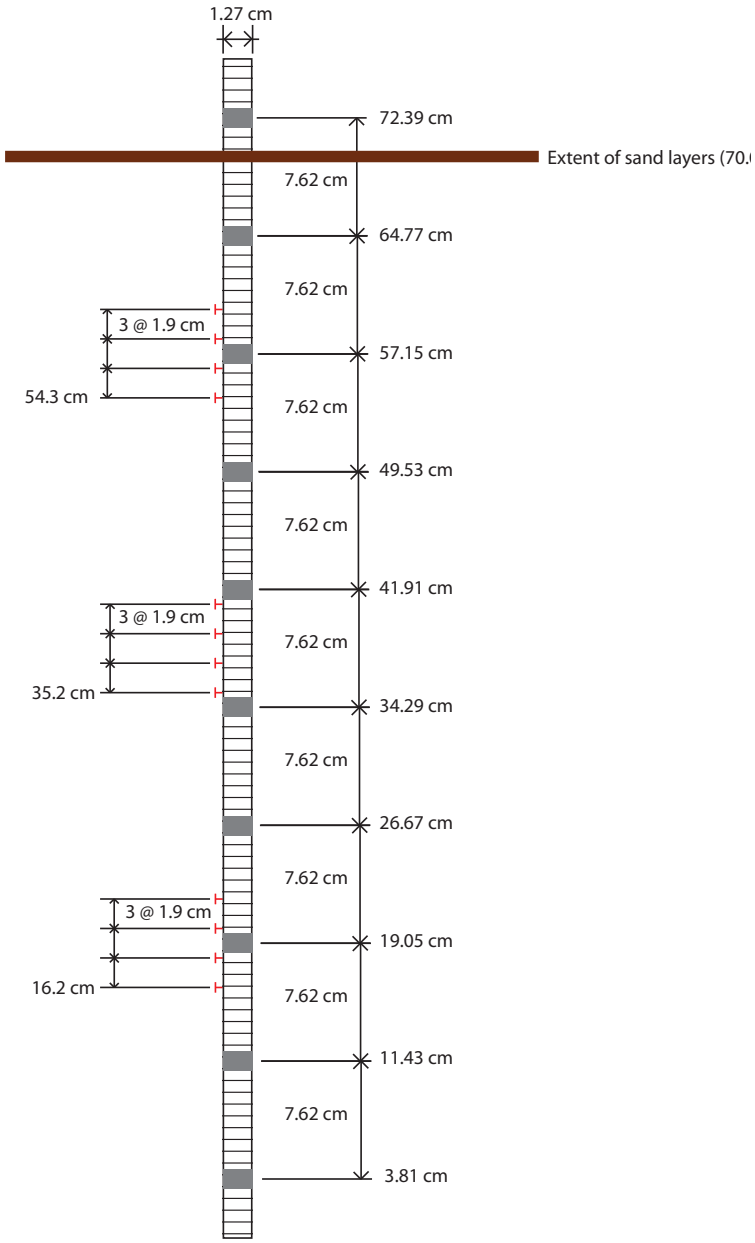

Figure A.2: Diagram of each well's construction. Fluid conductivity probes are labeled in red (center four probes were only ones used), while the gray bars represent bulk conductivity probes.

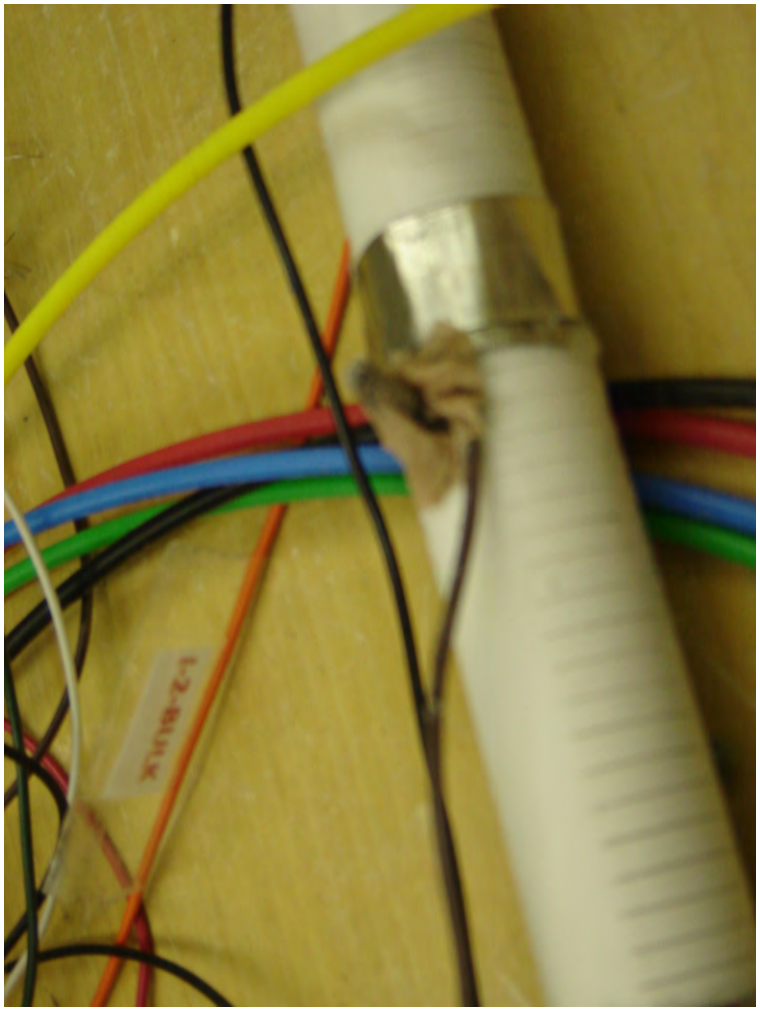

Figure A.3: Multilevel sampling ports with screen, created to take fluid samples from tank, but remained unused

This is displayed in Figure A.5. When it came time to pack the low conductivity cube, a plastic frame (20 cm x 20 cm x 20 cm) was used to hold the fine sand in place. A prototype of this is displayed in Figure A.7. Additionally, Figure A.8 shows the prototype being held in place at depth where the low conductivity cube will be placed. Figure A.6 shows a plan view of the tank cross section where the low conductivity cube is present.

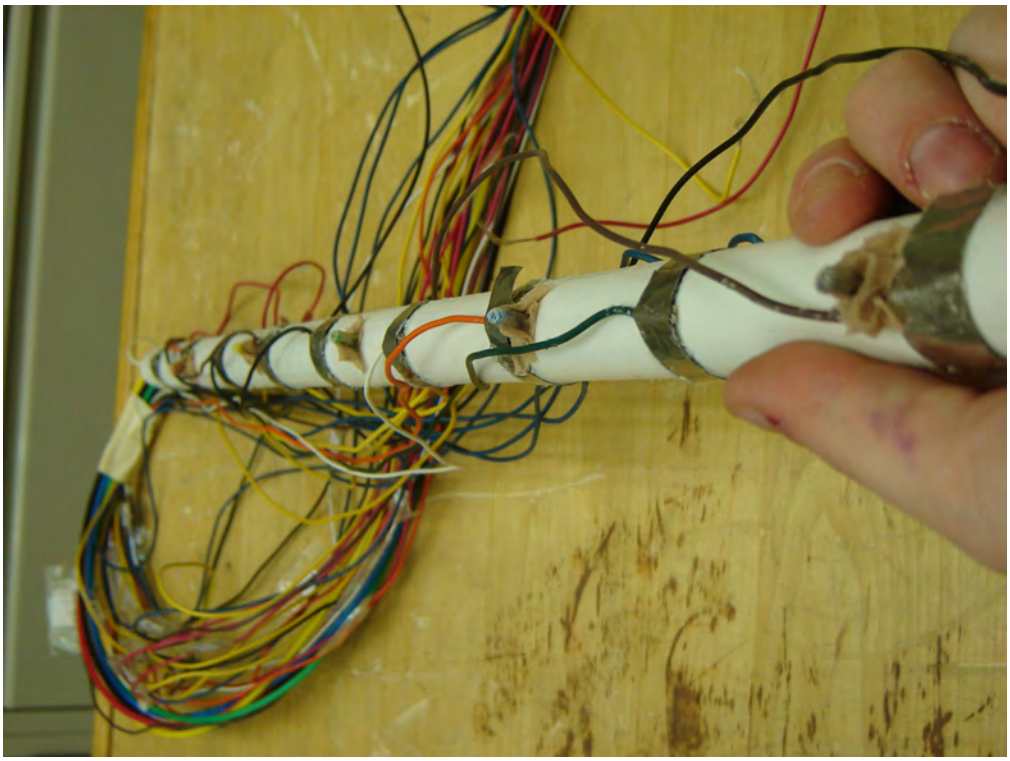

Figure A.4: Full shot of bulk probes and multi-level samplers (unused) along the length of one well

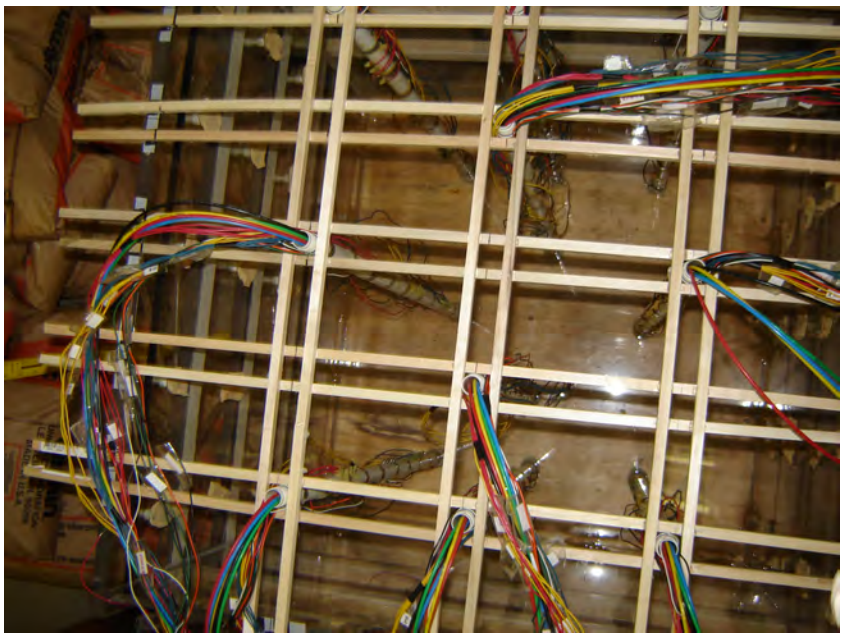

Figure A.5: Wooden frame used to hold wells in place, bottom of wells were held vertically with plumber's putty

A.3 Flow

Four manometers were installed across the length of the tank for spot observations of hydraulic gradient across the tank. These manometers are pictured in Figure A.9.

A.3.0.1 Constant Head Reservoir

A constant head reservoir was installed upstream of the inlets at a height of 1.72 m above the lab floor. This reservoir was fed by a small pump (Figure A.11 - Tetra Pond Water Garden Pump 550 GPH) to ensure that water was at the same level throughout each experiment (Figure A.10).

A.3.0.2 Inlets

All Twenty five inlet ports were used to inject tracer. These ports are pictured in Figure A.12. To prevent sand from leaving the inlet or outlet ports, hosiery was used to secure sand in place. Metal mesh was not an option as this would have interfered with electrical resistivity measurements.

A.3.0.3 Outlets

Outlet ports were symmetrical to inlet ports, except only the uppermost row of five ports were used at the outlet, with the bottom four rows being plugged. This was required to achieve steady state flow across the tank, as fully opening all twenty five ports caused transient flow.

A.4 Instrumentation - Probe Calibration

A.4.1 Geometric Factors

Before experimentally determining geometric factors, a MATLAB script (geom-dist.m) was created to narrow down geometric factors to values less than 0.5, to remove problematic measurements that occur due to large geometric factor values. (See script geom-dist.m with inputs distance.txt and electrodes.txt)

Before media packing, the tank was filled with water with known electrical resistivity (640 μS/cm). Voltage and current values were collected via the ERT machine. Using Ohm's law and the resistance-resistivity relationship, geometric factors (K) for each quadripole were solved for experimentally.

$$K = \frac{I}{V}\rho_{water,known} \tag{A.1}$$

A.4.2 Bulk Probe Configuration

Due to electrode number constraints on the electrical resistivity equipment (more instrumented electrodes than the machine could measure), bulk measurements were not taken at each well, but rather only at wells B, E, F, and I (see Figure A.6). At wells B, E, F, and I, measurements were taken along each well at various depths and between wells. The between well measurements are documented in Figure A.14. The green lines represent the six imaging planes created by taking cross well measurements between the combinations of wells. This configuration was chosen for its symmetry and inclusion of Well I, which is downstream of the low conductivity cube. The interested reader can find additional discarded configuration measurements (with different wells used for bulk conductivity measurements) in the master data folder under "Static Data".

A.5 Media - Porosity and Hydraulic Conductivity Measurements

While the tank was packed, but before steady state flow was established in the tank, static resistivity measurements were taken along each of the four bulk-wells (B,E,F,I) installed in the tank. These downwell measurements were used to plot resistivity vs. depth plots for each bulk conductivity well (B,E,F,I). Resistivity vs. depth plots were used to calculate Archie's law [17] formation factor, and calculate an estimated porosity value.

$$\theta = \left(\frac{\rho_{water}}{\rho_{rock,bulk}}\right)^{1/m} \tag{A.2}$$

Where $\frac{\rho_{water}}{\rho_{rock,bulk}}$ is the formation factor, based on water resistivity (ρ_{water}), and bulk resistivity ($\rho_{rock,bulk}$), and m is the cementation factor for unconsolidated sands (1.3).

Using this method, we estimated that porosity decreased from 0.34 to 0.31 due to overburden pressure of the tank.

Next, the relative decrease of porosity from 0.34 to 0.31 was used to calculate a relative decrease in hydraulic conductivity due to depth, using the Kozeny Carman equation.

$$K = \left(\frac{\rho g}{\mu}\right)\left[\frac{\theta^3}{(1-\theta)^2}\right]\left(\frac{d^2}{180}\right) \tag{A.3}$$

A relative decrease in porosity of 9% will create a hydraulic conductivity decrease of 30 %, so the hydraulic conductivity gradient with depth of the tank decreases from 0.005 m/s to 0.0036 m/s.

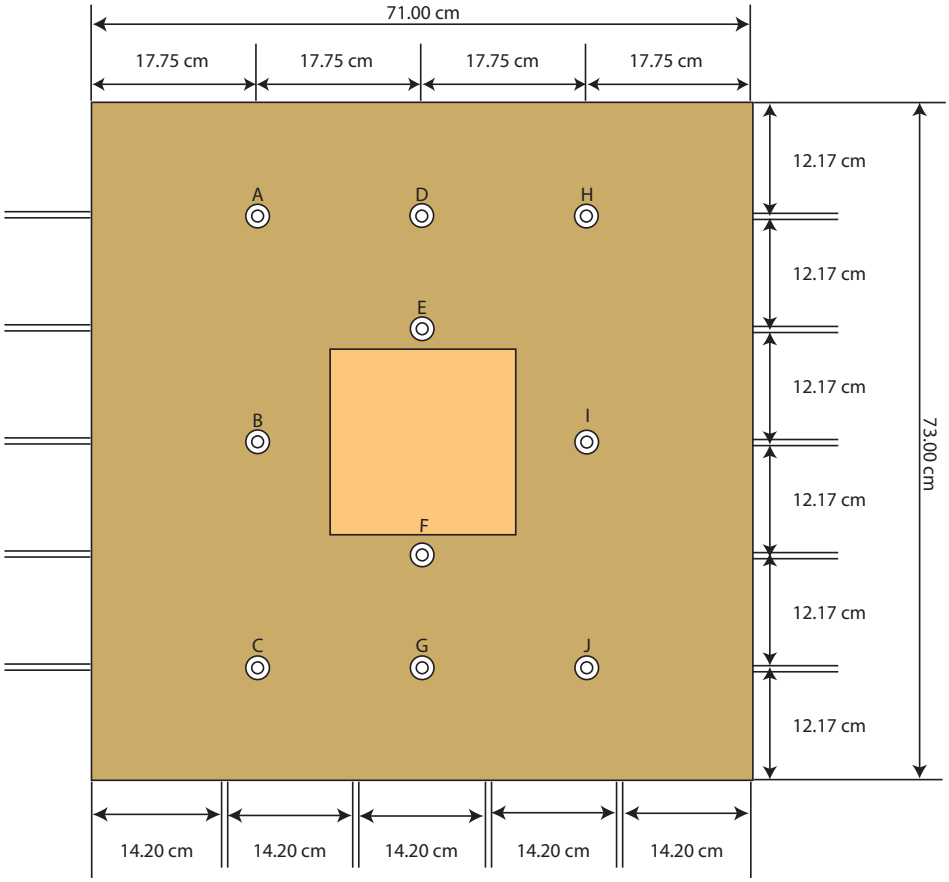

Figure A.6: Plan view of well placement in the tank

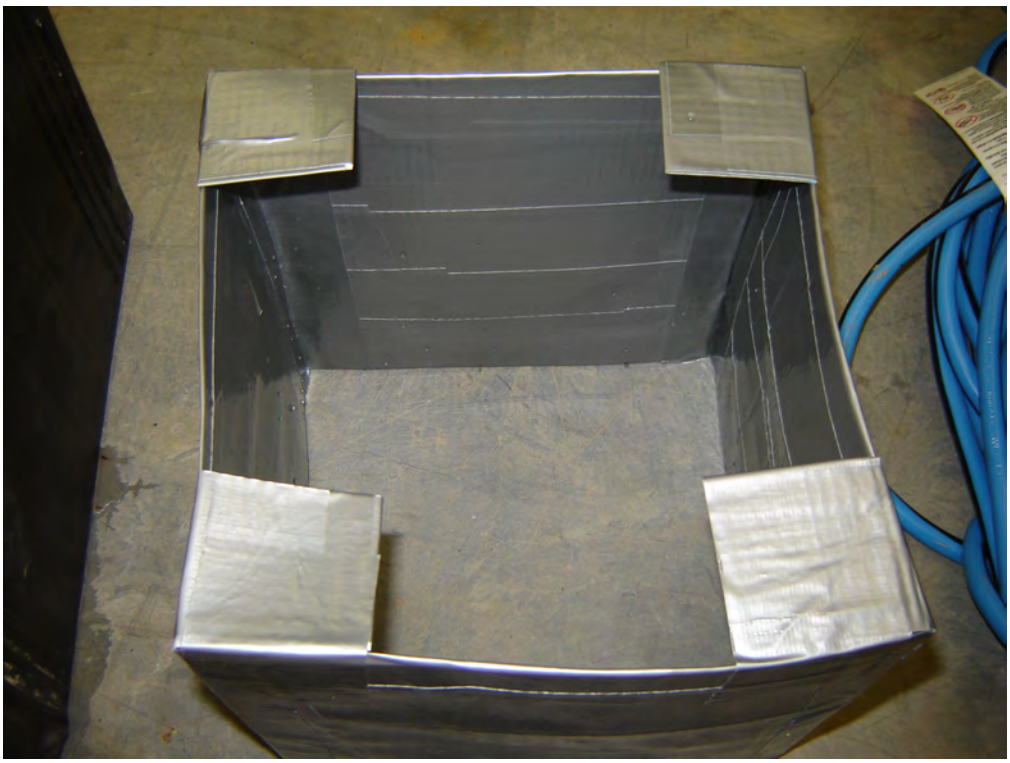

Figure A.7: Frame prototype used to hold low conductivity (K = 0.00014 m/s) sand cube in place while tank was packed

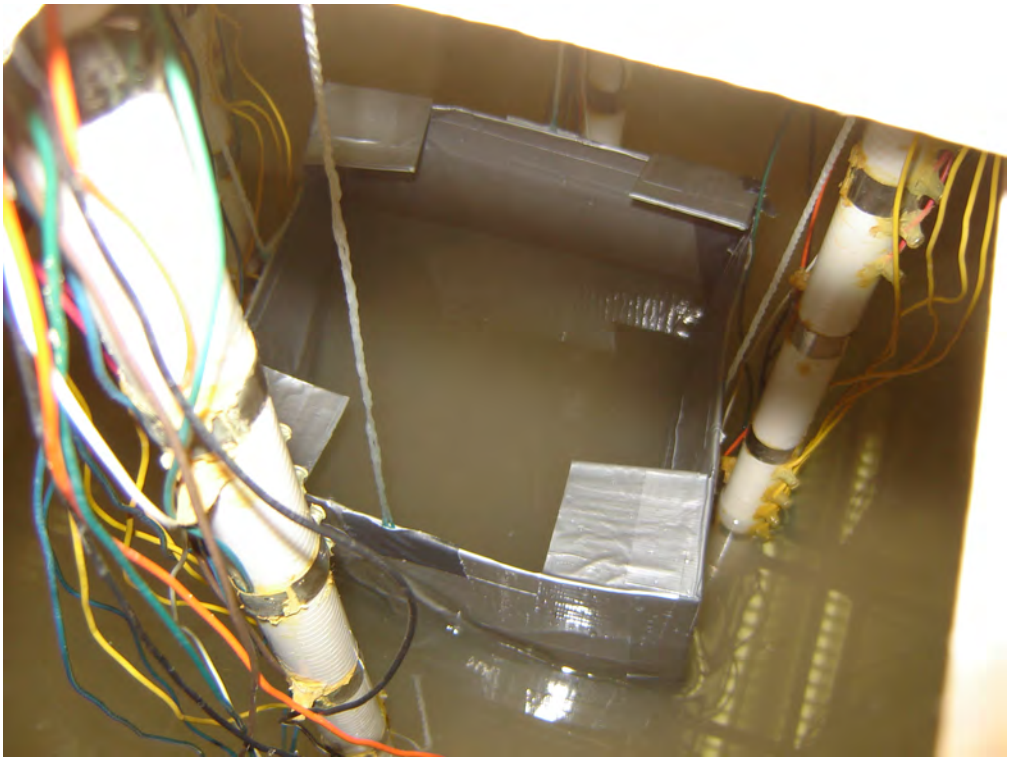

Figure A.8: Low conductivity sand frame being held in place to pack tank

Figure A.9: Four Manometers along the transverse length of the tank

(a) Constant head reservoir being fed by ground reservoir (required due to volume of water)

(b) Constant head reservoir overflow outlet

Figure A.10: Constant Head Reservoir

Figure A.11: Pump feeding constant head reservoir

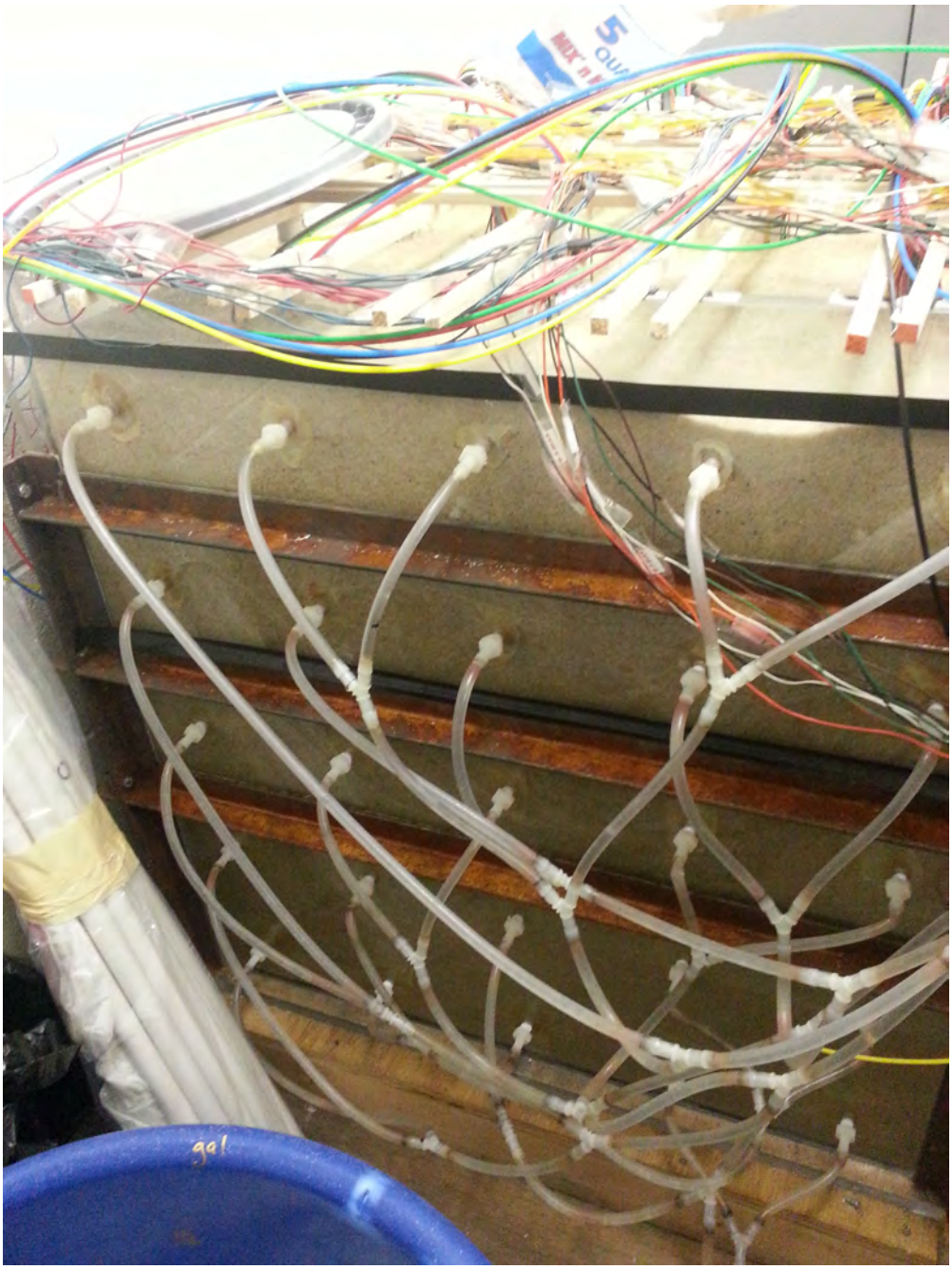

Figure A.12: Upstream view of inlet ports

Figure A.13: Downstream view of outlet ports

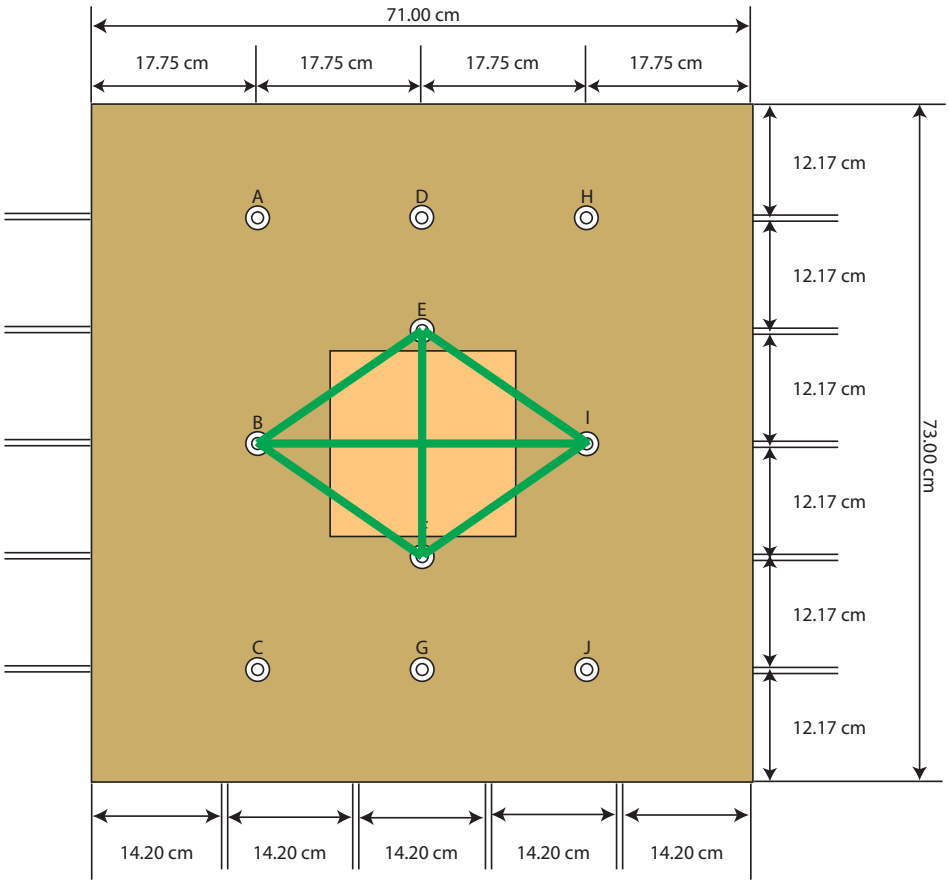

Figure A.14: Plan view of bulk conductivity imaging planes for wells B, E, F, and I

Appendix B

Exhaustive Experimental Data

This appendix contains experimental data for all eighteen tests conducted. This data includes the geophysical data from the bulk conductivity probes, the normalized concentration breakthrough curves for each test, the calculated temporal moments (and semi-invariants) and the calculated spatial moments for each test.

B.1 Plot Descriptions

B.1.1 Bulk Conductivity Plots

B.2 trade-offs

These plots represent the bulk conductivity measurements along wells B, E, F, and I. That is, each quadripole is located entirely on one well, with electrodes at different depths. The x axis of each plot is the measurement time of the first quadripole along a given well (after start of injection). Note that these measurements are not instantaneous, so the time axis varies on each plot.The y axis of each plot is distance from bottom of the tank in meters, providing a vertical profile of the tank at each of the four measurement wells. Frequency of bulk geophysical measurements (low, mid-range, high) affects the number of columns on the y-axis of each plot. Low-frequency geophysical measurements have a highly resolved y-axis with measurements at many depths, at the expense of the amount of time it takes to collect these measurements - i.e., temporal smearing. Conversely, high-

frequency geophysical measurements have a low resolution y-axis, but have many more measurements in time to compensate. The trade-off between frequency of measurements and temporal smearing is an area for future study that should be considered. Note that each color axis is from 0 - 250 % change from background conditions. This was chosen to consistently compare plots across tests that had varying injection concentrations (0.25 g/L, 0.55 g/L, 0.75 g/L).

B.2.1 Normalized Well Concentration Plots

These plots are normalized concentration breakthrough curves for each well (A-J) as well as normalized breakthrough at the inlet and outlet ports (plotted in black). Note that upstream wells are plotted in "cold" colors, and the colors become "warmer" as one moves from upstream to downstream wells. See Figure A.6 for a reference on well location.

B.2.2 Temporal Moments

Based on the normalized concentration plots, temporal moments were calculated for each well. Note that due to tailing behavior, temporal moments do not always behave as expected (e.g., variance may decrease from upstream to downstream). For future analysis, one should consider looking at this data using truncated temporal moment analysis [29].

B.3 0.55 g/L, Mid-Range Frequency Geophysical Measurements, 25 Injection Ports

B.3.1 Test 1

Experimental values include: 0.55 g/L, Mid-Range Frequency Geophysical Measurements, 25 Injection Ports, this test is labeled Test09 in the data folder. Results for bulk conductivity are displayed in B.1, fluid conductivity in B.2, and temporal moments in B.1.

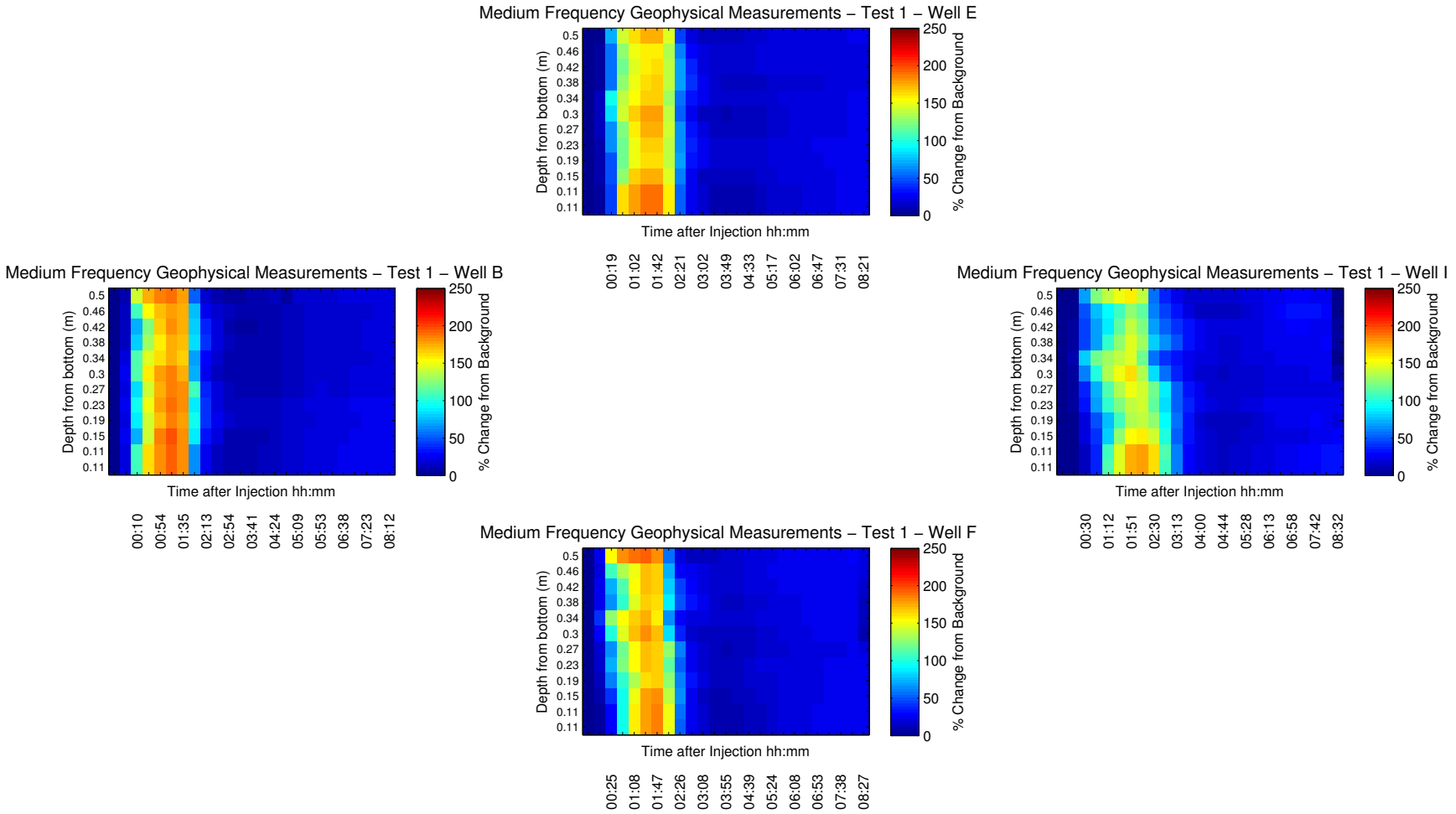

Figure B.1: Downwell Bulk Conductivity Measurements for 0.55 g/L, Mid-Range Frequency Geophysical Measurements, 25 Injection Ports (Test09)

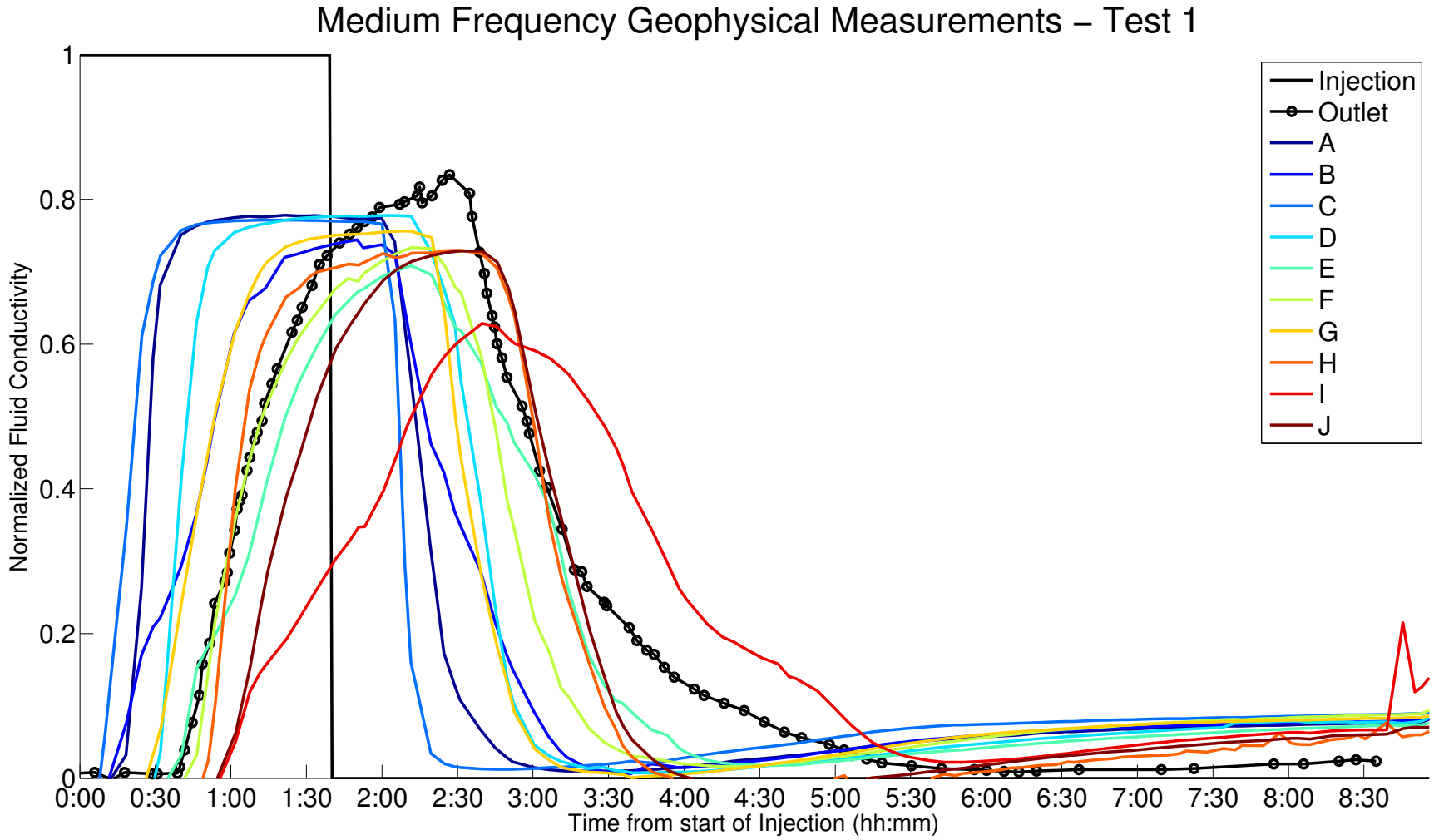

Figure B.2: Fluid Conductivity Measurements at all Wells for 0.55 g/L, Mid-Range Frequency Geophysical Measurements, 25 Injection Ports (Test09)

Well	**Mean Arrival Time (s)**	**Variance (s^2)**	**Skew**	**Kurtosis**	**Semi-invariant m3**	**Semi-invariant m2**	**Semi-invariant m1**	**Semi-invariant m0**
A	9180	8580	1.9	1.09	2.03E+13	8.48E+08	4.93E+04	5.38
B	10360	8630	1.75	0.48	2.21E+13	9.36E+08	5.34E+04	5.15
C	9700	9260	1.83	0.69	2.50E+13	1.02E+09	5.50E+04	5.67
D	9780	8160	1.82	0.83	2.08E+13	8.97E+08	5.41E+04	5.52
E	11320	7770	1.62	0.07	2.10E+13	9.46E+08	5.68E+04	5.02
F	11430	8240	1.64	0.10	2.25E+13	9.71E+08	5.59E+04	4.89
G	10650	8610	1.73	0.40	2.34E+13	9.88E+08	5.61E+04	5.27
H	10680	7460	1.68	0.38	2.04E+13	9.31E+08	5.86E+04	5.49
I	13640	7570	1.42	-0.68	2.99E+13	1.35E+09	7.58E+04	5.55
J	11420	7400	1.61	0.08	1.92E+13	8.77E+08	5.40E+04	4.73

Table B.1: Temporal Moments - 0.55 g/L, Mid-Range Frequency Geophysical Measurements, 25 Injection Ports - (Test09)

B.3.2 Test 2

Experimental values include: 0.55 g/L, Mid-Range Frequency Geophysical Measurements, 25 Injection Ports, this test is labeled Test10 in the data folder. Results for bulk conductivity are displayed in B.3, fluid conductivity in B.4, and temporal moments in B.2.

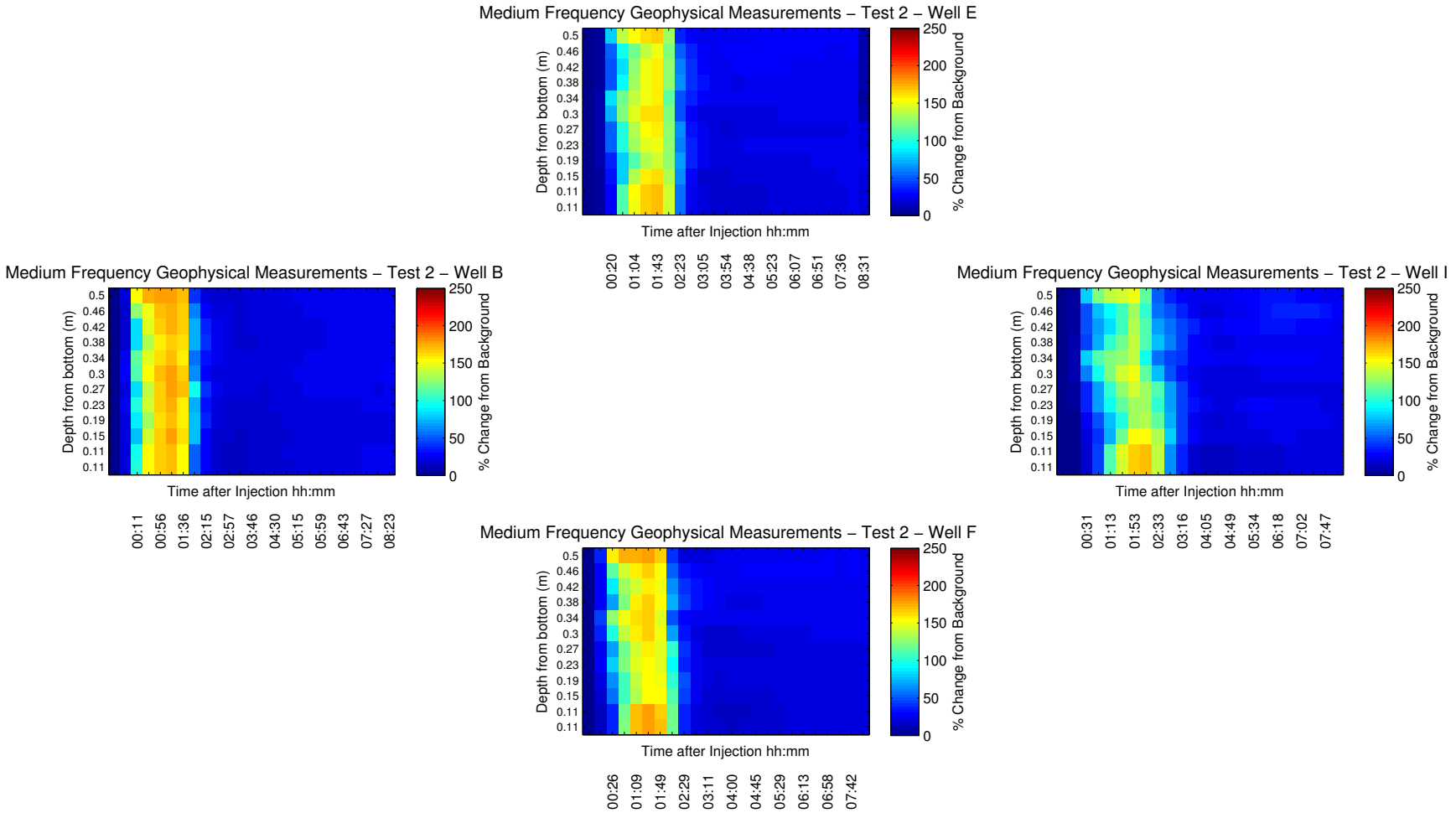

Figure B.3: Downwell Bulk Conductivity Measurements for 0.55 g/L, Mid-Range Frequency Geophysical Measurements, 25 Injection Ports (Test10)

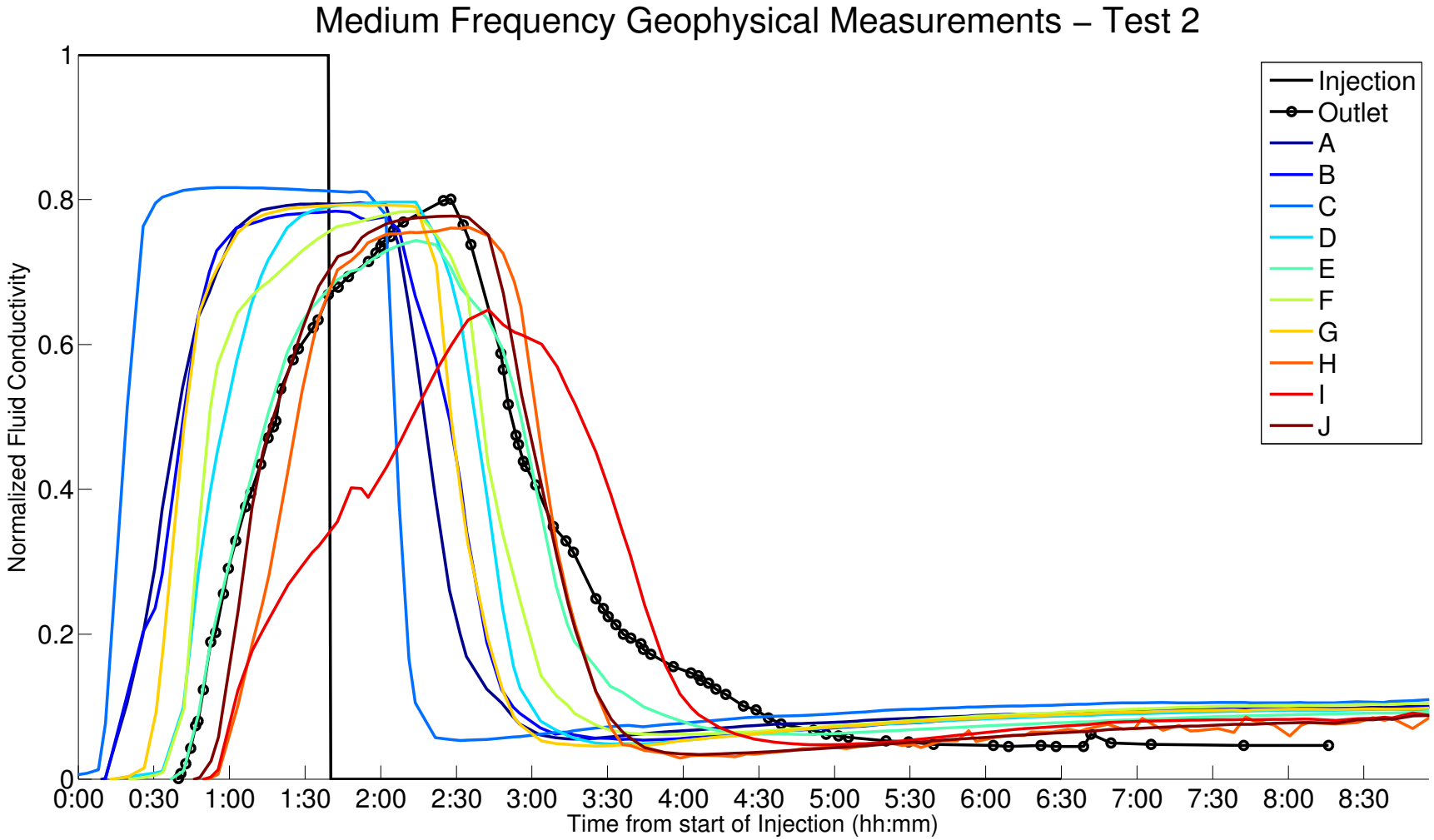

Figure B.4: Fluid Conductivity Measurements at all Wells for 0.55 g/L, Mid-Range Frequency Geophysical Measurements, 25 Injection Ports (Test10)

Well	**Mean Arrival Time (s)**	**Variance (s^2)**	**Skew**	**Kurtosis**	**Semi-invariant m3**	**Semi-invariant m2**	**Semi-invariant m1**	**Semi-invariant m0**
A	10530	8810	1.72	0.32	2.61E+13	1.10E+09	6.17E+04	5.86
B	10390	8610	1.73	0.4	2.53E+13	1.08E+09	6.16E+04	5.93
C	9900	9190	1.79	0.52	2.74E+13	1.14E+09	6.16E+04	6.23
D	11080	8310	1.66	0.14	2.45E+13	1.06E+09	6.14E+04	5.55
E	11770	7890	1.57	-0.14	2.50E+13	1.12E+09	6.56E+04	5.57
F	11140	8280	1.65	0.12	2.53E+13	1.10E+09	6.38E+04	5.73
G	10500	8500	1.72	0.37	2.46E+13	1.06E+09	6.07E+04	5.78
H	12010	7710	1.55	-0.2	2.39E+13	1.08E+09	6.36E+04	5.29
I	13120	7540	1.45	-0.58	2.43E+13	1.11E+09	6.35E+04	4.84
J	11600	7710	1.59	-0.05	2.35E+13	1.06E+09	6.34E+04	5.47

Table B.2: Temporal Moments - 0.55 g/L, Mid-Range Frequency Geophysical Measurements, 25 Injection Ports - (Test10)

B.3.3 Test 3

Experimental values include: 0.55 g/L, Mid-Range Frequency Geophysical Measurements, 25 Injection Ports, this test is labeled Test11 in the data folder. Results for bulk conductivity are displayed in B.5, fluid conductivity in B.6, and temporal moments in B.3.

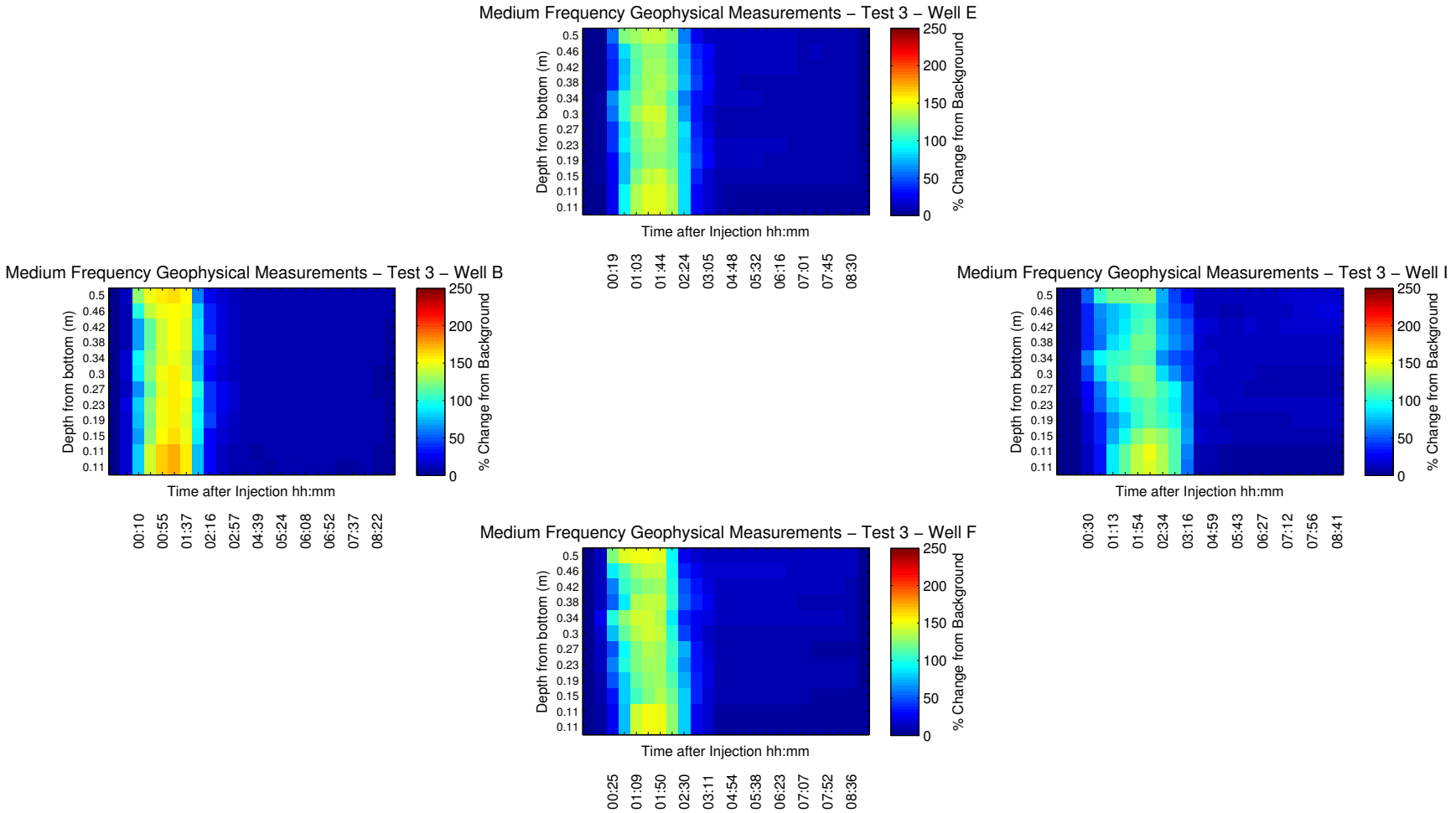

Figure B.5: Downwell Bulk Conductivity Measurements for 0.55 g/L, Mid-Range Frequency Geophysical Measurements, 25 Injection Ports (Test11)

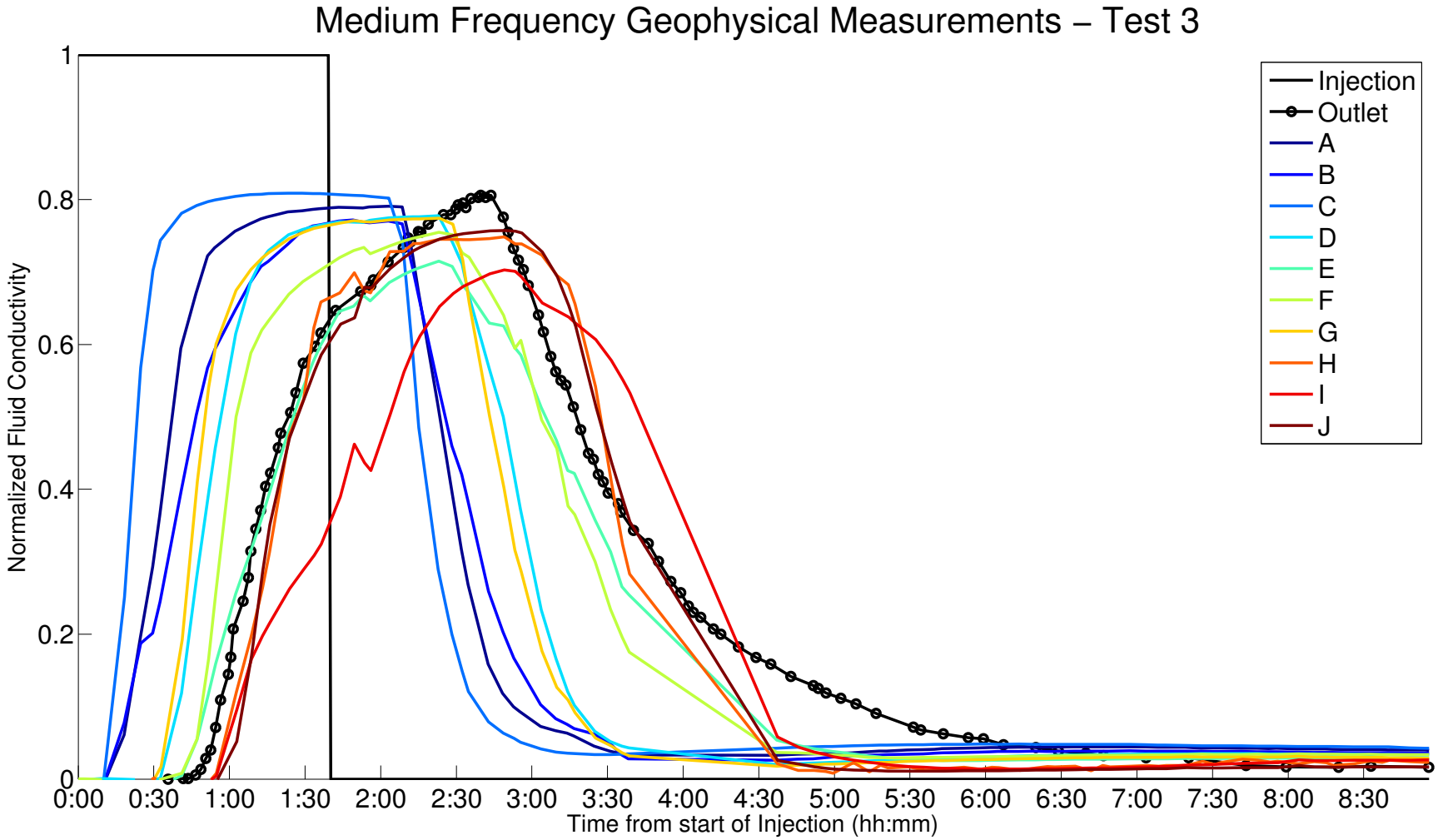

Figure B.6: Fluid Conductivity Measurements at all Wells for 0.55 g/L, Mid-Range Frequency Geophysical Measurements, 25 Injection Ports (Test11)

Well	**Mean Arrival Time (s)**	**Variance (s^2)**	**Skew**	**Kurtosis**	**Semi-invariant m3**	**Semi-invariant m2**	**Semi-invariant m1**	**Semi-invariant m0**
A	14090	10460	1.46	-0.69	1.45E+14	5.64E+09	2.58E+05	18.31
B	13940	10340	1.47	-0.66	1.23E+14	4.83E+09	2.23E+05	16.02
C	13880	10570	1.47	-0.65	1.46E+14	5.67E+09	2.59E+05	18.63
D	14300	10230	1.45	-0.72	1.46E+14	5.72E+09	2.65E+05	18.5
E	14630	9930	1.42	-0.80	1.38E+14	5.52E+09	2.58E+05	17.64
F	11890	8450	1.6	-0.040	3.77E+13	1.62E+09	9.03E+04	7.59
G	11360	9050	1.69	0.25	3.81E+13	1.55E+09	8.36E+04	7.36
H	12310	8040	1.58	-0.04	3.42E+13	1.48E+09	8.40E+04	6.82
I	12640	7250	1.5	-0.27	2.62E+13	1.20E+09	7.14E+04	5.65
J	12480	8010	1.53	-0.26	3.79E+13	1.67E+09	9.49E+04	7.61

Table B.3: Temporal Moments - 0.55 g/L, Mid-Range Frequency Geophysical Measurements, 25 Injection Ports - (Test11)

B.4 0.55 g/L, Low Frequency Geophysical Measurements, 25 Injection Ports

B.4.1 Test 1

Experimental values include: 0.55 g/L, Low Frequency Geophysical Measurements, 25 Injection Ports, this test is labeled Test17 in the data folder. Results for bulk conductivity are displayed in B.7, fluid conductivity in B.8, and temporal moments in B.4.

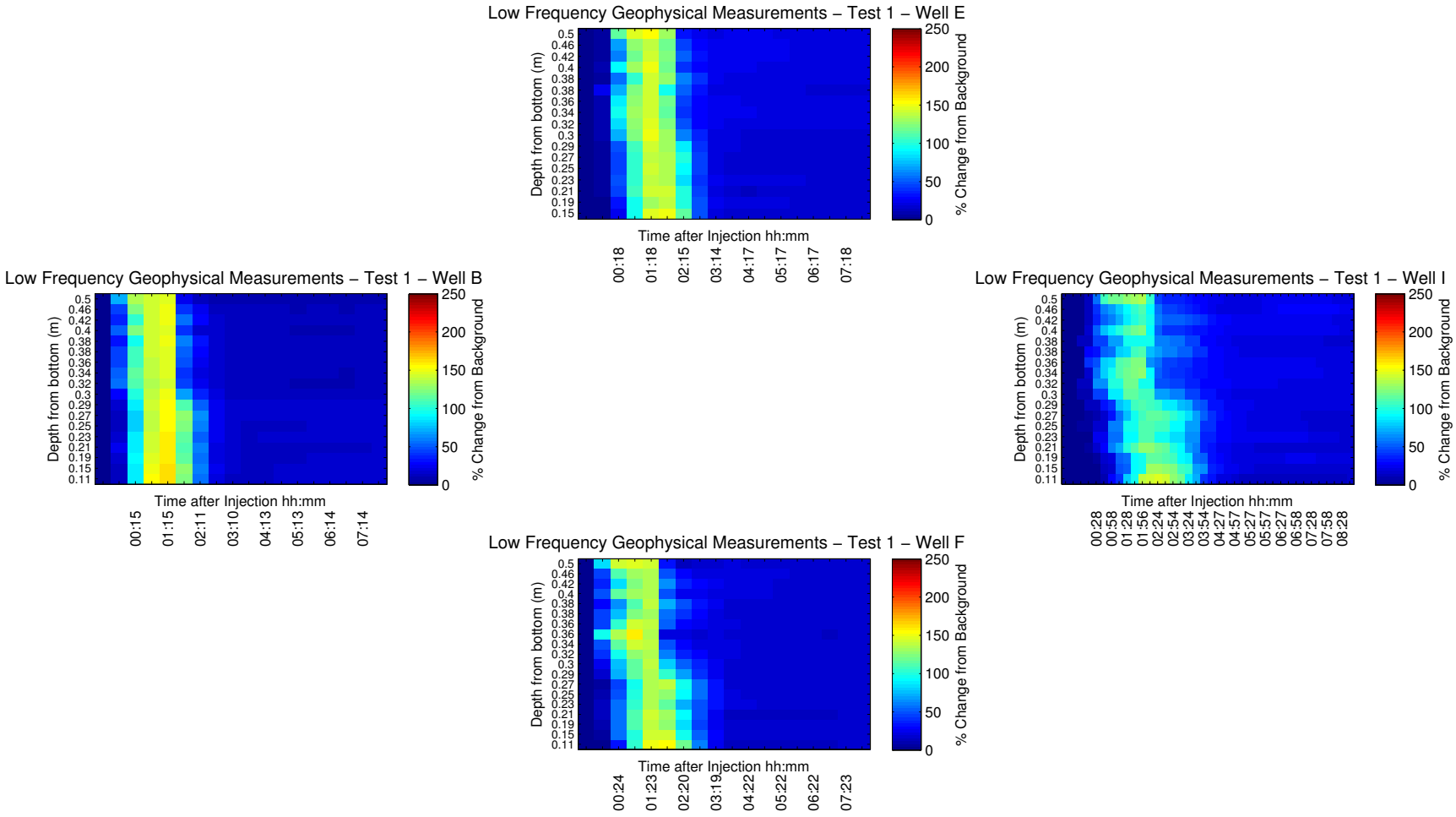

Figure B.7: Downwell Bulk Conductivity Measurements for 0.55 g/L, Low Frequency Geophysical Measurements, 25 Injection Ports (Test17)

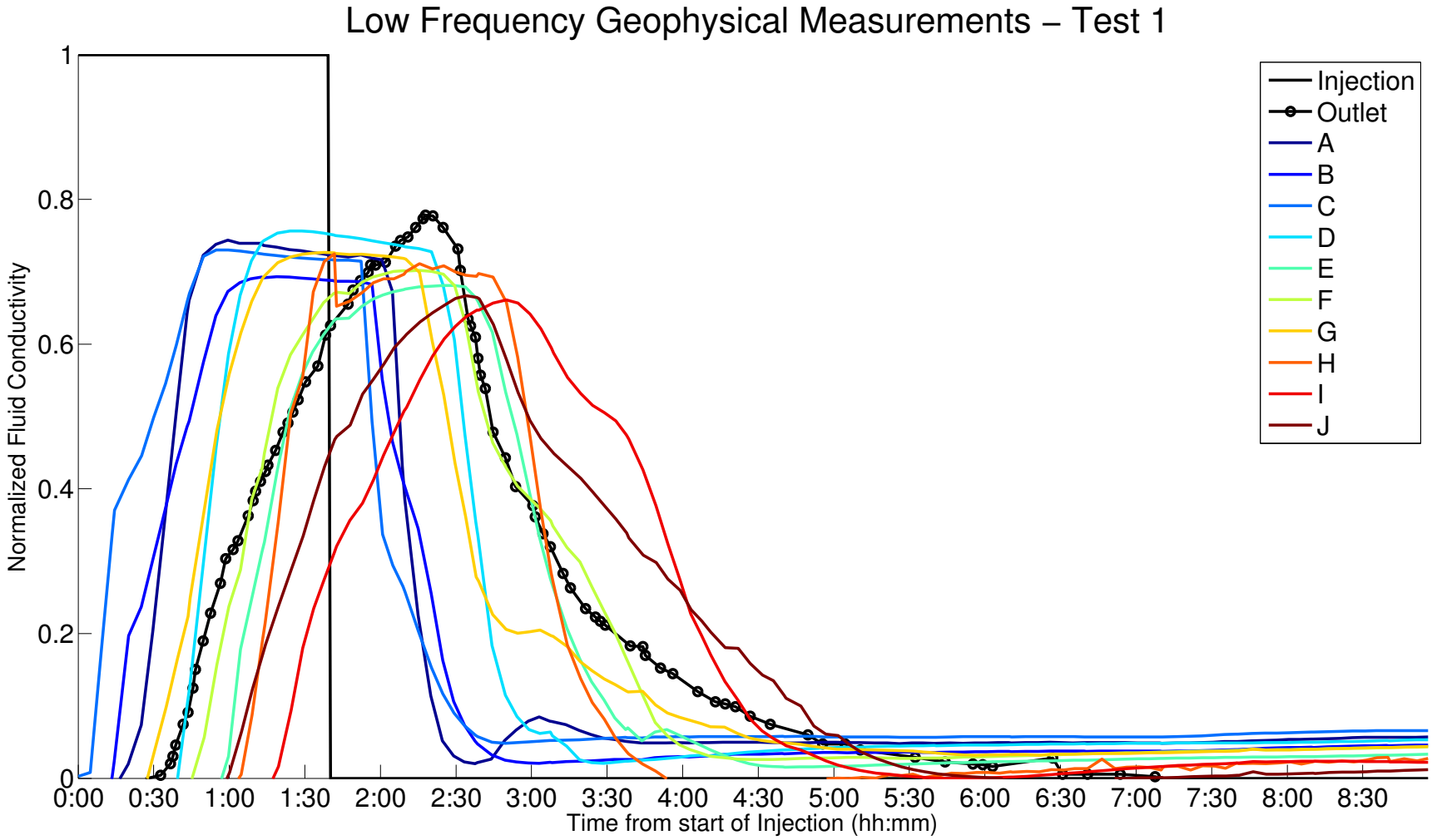

Figure B.8: Fluid Conductivity Measurements at all Wells for 0.55 g/L, Low Frequency Geophysical Measurements, 25 Injection Ports (Test17)

Well	**Mean Arrival Time (s)**	**Variance (s^2)**	**Skew**	**Kurtosis**	**Semi-invariant m3**	**Semi-invariant m2**	**Semi-invariant m1**	**Semi-invariant m0**
A	10150	8660	1.75	0.44	2.20E+13	9.45E+08	5.39E+04	5.31
B	10130	8770	1.75	0.45	2.22E+13	9.46E+08	5.33E+04	5.27
C	9880	9050	1.77	0.49	2.47E+13	1.04E+09	5.72E+04	5.79
D	10590	7990	1.69	0.3	2.11E+13	9.40E+08	5.65E+04	5.34
E	11640	7400	1.55	-0.17	2.09E+13	9.75E+08	5.97E+04	5.12
F	11300	7360	1.58	-0.07	2.11E+13	9.90E+08	6.15E+04	5.44
G	10530	7690	1.66	0.22	2.09E+13	9.64E+08	5.97E+04	5.67
H	11180	7170	1.59	0.01	1.83E+13	8.67E+08	5.50E+04	4.92
I	12530	6140	1.39	-0.7	1.84E+13	9.51E+08	6.12E+04	4.88
J	11770	6040	1.41	-0.61	1.71E+13	9.13E+08	6.14E+04	5.22

Table B.4: Temporal Moments - 0.55 g/L, Low Frequency Geophysical Measurements, 25 Injection Ports - (Test17)

B.4.2 Test 2

Experimental values include: 0.55 g/L, Low Frequency Geophysical Measurements, 25 Injection Ports, this test is labeled Test18 in the data folder. Results for bulk conductivity are displayed in B.9, fluid conductivity in B.10, and temporal moments in B.5.

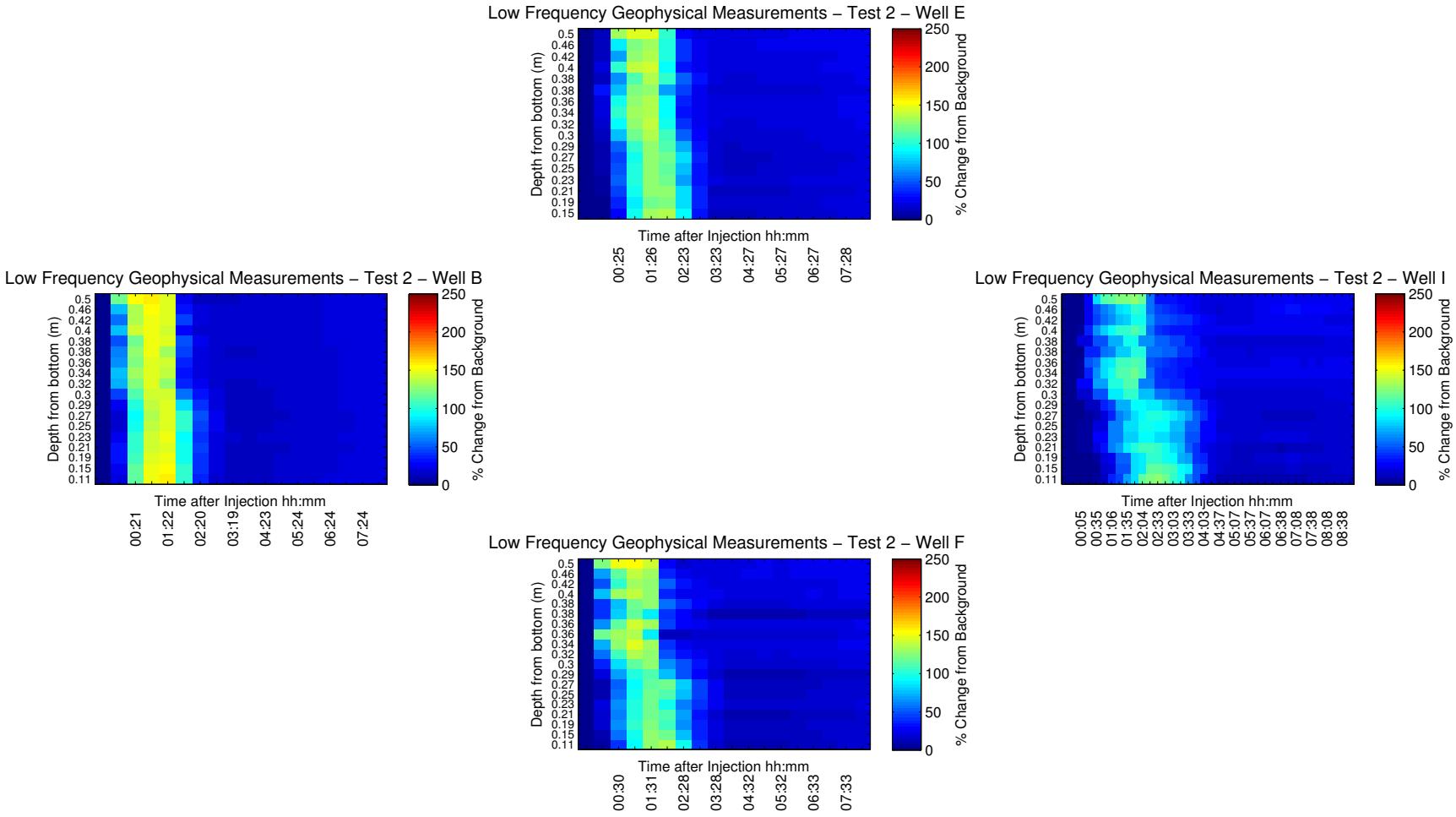

Figure B.9: Downwell Bulk Conductivity Measurements for 0.55 g/L, Low Frequency Geophysical Measurements, 25 Injection Ports (Test18)

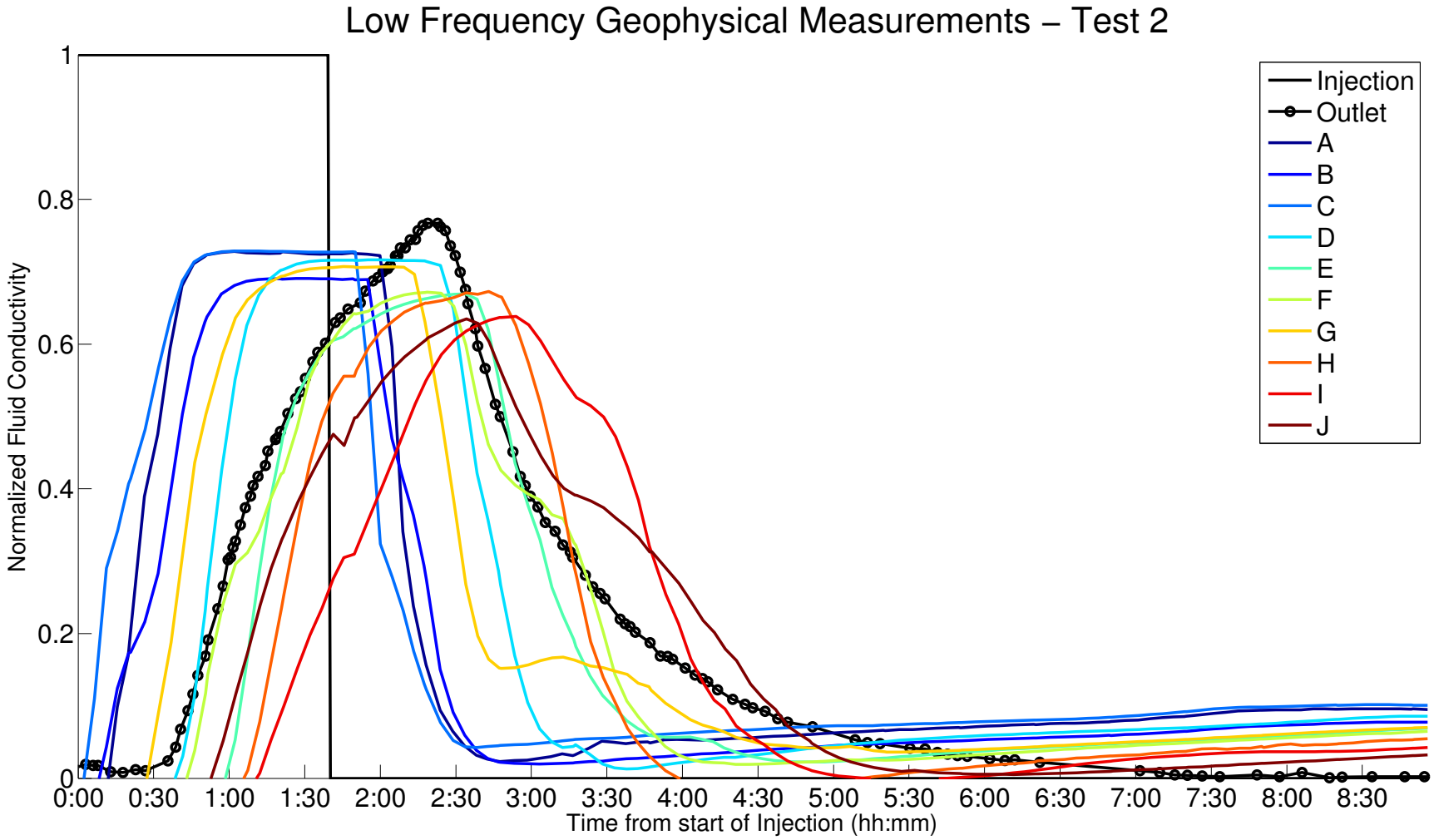

Figure B.10: Fluid Conductivity Measurements at all Wells for 0.55 g/L, Low Frequency Geophysical Measurements, 25 Injection Ports (Test18)

Well	**Mean Arrival Time (s)**	**Variance (s^2)**	**Skew**	**Kurtosis**	**Semi-invariant m3**	**Semi-invariant m2**	**Semi-invariant m1**	**Semi-invariant m0**
A	11030	9640	1.7	0.17	3.19E+13	1.28E+09	6.58E+04	5.96
B	11140	9560	1.69	0.14	3.04E+13	1.22E+09	6.32E+04	5.67
C	10880	9840	1.71	0.18	3.30E+13	1.32E+09	6.67E+04	6.13
D	11620	8770	1.64	0.05	2.83E+13	1.18E+09	6.49E+04	5.58
E	12580	8210	1.54	-0.29	2.78E+13	1.20E+09	6.69E+04	5.32
F	11870	8000	1.58	-0.09	2.47E+13	1.09E+09	6.32E+04	5.32
G	10990	8460	1.67	0.21	2.64E+13	1.14E+09	6.50E+04	5.91
H	12430	7930	1.54	-0.24	2.47E+13	1.08E+09	6.20E+04	4.99
I	12800	6890	1.44	-0.55	2.12E+13	1.01E+09	6.13E+04	4.79
J	11730	6660	1.48	-0.37	1.92E+13	9.62E+08	6.20E+04	5.29

Table B.5: Temporal Moments - 0.55 g/L, Low Frequency Geophysical Measurements, 25 Injection Ports - (Test18)

B.4.3 Test 3

Experimental values include: 0.55 g/L, Low Frequency Geophysical Measurements, 25 Injection Ports, this test is labeled Test19 in the data folder. Results for bulk conductivity are displayed in B.11, fluid conductivity in B.12, and temporal moments in B.6.

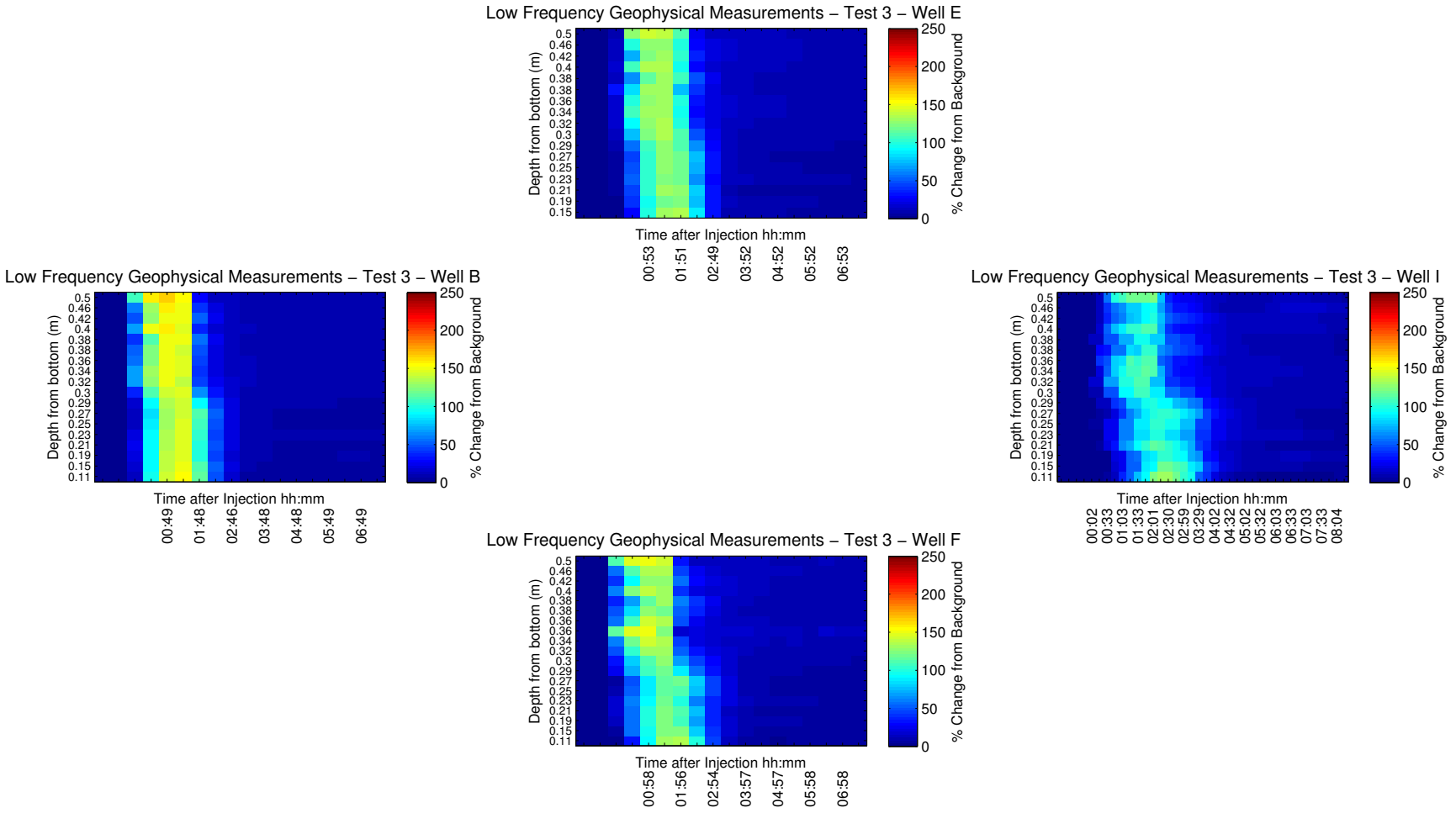

Figure B.11: Downwell Bulk Conductivity Measurements for 0.55 g/L, Low Frequency Geophysical Measurements, 25 Injection Ports (Test19)

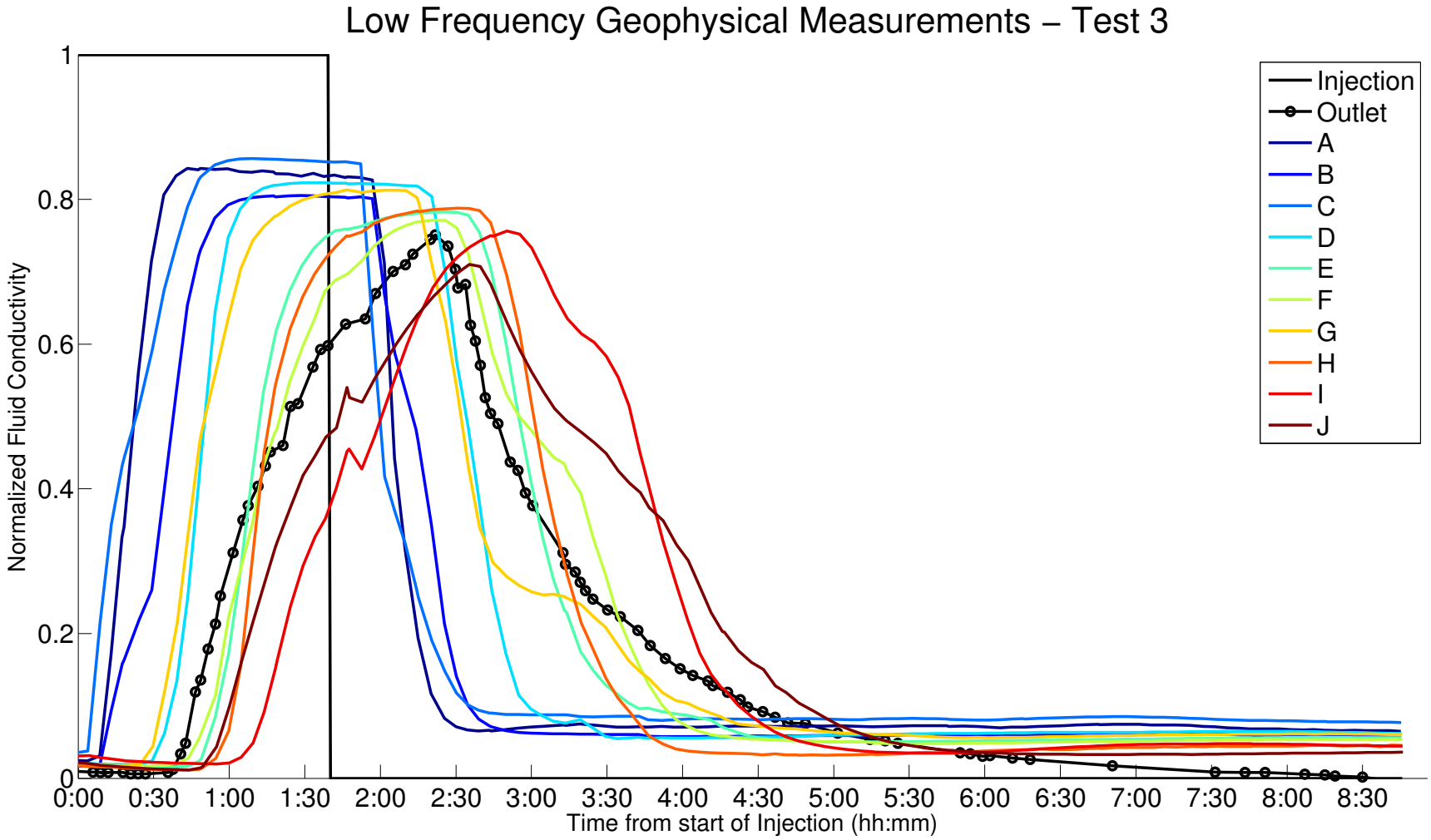

Figure B.12: Fluid Conductivity Measurements at all Wells for 0.55 g/L, Low Frequency Geophysical Measurements, 25 Injection Ports (Test19)

Well	**Mean Arrival Time (s)**	**Variance (s^2)**	**Skew**	**Kurtosis**	**Semi-invariant m3**	**Semi-invariant m2**	**Semi-invariant m1**	**Semi-invariant m0**
A	7400	6950	2.03	1.85	1.09E+13	5.30E+08	3.81E+04	5.14
B	7700	6610	1.96	1.64	9.52E+12	4.79E+08	3.58E+04	4.66
C	7560	7140	2	1.71	1.16E+13	5.58E+08	3.90E+04	5.16
D	8400	6160	1.8	1.04	1.00E+13	5.33E+08	4.13E+04	4.91
E	9480	5650	1.58	0.13	1.01E+13	5.82E+08	4.53E+04	4.78
F	9630	5440	1.52	-0.08	9.76E+12	5.80E+08	4.56E+04	4.74
G	8750	5980	1.69	0.57	1.06E+13	5.92E+08	4.61E+04	5.27
H	9310	5150	1.55	0.08	8.58E+12	5.22E+08	4.29E+04	4.61
I	10790	4670	1.31	-0.9	9.72E+12	6.30E+08	4.92E+04	4.55
J	10570	4880	1.33	-0.89	1.02E+13	6.59E+08	5.14E+04	4.86

Table B.6: Temporal Moments - 0.55 g/L, Low Frequency Geophysical Measurements, 25 Injection Ports - (Test19)

B.5 0.55 g/L, High Frequency Geophysical Measurements, 25 Injection Ports

Experimental values include: 0.55 g/L, High Frequency Geophysical Measurements, 25 Injection Ports, this test is labeled Test14 in the data folder. Results for bulk conductivity are displayed in B.13, fluid conductivity in B.14, and temporal moments in B.7.

B.5.1 Test 1

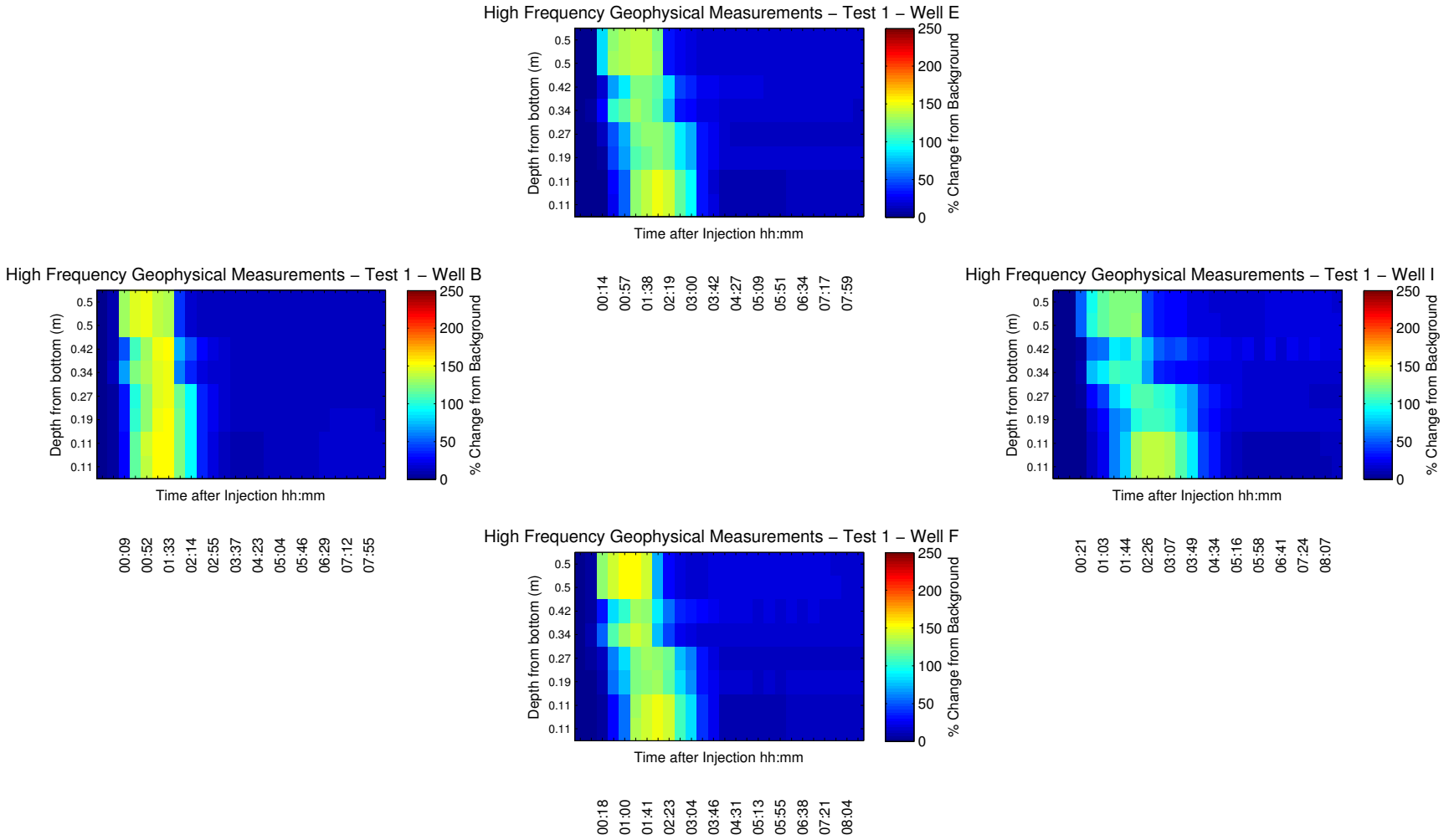

Figure B.13: Downwell Bulk Conductivity Measurements for 0.55 g/L, High Frequency Geophysical Measurements, 25 Injection Ports (Test14)

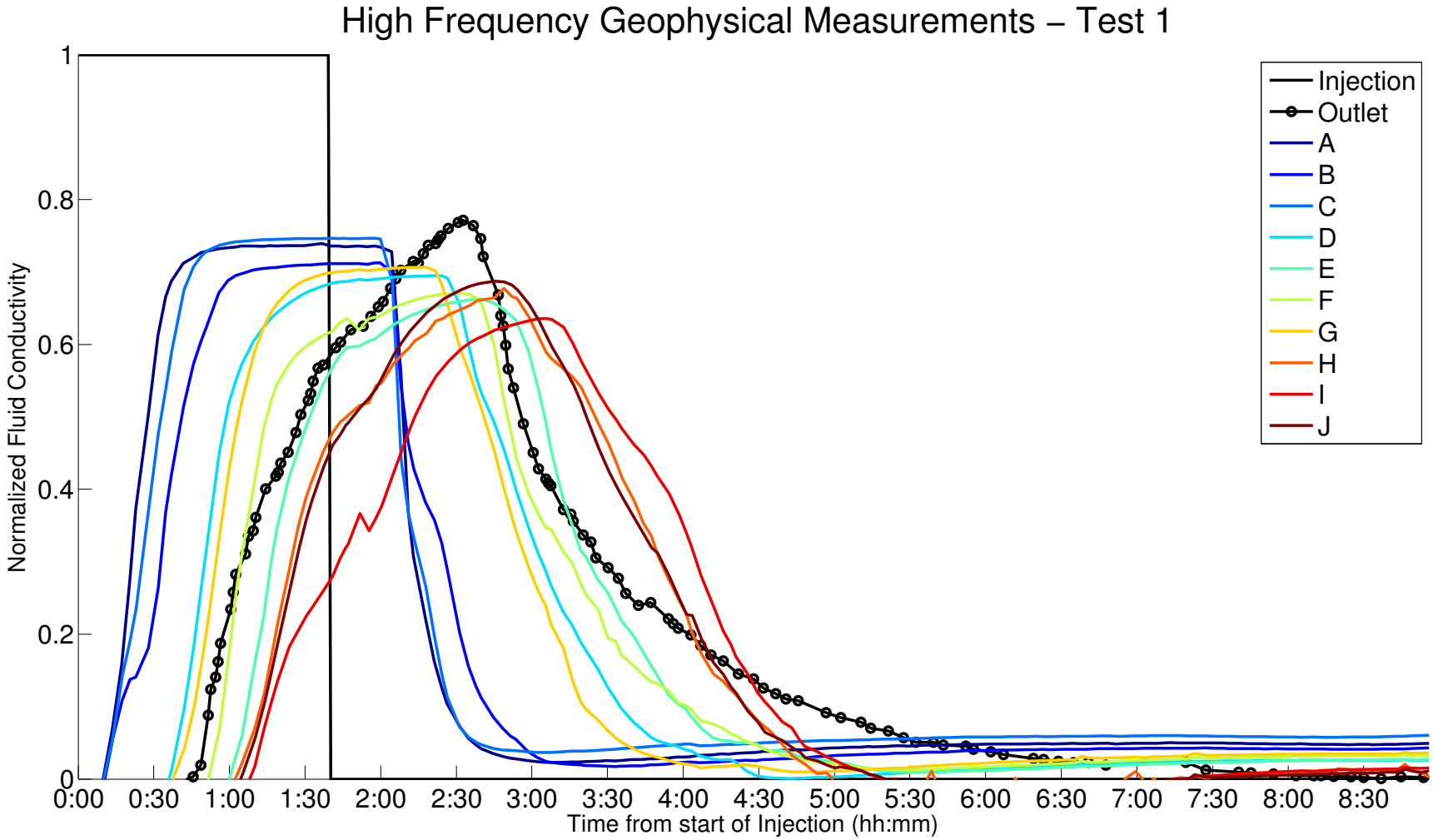

Figure B.14: Fluid Conductivity Measurements at all Wells for 0.55 g/L, High Frequency Geophysical Measurements, 25 Injection Ports (Test14)

Well	**Mean Arrival Time (s)**	**Variance (s^2)**	**Skew**	**Kurtosis**	**Semi-invariant m3**	**Semi-invariant m2**	**Semi-invariant m1**	**Semi-invariant m0**
A	9350	8570	1.85	0.86	2.07E+13	8.82E+08	5.12E+04	5.48
B	9870	8480	1.79	0.63	2.08E+13	8.95E+08	5.21E+04	5.28
C	9900	8770	1.79	0.59	2.29E+13	9.70E+08	5.49E+04	5.55
D	10310	7260	1.68	0.35	1.87E+13	8.85E+08	5.74E+04	5.57
E	11890	7050	1.51	-0.3	2.11E+13	1.01E+09	6.29E+04	5.29
F	11390	7250	1.56	-0.11	2.09E+13	9.87E+08	6.17E+04	5.41
G	10500	7500	1.68	0.34	1.90E+13	8.73E+08	5.51E+04	5.24
H	11930	6500	1.45	-0.48	2.03E+13	1.03E+09	6.68E+04	5.6
I	12360	5930	1.38	-0.71	1.77E+13	9.35E+08	6.15E+04	4.98
J	11680	6010	1.43	-0.51	1.71E+13	9.07E+08	6.14E+04	5.26

Table B.7: Temporal Moments - 0.55 g/L, High Frequency Geophysical Measurements, 25 Injection Ports - (Test14)

B.5.2 Test 2

Experimental values include: 0.55 g/L, High Frequency Geophysical Measurements, 25 Injection Ports, this test is labeled Test15 in the data folder. Results for bulk conductivity are displayed in B.15, fluid conductivity in B.16, and temporal moments in B.8.

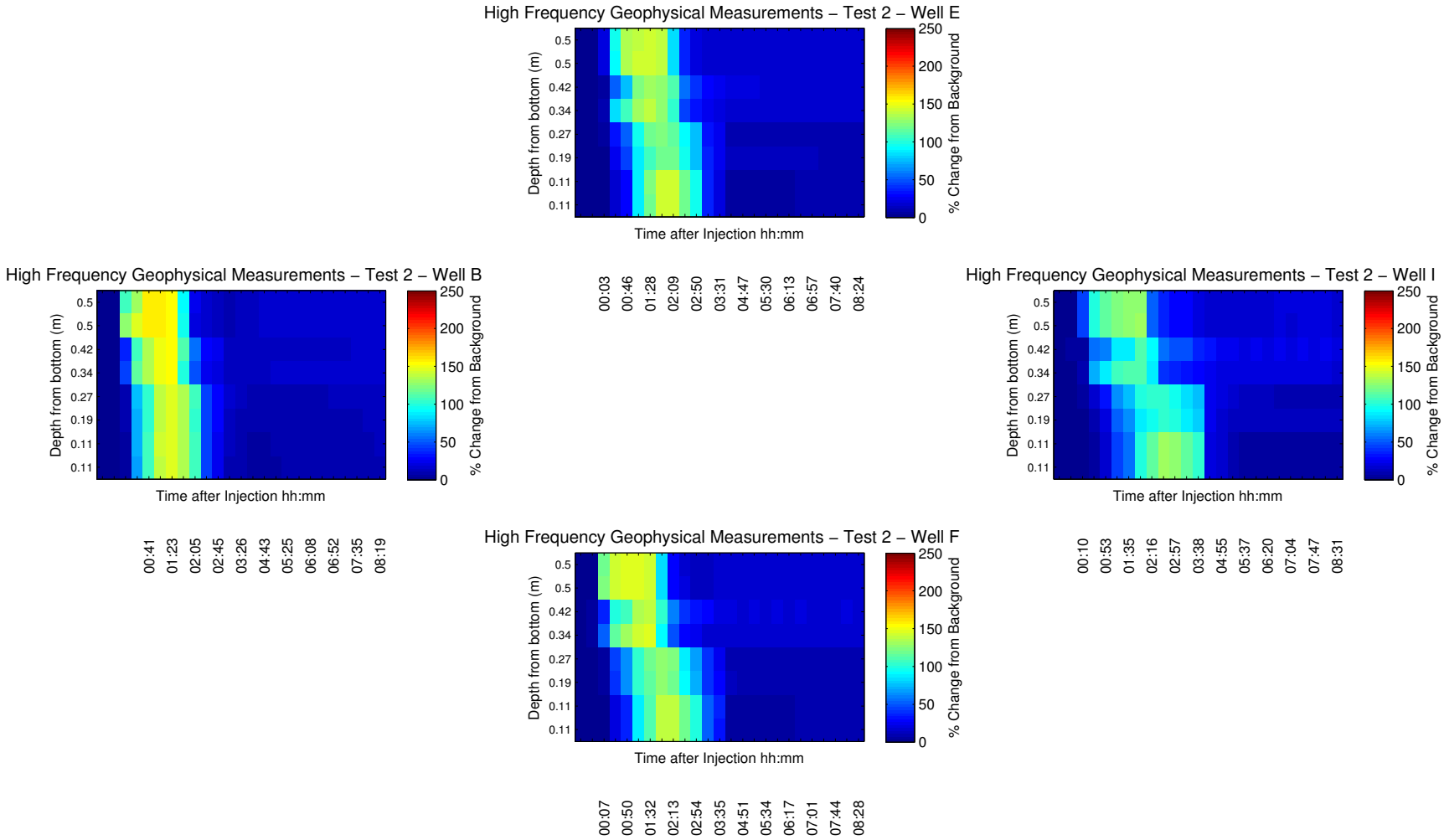

Figure B.15: Downwell Bulk Conductivity Measurements for 0.55 g/L, High Frequency Geophysical Measurements, 25 Injection Ports (Test15)

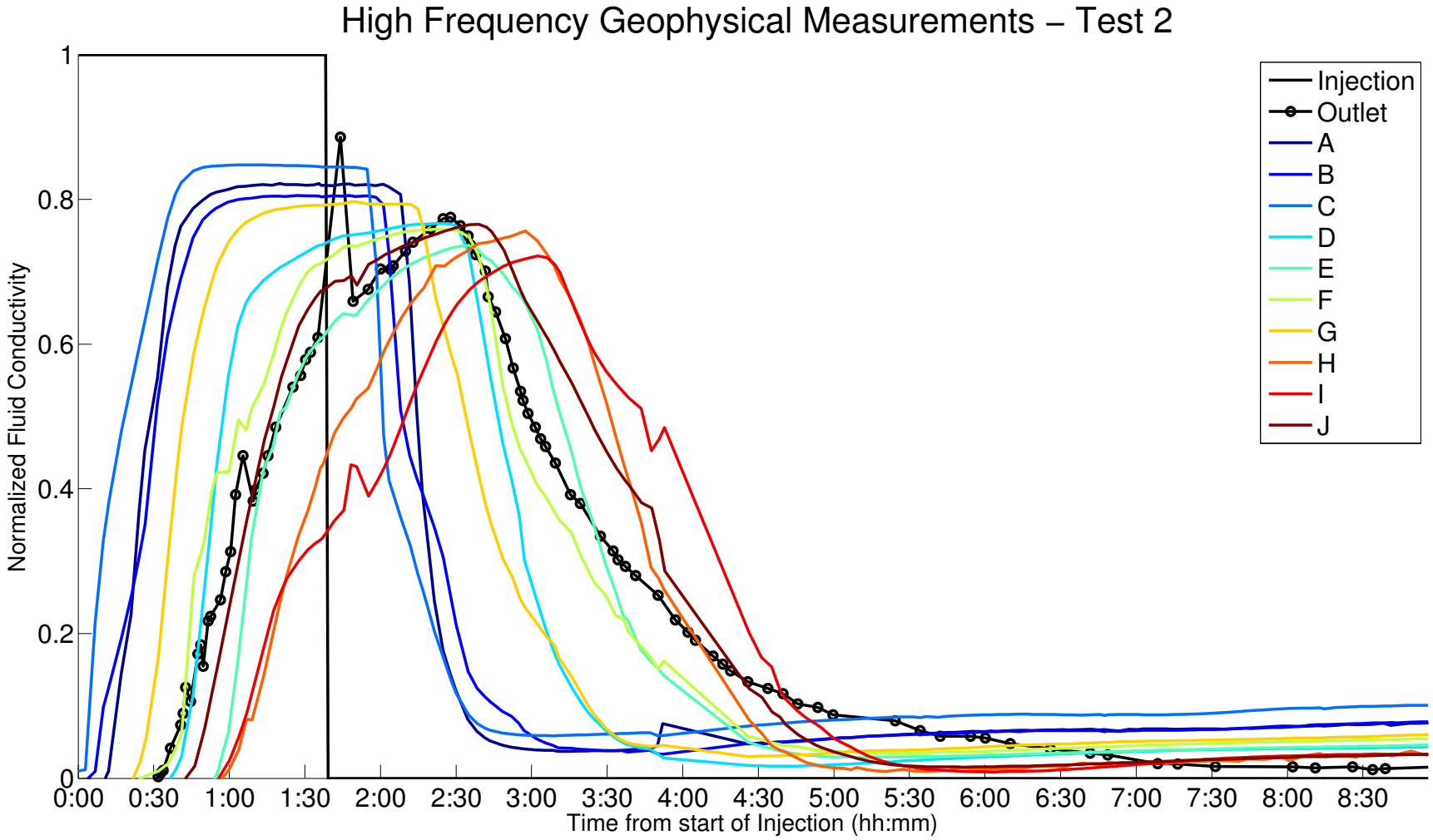

Figure B.16: Fluid Conductivity Measurements at all Wells for 0.55 g/L, High Frequency Geophysical Measurements, 25 Injection Ports (Test15)

Well	**Mean Arrival Time (s)**	**Variance (s^2)**	**Skew**	**Kurtosis**	**Semi-invariant m3**	**Semi-invariant m2**	**Semi-invariant m1**	**Semi-invariant m0**
A	8970	8210	1.9	1.14	1.96E+13	8.47E+08	5.14E+04	5.73
B	8970	8230	1.9	1.15	1.92E+13	8.27E+08	5.00E+04	5.58
C	8990	8740	1.9	1.05	2.27E+13	9.52E+08	5.45E+04	6.05
D	9480	6680	1.75	0.76	1.41E+13	6.98E+08	4.92E+04	5.19
E	10850	6350	1.54	-0.1	1.63E+13	8.43E+08	5.79E+04	5.33
F	10130	6610	1.63	0.26	1.66E+13	8.40E+08	5.82E+04	5.75
G	8980	7060	1.84	1.11	1.55E+13	7.36E+08	5.06E+04	5.64
H	11270	5720	1.43	-0.47	1.54E+13	8.49E+08	5.99E+04	5.31
I	11740	5340	1.35	-0.8	1.52E+13	8.76E+08	6.18E+04	5.27
J	10470	5680	1.48	-0.28	1.53E+13	8.67E+08	6.40E+04	6.11

Table B.8: Temporal Moments - 0.55 g/L, High Frequency Geophysical Measurements, 25 Injection Ports - (Test15)

B.5.3 Test 3

Experimental values include: 0.55 g/L, High Frequency Geophysical Measurements, 25 Injection Ports, this test is labeled Test16 in the data folder. Results for bulk conductivity are displayed in B.17, fluid conductivity in B.18, and temporal moments in B.9.

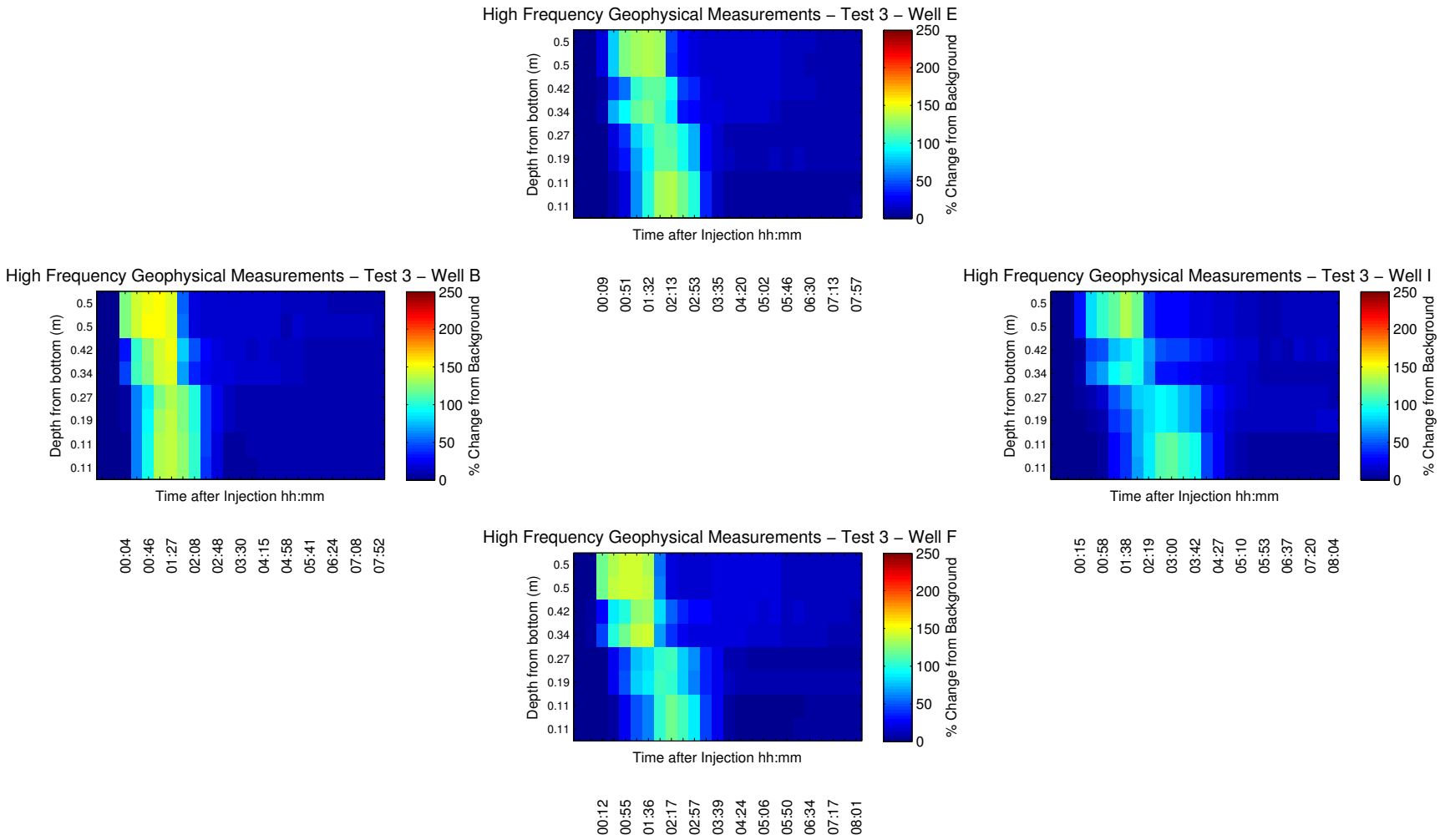

Figure B.17: Downwell Bulk Conductivity Measurements for 0.55 g/L, High Frequency Geophysical Measurements, 25 Injection Ports (Test16)

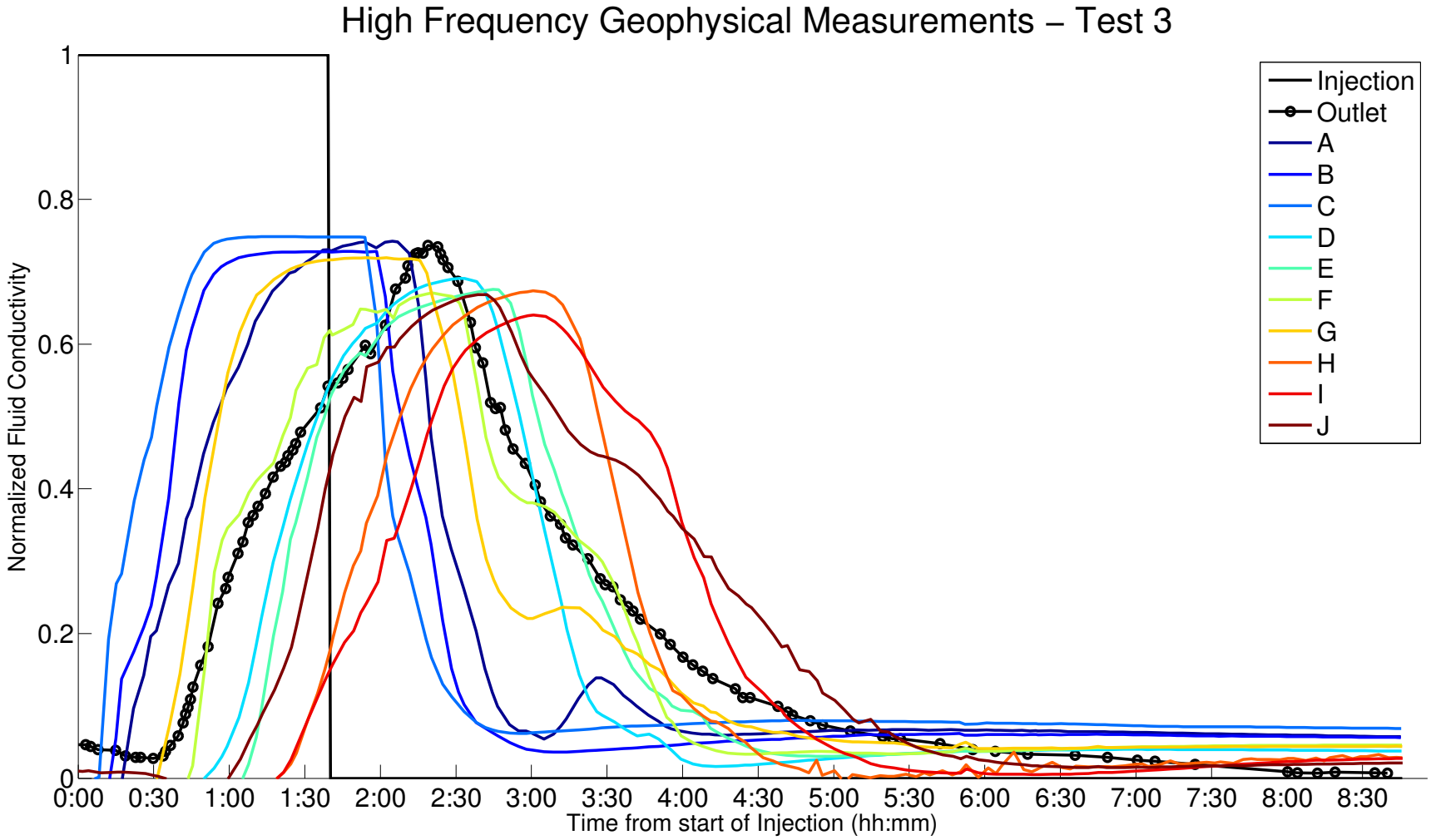

Figure B.18: Fluid Conductivity Measurements at all Wells for 0.55 g/L, High Frequency Geophysical Measurements, 25 Injection Ports (Test16)

Well	**Mean Arrival Time (s)**	**Variance (s^2)**	**Skew**	**Kurtosis**	**Semi-invariant m3**	**Semi-invariant m2**	**Semi-invariant m1**	**Semi-invariant m0**
A	9720	7470	1.7	0.36	1.52E+13	7.28E+08	4.71E+04	4.85
B	9080	7760	1.81	0.74	1.47E+13	6.82E+08	4.34E+04	4.77
C	8990	8010	1.81	0.72	1.60E+13	7.36E+08	4.56E+04	5.08
D	10800	6490	1.54	-0.16	1.28E+13	6.62E+08	4.50E+04	4.17
E	11360	6440	1.47	-0.42	1.48E+13	7.71E+08	5.13E+04	4.52
F	10400	6480	1.56	-0.07	1.37E+13	7.15E+08	4.96E+04	4.77
G	9880	6820	1.62	0.14	1.52E+13	7.77E+08	5.33E+04	5.39
H	11540	5350	1.36	-0.73	1.08E+13	6.25E+08	4.46E+04	3.86
I	12090	4810	1.27	-1.08	1.13E+13	6.86E+08	4.90E+04	4.05
J	11440	5060	1.3	-1.02	1.26E+13	7.74E+08	5.66E+04	4.95

Table B.9: Temporal Moments - 0.55 g/L, High Frequency Geophysical Measurements, 25 Injection Ports - (Test16)

B.6 0.25 g/L, Mid-Range Frequency Geophysical Measurements, 25 Injection Ports

Experimental values include: 0.25 g/L, Mid-Range Frequency Geophysical Measurements, 25 Injection Ports, this test is labeled Test12 in the data folder. Results for bulk conductivity are displayed in B.19, fluid conductivity in B.20, and temporal moments in B.10.

B.6.1 Test 1

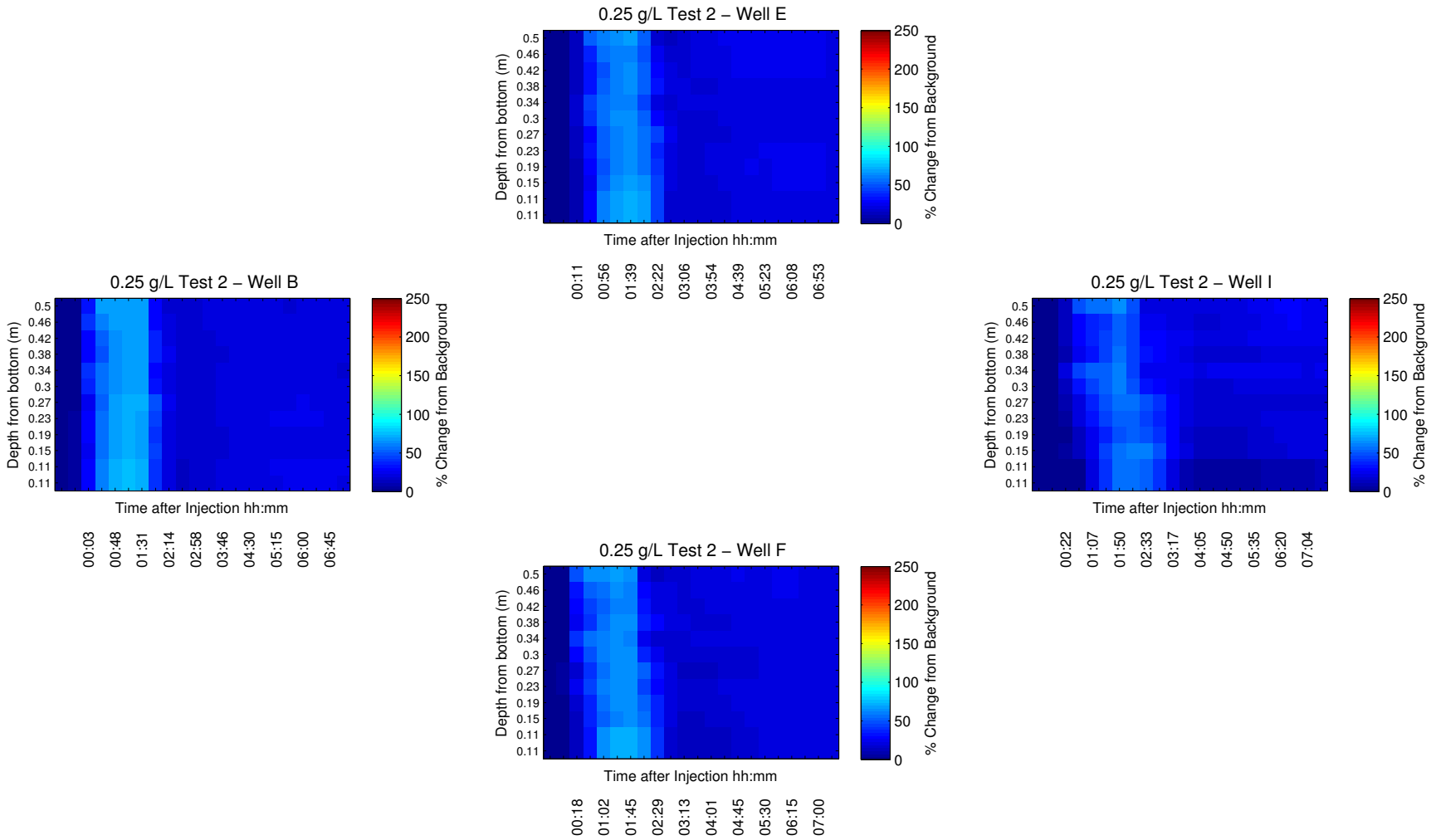

Figure B.19: Downwell Bulk Conductivity Measurements for 0.25 g/L, Mid-Range Frequency Geophysical Measurements, 25 Injection Ports (Test12)

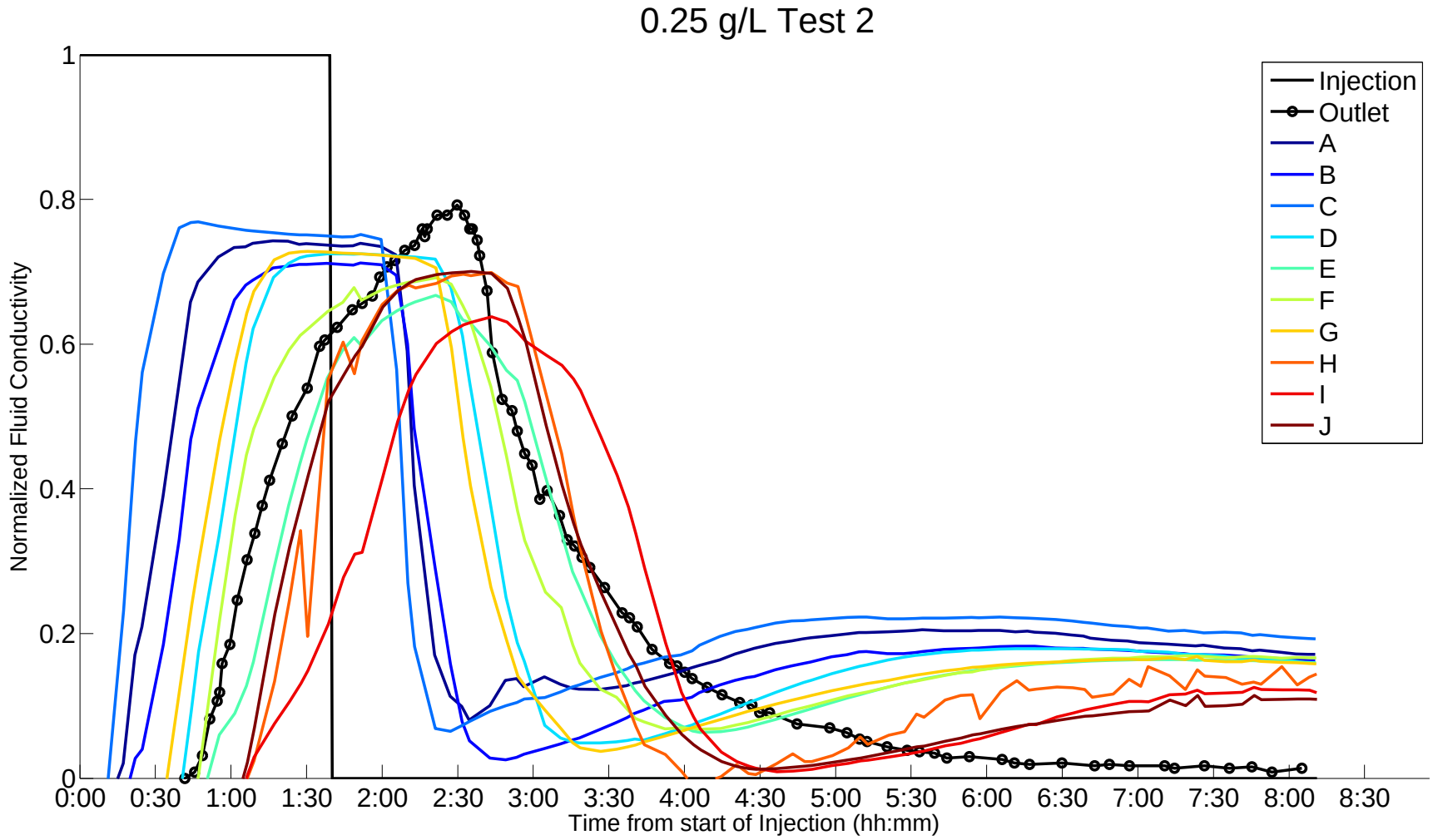

Figure B.20: Fluid Conductivity Measurements at all Wells for 0.25 g/L, Mid-Range Frequency Geophysical Measurements, 25 Injection Ports (Test12)

Well	**Mean Arrival Time (s)**	**Variance (s^2)**	**Skew**	**Kurtosis**	**Semi-invariant m3**	**Semi-invariant m2**	**Semi-invariant m1**	**Semi-invariant m0**
A	12280	8550	1.45	-0.71	8.73E+13	4.01E+09	2.20E+05	17.92
B	12720	8610	1.43	-0.78	8.74E+13	3.97E+09	2.14E+05	16.84
C	12120	8790	1.47	-0.68	9.51E+13	4.33E+09	2.34E+05	19.33
D	12900	8120	1.42	-0.8	8.19E+13	3.79E+09	2.10E+05	16.28
E	13840	7670	1.35	-0.99	8.50E+13	3.97E+09	2.19E+05	15.85
F	13180	7930	1.4	-0.85	8.34E+13	3.87E+09	2.16E+05	16.36
G	12510	8240	1.45	-0.7	7.90E+13	3.64E+09	2.03E+05	16.2
H	13500	7500	1.37	-0.91	7.18E+13	3.38E+09	1.92E+05	14.19
I	13740	7060	1.34	-0.99	6.37E+13	3.08E+09	1.77E+05	12.9
J	12920	7190	1.39	-0.81	6.35E+13	3.08E+09	1.82E+05	14.08

Table B.10: Temporal Moments - 0.25 g/L, Mid-Range Frequency Geophysical Measurements, 25 Injection Ports - (Test12)

B.6.2 Test 2

Experimental values include: 0.25 g/L, Mid-Range Frequency Geophysical Measurements, 25 Injection Ports, this test is labeled Test13 in the data folder. Results for bulk conductivity are displayed in B.21, fluid conductivity in B.22, and temporal moments in B.11.

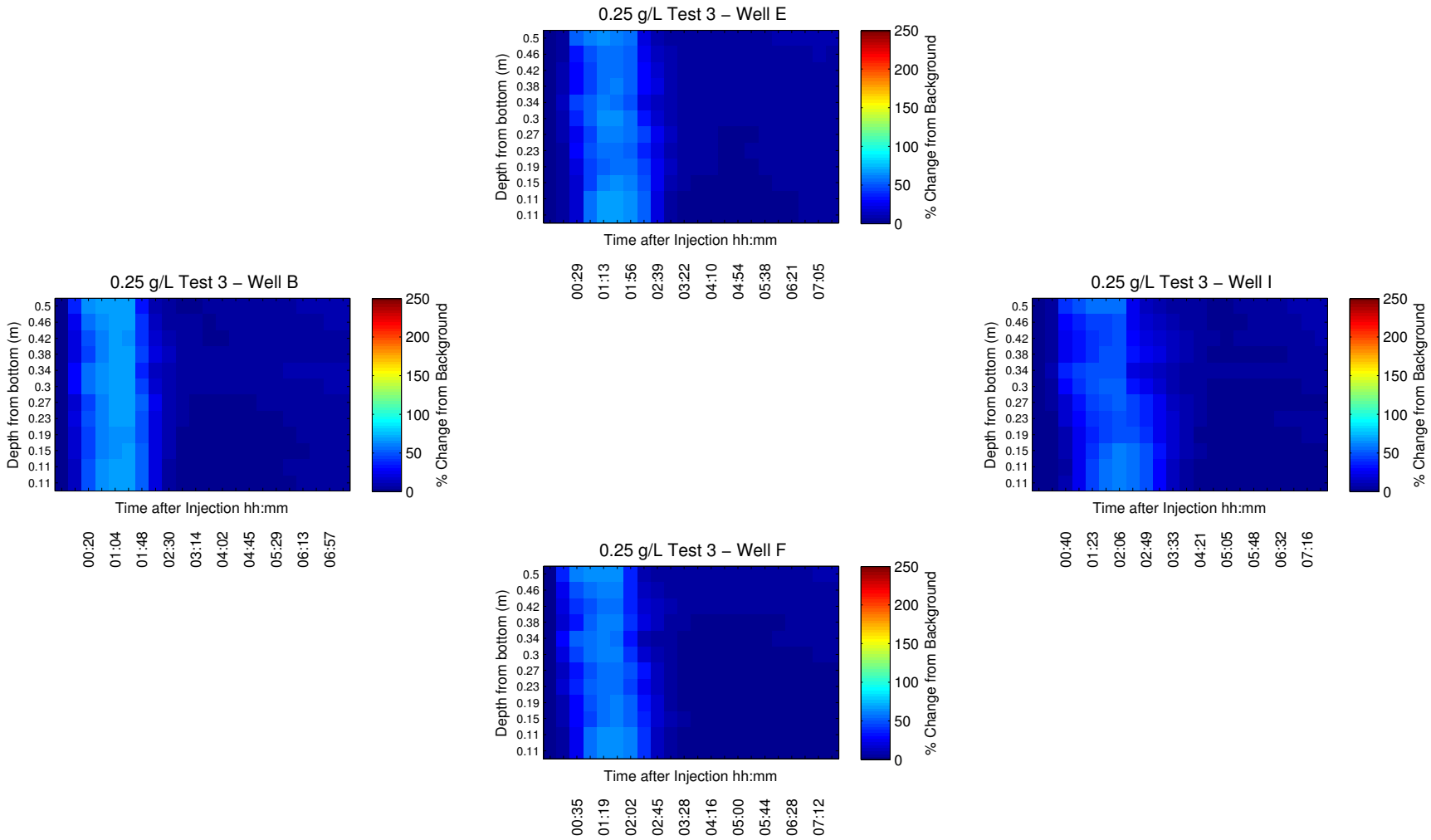

Figure B.21: Downwell Bulk Conductivity Measurements for 0.25 g/L, Mid-Range Frequency Geophysical Measurements, 25 Injection Ports (Test13)

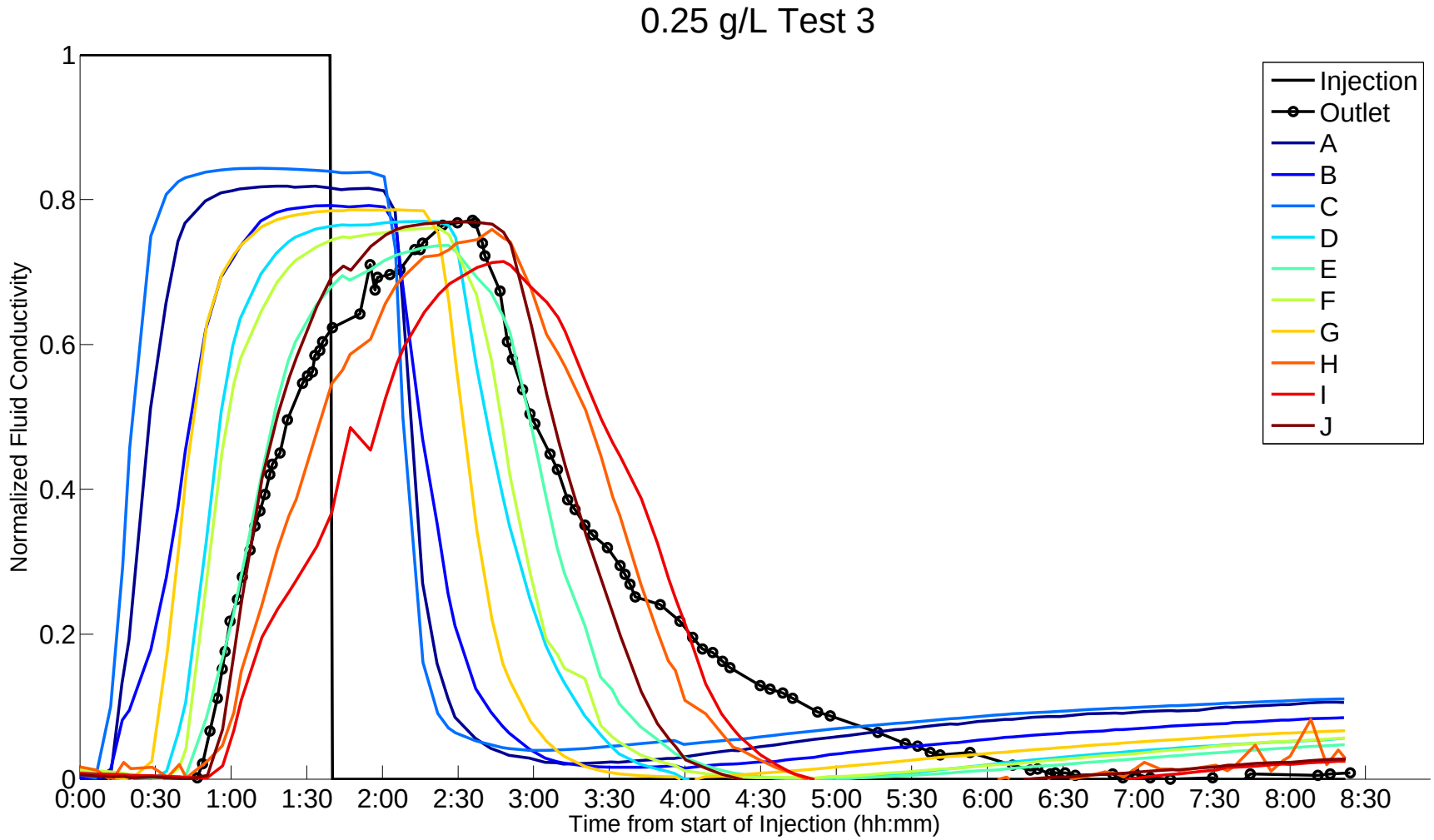

Figure B.22: Fluid Conductivity Measurements at all Wells for 0.25 g/L, Mid-Range Frequency Geophysical Measurements, 25 Injection Ports (Test13)

Well	**Mean Arrival Time (s)**	**Variance (s^2)**	**Skew**	**Kurtosis**	**Semi-invariant m3**	**Semi-invariant m2**	**Semi-invariant m1**	**Semi-invariant m0**
A	8440	7690	1.89	1.08	3.33E+13	1.54E+09	9.97E+04	11.82
B	8320	7060	1.9	1.25	2.55E+13	1.23E+09	8.58E+04	10.31
C	8290	7750	1.9	1.11	3.52E+13	1.63E+09	1.05E+05	12.66
D	8290	5550	1.76	0.97	1.87E+13	1.06E+09	8.86E+04	10.68
E	8900	4850	1.55	0.16	1.60E+13	1.01E+09	8.77E+04	9.85
F	8290	5170	1.7	0.82	1.63E+13	9.82E+08	8.53E+04	10.29
G	8040	6160	1.88	1.39	2.12E+13	1.11E+09	8.71E+04	10.84
H	10270	5640	1.45	-0.41	2.92E+13	1.72E+09	1.28E+05	12.5
I	10130	4320	1.31	-0.89	1.81E+13	1.26E+09	1.05E+05	10.39
J	8920	4230	1.43	-0.31	1.48E+13	1.05E+09	9.62E+04	10.79

Table B.11: Temporal Moments - 0.25 g/L, Mid-Range Frequency Geophysical Measurements, 25 Injection Ports - (Test13)

B.6.3 Test 3

Experimental values include: 0.25 g/L, Mid-Range Frequency Geophysical Measurements, 25 Injection Ports, this test is labeled Test22 in the data folder. Results for bulk conductivity are displayed in B.23, fluid conductivity in B.24, and temporal moments in B.12.

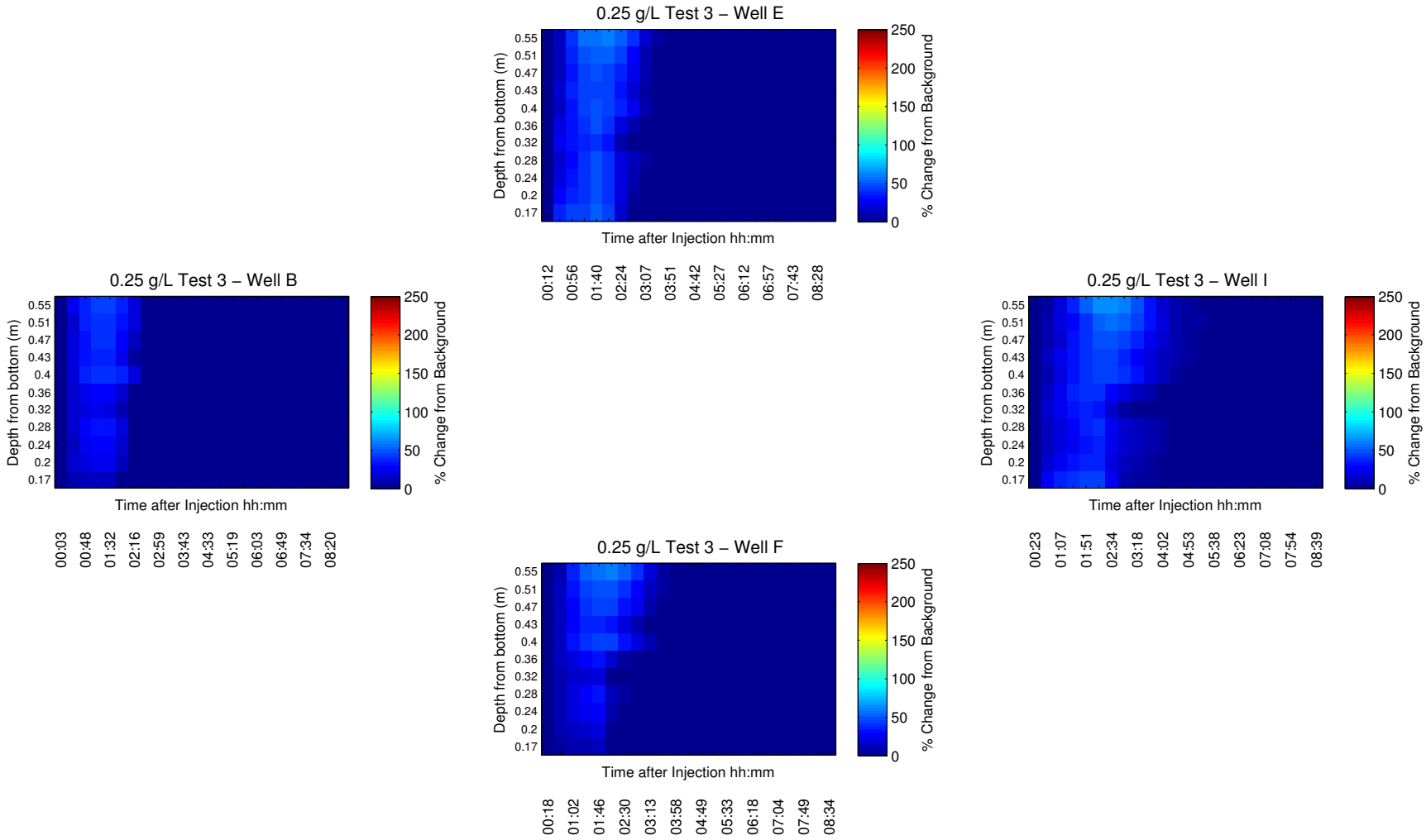

Figure B.23: Downwell Bulk Conductivity Measurements for 0.25 g/L, Mid-Range Frequency Geophysical Measurements, 25 Injection Ports (Test22)

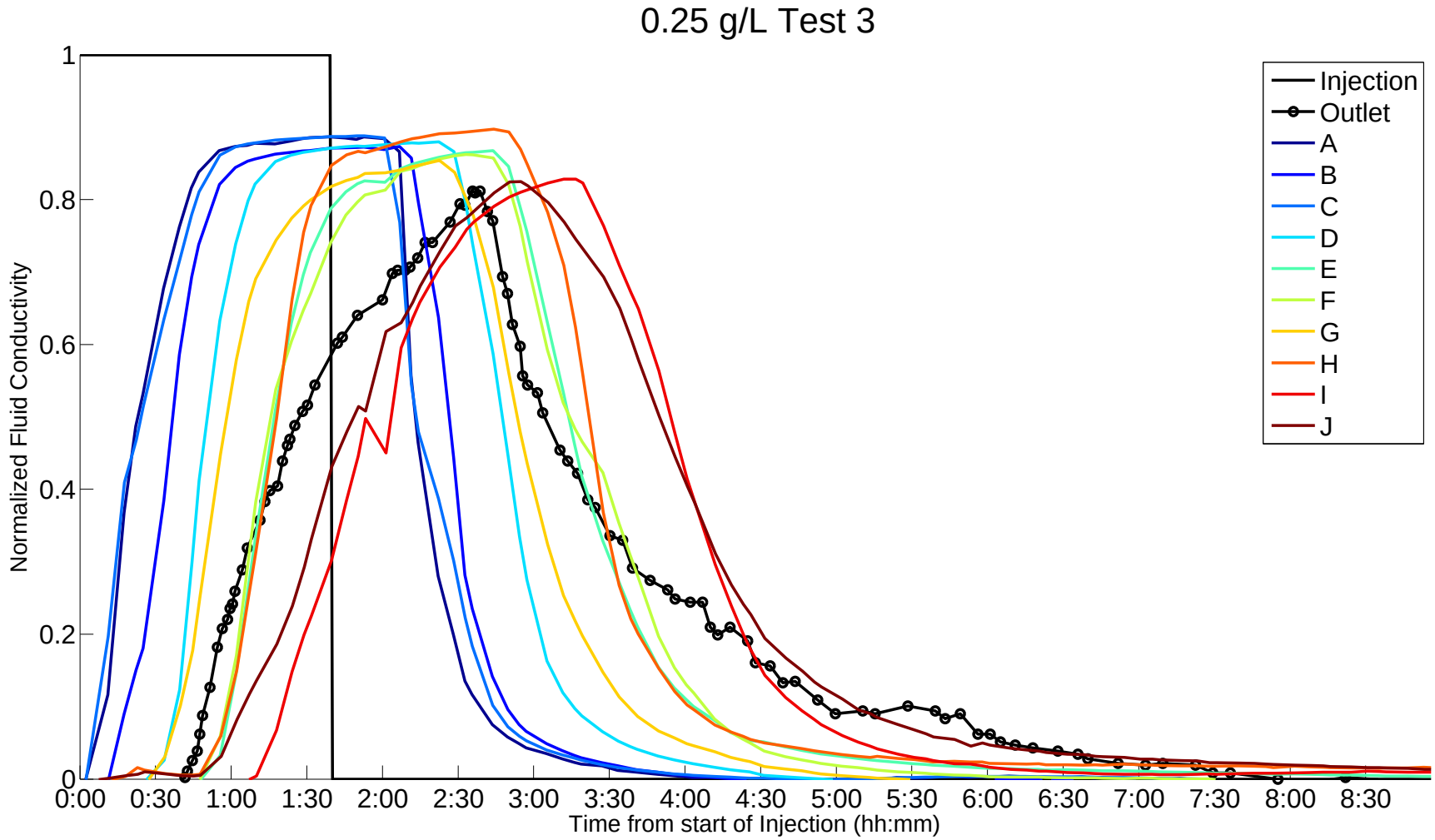

Figure B.24: Fluid Conductivity Measurements at all Wells for 0.25 g/L, Mid-Range Frequency Geophysical Measurements, 25 Injection Ports (Test22)

Well	**Mean Arrival Time (s)**	**Variance (s^2)**	**Skew**	**Kurtosis**	**Semi-invariant m3**	**Semi-invariant m2**	**Semi-invariant m1**	**Semi-invariant m0**
A	5310	3200	1.72	1.57	5.67E+12	5.32E+08	7.35E+04	13.83
B	5900	2890	1.44	-0.07	5.55E+12	5.84E+08	7.98E+04	13.53
C	5340	3050	1.59	0.75	5.16E+12	5.28E+08	7.46E+04	13.97
D	7130	3100	1.34	-0.68	9.15E+12	8.80E+08	1.04E+05	14.58
E	9600	4660	1.44	-0.34	2.74E+13	1.79E+09	1.51E+05	15.69
F	9370	4140	1.36	-0.66	2.28E+13	1.64E+09	1.46E+05	15.6
G	7790	3470	1.35	-0.65	1.22E+13	1.06E+09	1.14E+05	14.6
H	9580	4590	1.43	-0.34	2.82E+13	1.85E+09	1.57E+05	16.44
I	11730	4700	1.29	-0.99	4.07E+13	2.50E+09	1.84E+05	15.66
J	11530	4830	1.29	-1.04	4.14E+13	2.57E+09	1.90E+05	16.47

Table B.12: Temporal Moments - 0.25 g/L, Mid-Range Frequency Geophysical Measurements, 25 Injection Ports - (Test22)

B.7 0.75 g/L, Mid-Range Frequency Geophysical Measurements, 25 Injection Ports

Experimental values include: 0.75 g/L, Mid-Range Frequency Geophysical Measurements, 25 Injection Ports, this test is labeled Test05 in the data folder. Results for bulk conductivity are displayed in B.25, fluid conductivity in B.26, and temporal moments in B.13.

B.7.1 Test 1

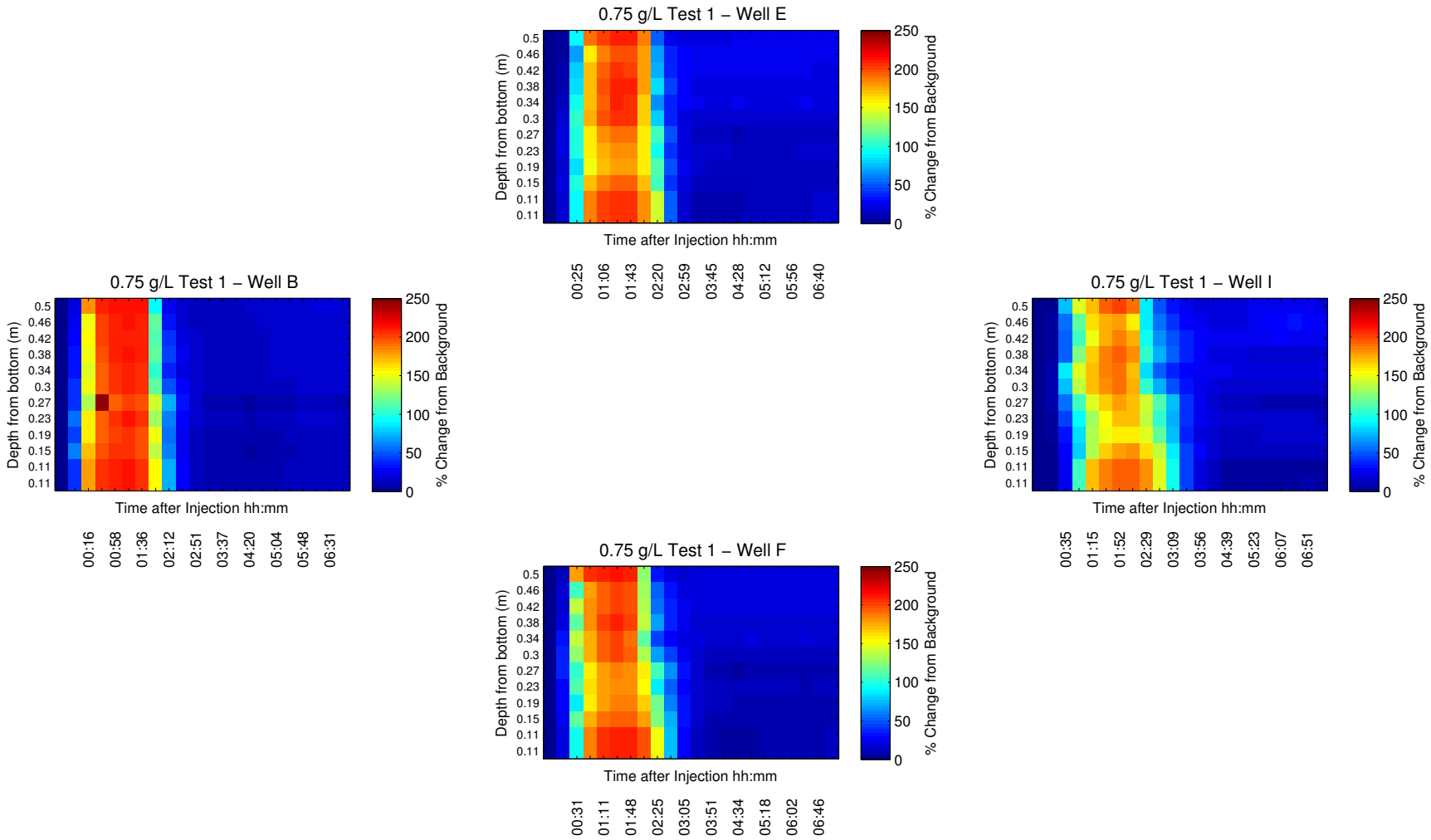

Figure B.25: Downwell Bulk Conductivity Measurements for 0.75 g/L, Mid-Range Frequency Geophysical Measurements, 25 Injection Ports (Test05)

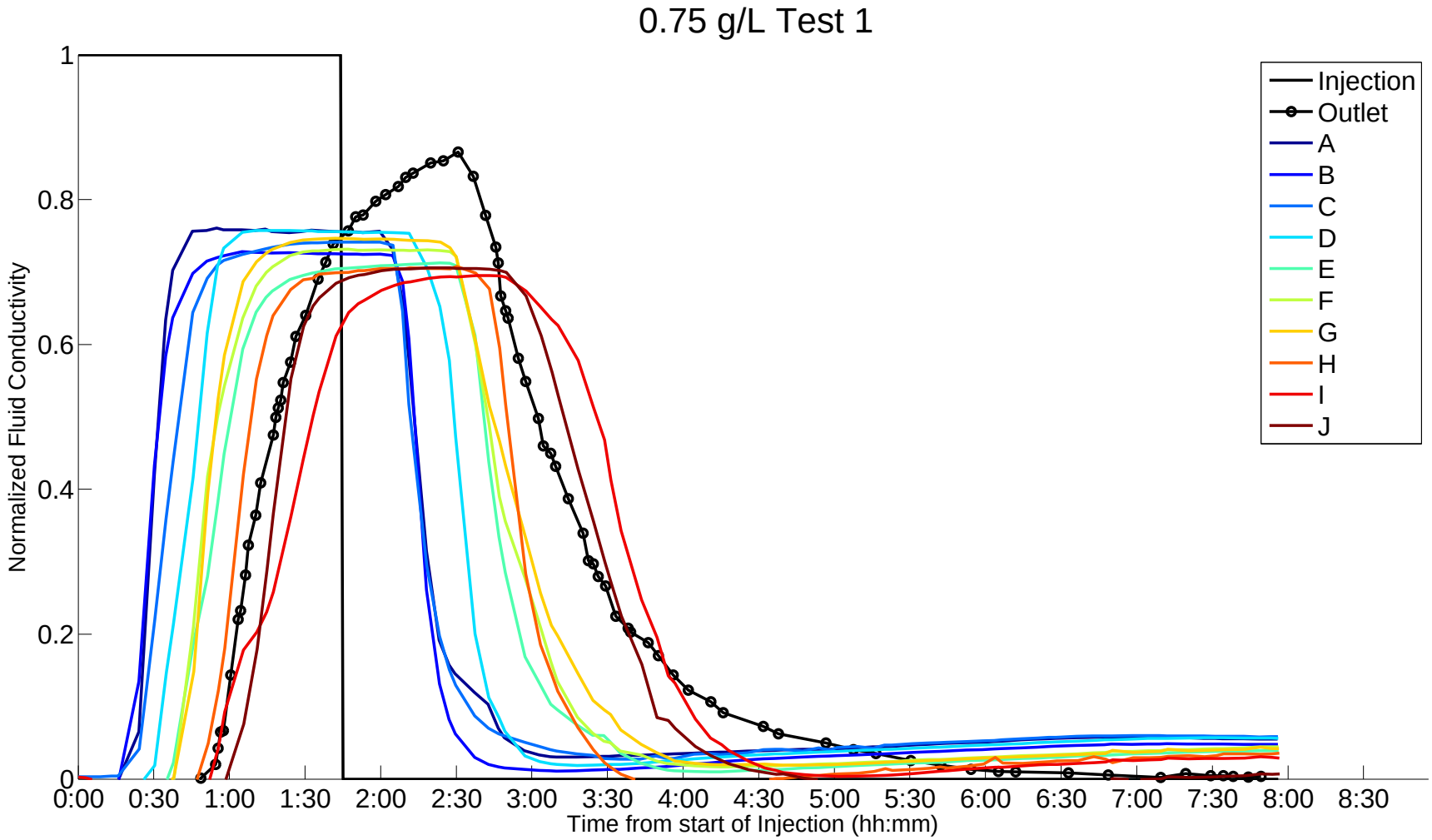

Figure B.26: Fluid Conductivity Measurements at all Wells for 0.75 g/L, Mid-Range Frequency Geophysical Measurements, 25 Injection Ports (Test05)

Well	**Mean Arrival Time (s)**	**Variance (s^2)**	**Skew**	**Kurtosis**	**Semi-invariant m3**	**Semi-invariant m2**	**Semi-invariant m1**	**Semi-invariant m0**
A	8030	6600	1.83	0.92	7.73E+12	4.07E+08	3.03E+04	3.77
B	7860	6620	1.86	1.08	7.18E+12	3.74E+08	2.79E+04	3.54
C	7910	6390	1.84	1.05	6.37E+12	3.40E+08	2.60E+04	3.29
D	8480	6270	1.75	0.65	7.44E+12	4.04E+08	3.08E+04	3.64
E	8930	5770	1.63	0.24	7.02E+12	4.05E+08	3.20E+04	3.58
F	8760	5590	1.63	0.27	6.81E+12	4.03E+08	3.27E+04	3.73
G	8580	5250	1.61	0.23	6.17E+12	3.82E+08	3.24E+04	3.77
H	9080	5430	1.58	0.11	6.34E+12	3.78E+08	3.07E+04	3.38
I	10100	4730	1.36	-0.75	7.11E+12	4.68E+08	3.80E+04	3.76
J	9320	3930	1.32	-0.86	4.82E+12	3.61E+08	3.29E+04	3.53

Table B.13: Temporal Moments - 0.75 g/L, Mid-Range Frequency Geophysical Measurements, 25 Injection Ports - (Test05)

B.7.2 Test 2

Experimental values include: 0.75 g/L, Mid-Range Frequency Geophysical Measurements, 25 Injection Ports, this test is labeled Test20 in the data folder. Results for bulk conductivity are displayed in B.27, fluid conductivity in B.28, and temporal moments in B.14.

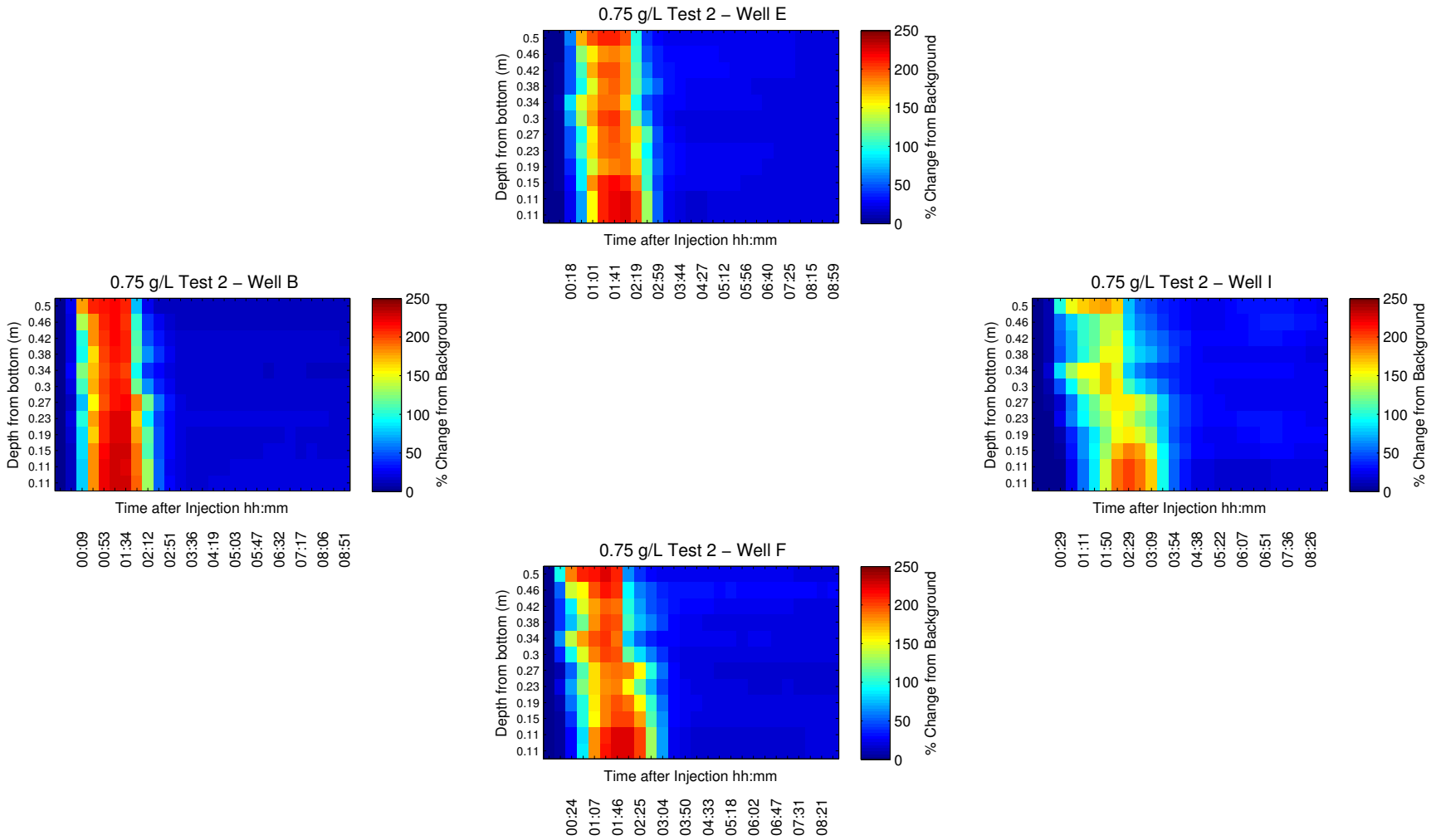

Figure B.27: Downwell Bulk Conductivity Measurements for 0.75 g/L, Mid-Range Frequency Geophysical Measurements, 25 Injection Ports (Test20)

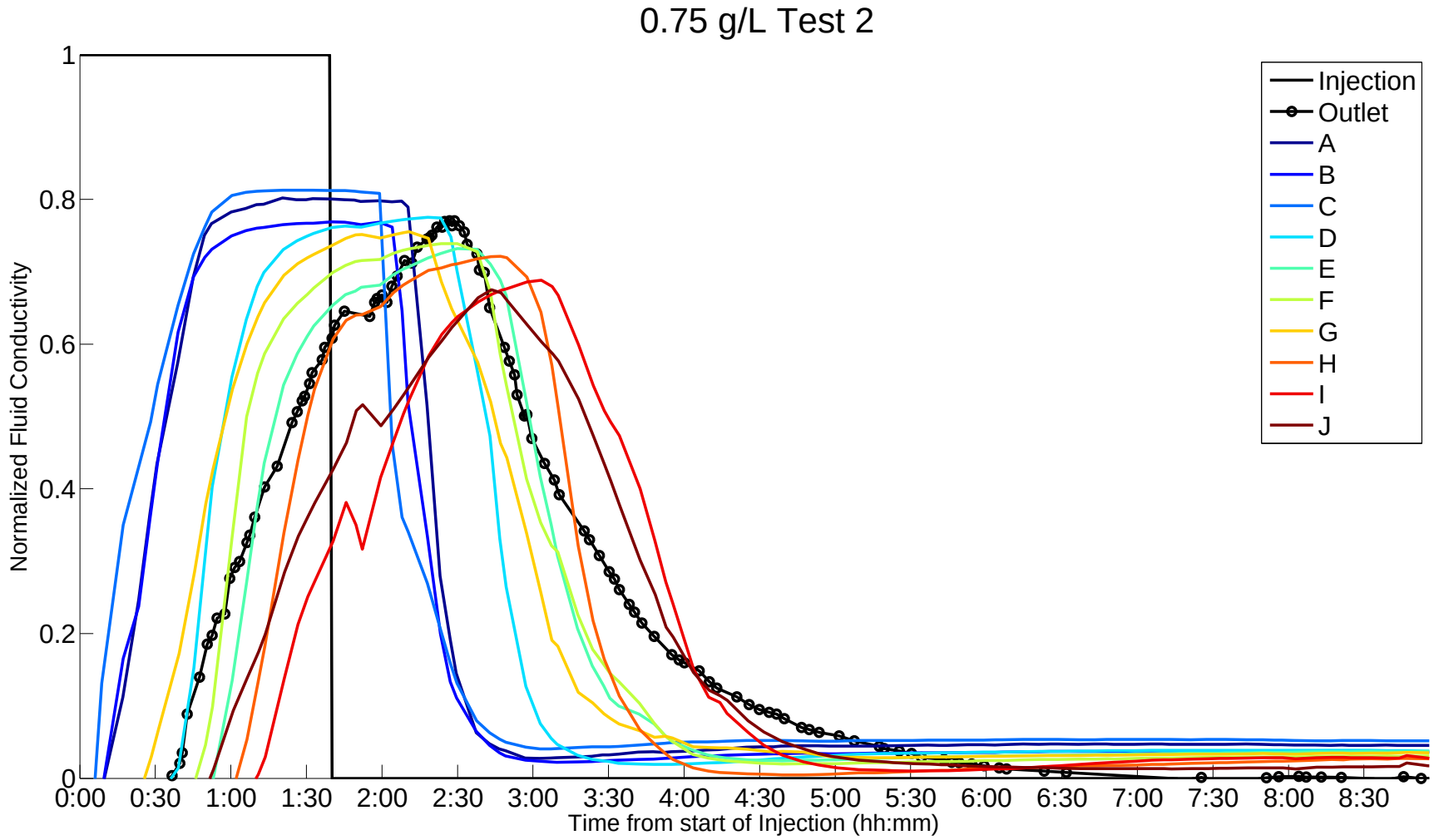

Figure B.28: Fluid Conductivity Measurements at all Wells for 0.75 g/L, Mid-Range Frequency Geophysical Measurements, 25 Injection Ports (Test20)

Well	**Mean Arrival Time (s)**	**Variance (s^2)**	**Skew**	**Kurtosis**	**Semi-invariant m3**	**Semi-invariant m2**	**Semi-invariant m1**	**Semi-invariant m0**
A	9700	8690	1.85	0.88	1.82E+13	7.58E+08	4.34E+04	4.47
B	9600	8750	1.86	0.94	1.73E+13	7.17E+08	4.08E+04	4.25
C	9500	8920	1.87	0.94	1.85E+13	7.60E+08	4.26E+04	4.48
D	10500	8040	1.74	0.54	1.65E+13	7.19E+08	4.31E+04	4.11
E	11730	7810	1.6	0	1.85E+13	8.23E+08	4.86E+04	4.14
F	11090	7650	1.65	0.22	1.74E+13	7.84E+08	4.79E+04	4.32
G	10440	7790	1.72	0.5	1.67E+13	7.44E+08	4.58E+04	4.38
H	11710	7390	1.58	-0.01	1.62E+13	7.39E+08	4.51E+04	3.85
I	12850	7000	1.45	-0.51	1.74E+13	8.22E+08	4.93E+04	3.84
J	11980	6730	1.48	-0.35	1.50E+13	7.35E+08	4.66E+04	3.89

Table B.14: Temporal Moments - 0.75 g/L, Mid-Range Frequency Geophysical Measurements, 25 Injection Ports - (Test20)

B.7.3 Test 3

Experimental values include: 0.75 g/L, Mid-Range Frequency Geophysical Measurements, 25 Injection Ports, this test is labeled Test21 in the data folder. Results for bulk conductivity are displayed in B.29, fluid conductivity in B.30, and temporal moments in B.15.

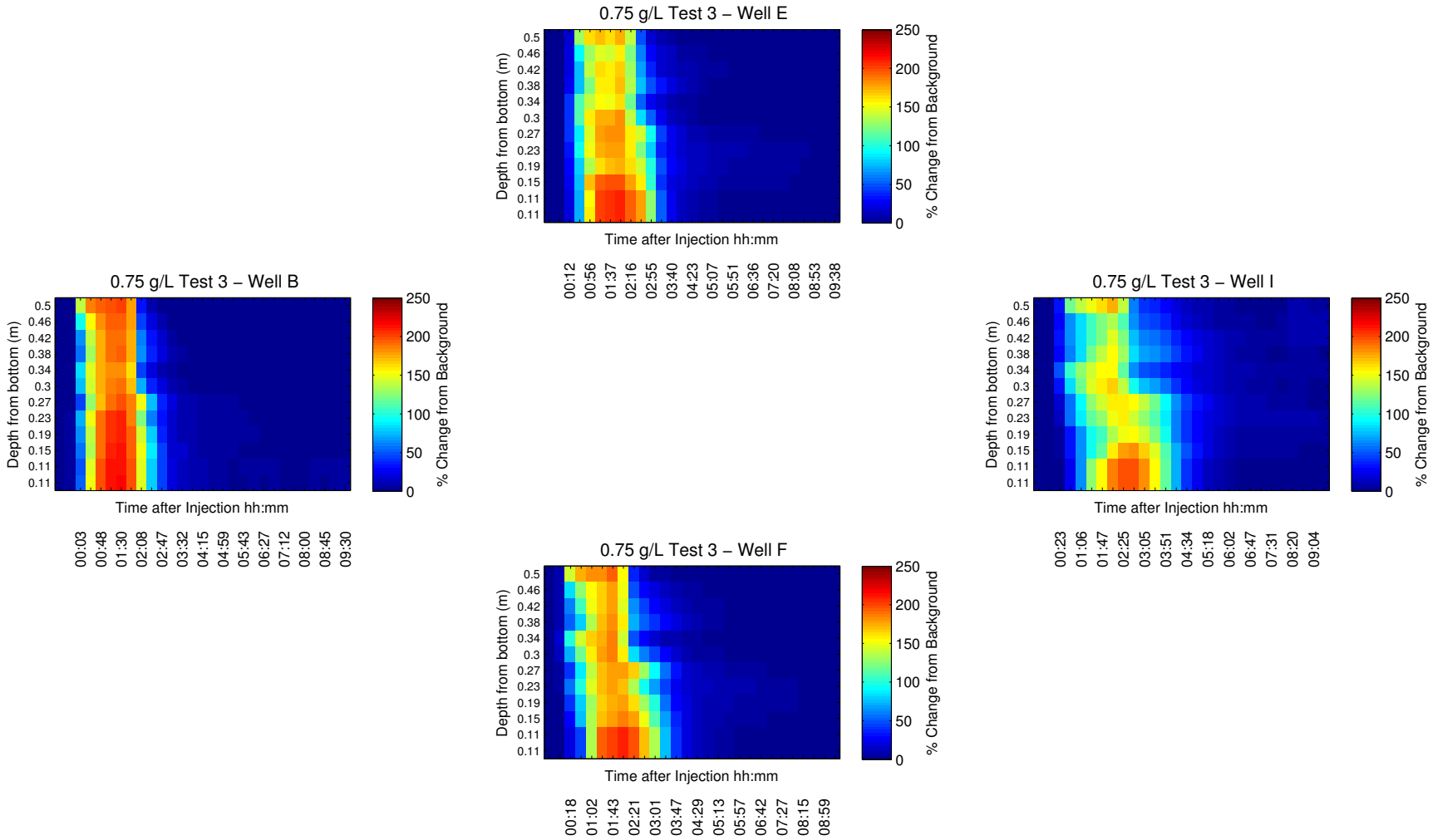

Figure B.29: Downwell Bulk Conductivity Measurements for 0.75 g/L, Mid-Range Frequency Geophysical Measurements, 25 Injection Ports (Test21)

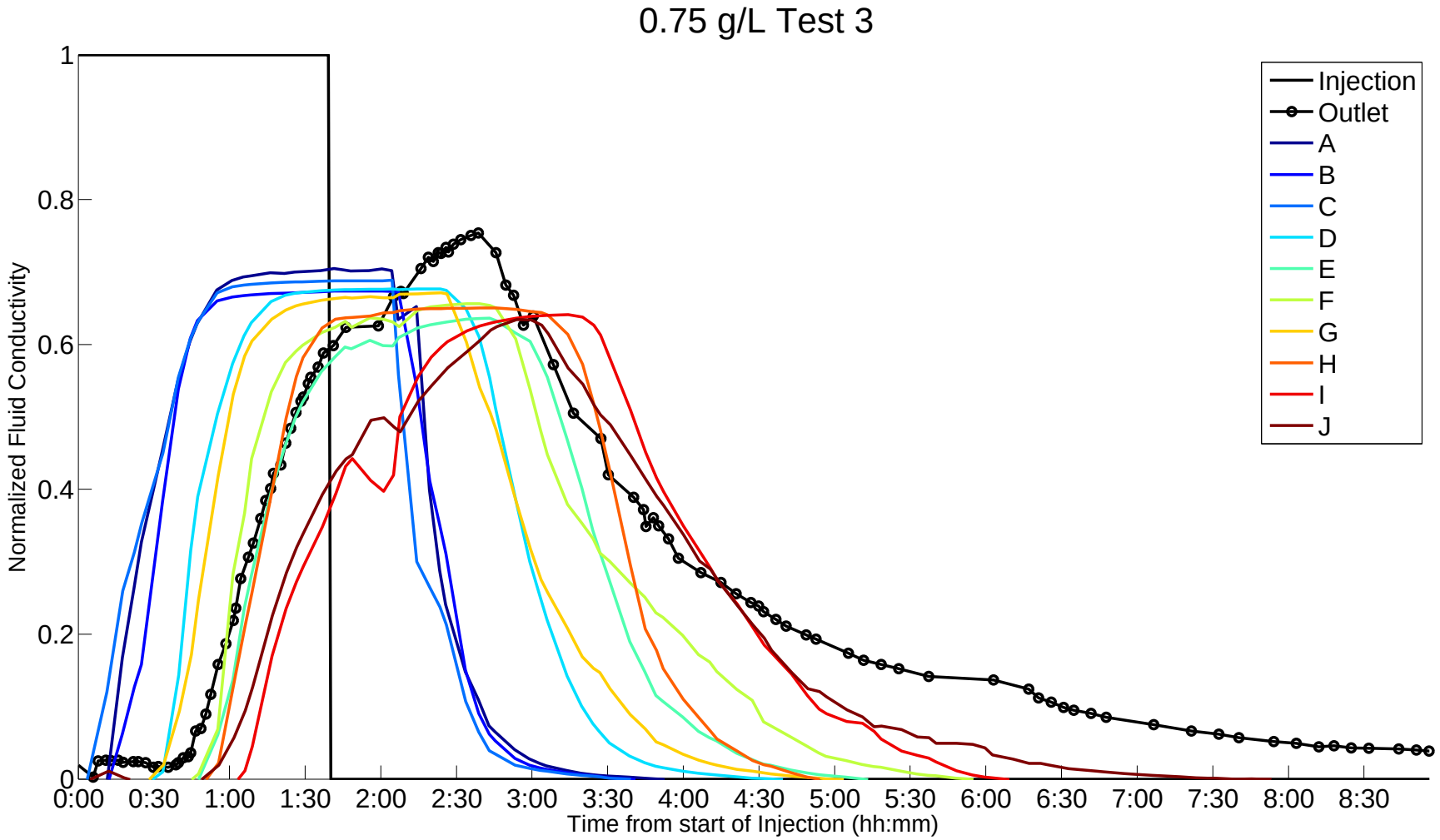

Figure B.30: Fluid Conductivity Measurements at all Wells for 0.75 g/L, Mid-Range Frequency Geophysical Measurements, 25 Injection Ports (Test21)

Well	**Mean Arrival Time (s)**	**Variance (s^2)**	**Skew**	**Kurtosis**	**Semi-invariant m3**	**Semi-invariant m2**	**Semi-invariant m1**	**Semi-invariant m0**
A	6110	4660	2.2	4.12	2.99E+12	1.77E+08	1.83E+04	3
B	6210	4600	2.16	3.92	2.83E+12	1.70E+08	1.76E+04	2.84
C	5770	4510	2.26	4.68	2.54E+12	1.53E+08	1.65E+04	2.86
D	7320	3560	1.47	0.11	2.55E+12	2.13E+08	2.35E+04	3.21
E	9340	4370	1.41	-0.36	5.04E+12	3.46E+08	3.04E+04	3.25
F	9380	4320	1.36	-0.66	5.38E+12	3.83E+08	3.36E+04	3.59
G	7750	3890	1.49	0.15	3.11E+12	2.40E+08	2.48E+04	3.19
H	9130	3360	1.22	-1.25	3.88E+12	3.28E+08	3.17E+04	3.47
I	11070	4000	1.21	-1.31	6.90E+12	4.85E+08	3.88E+04	3.5
J	11090	4390	1.23	-1.3	7.43E+12	5.08E+08	3.96E+04	3.57

Table B.15: Temporal Moments - 0.75 g/L, Mid-Range Frequency Geophysical Measurements, 25 Injection Ports - (Test21)

B.8 0.55 g/L, Mid-Range Frequency Geophysical Measurements, 9 Injection Ports

Experimental values include: 0.55 g/L, Mid-Range Frequency Geophysical Measurements, 9 Injection Ports, this test is labeled Test06 in the data folder. Results for bulk conductivity are displayed in B.31, fluid conductivity in B.32, and temporal moments in B.16.

B.8.1 Test 1

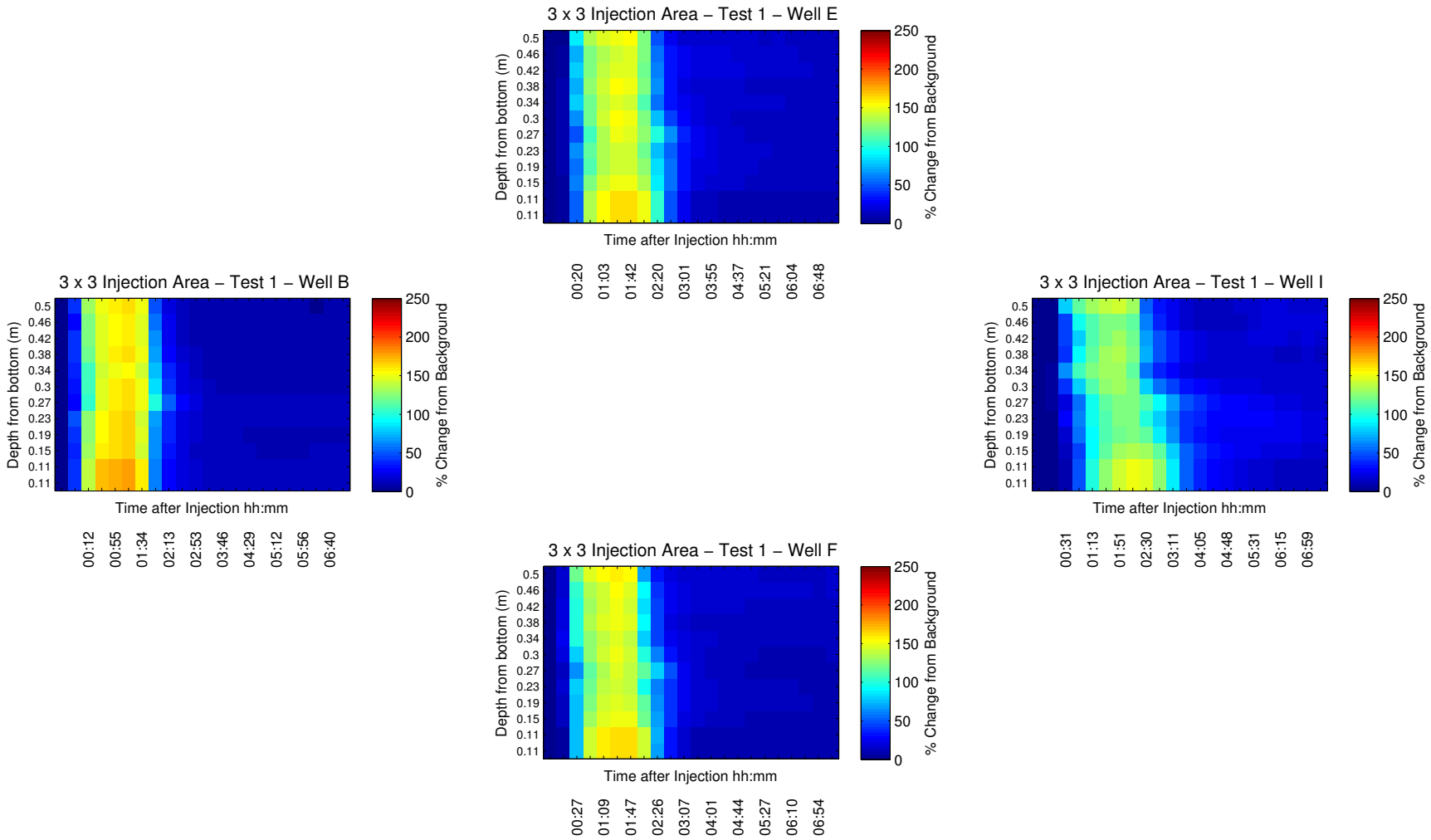

Figure B.31: Downwell Bulk Conductivity Measurements for 0.55 g/L, Mid-Range Frequency Geophysical Measurements, 9 Injection Ports (Test06)

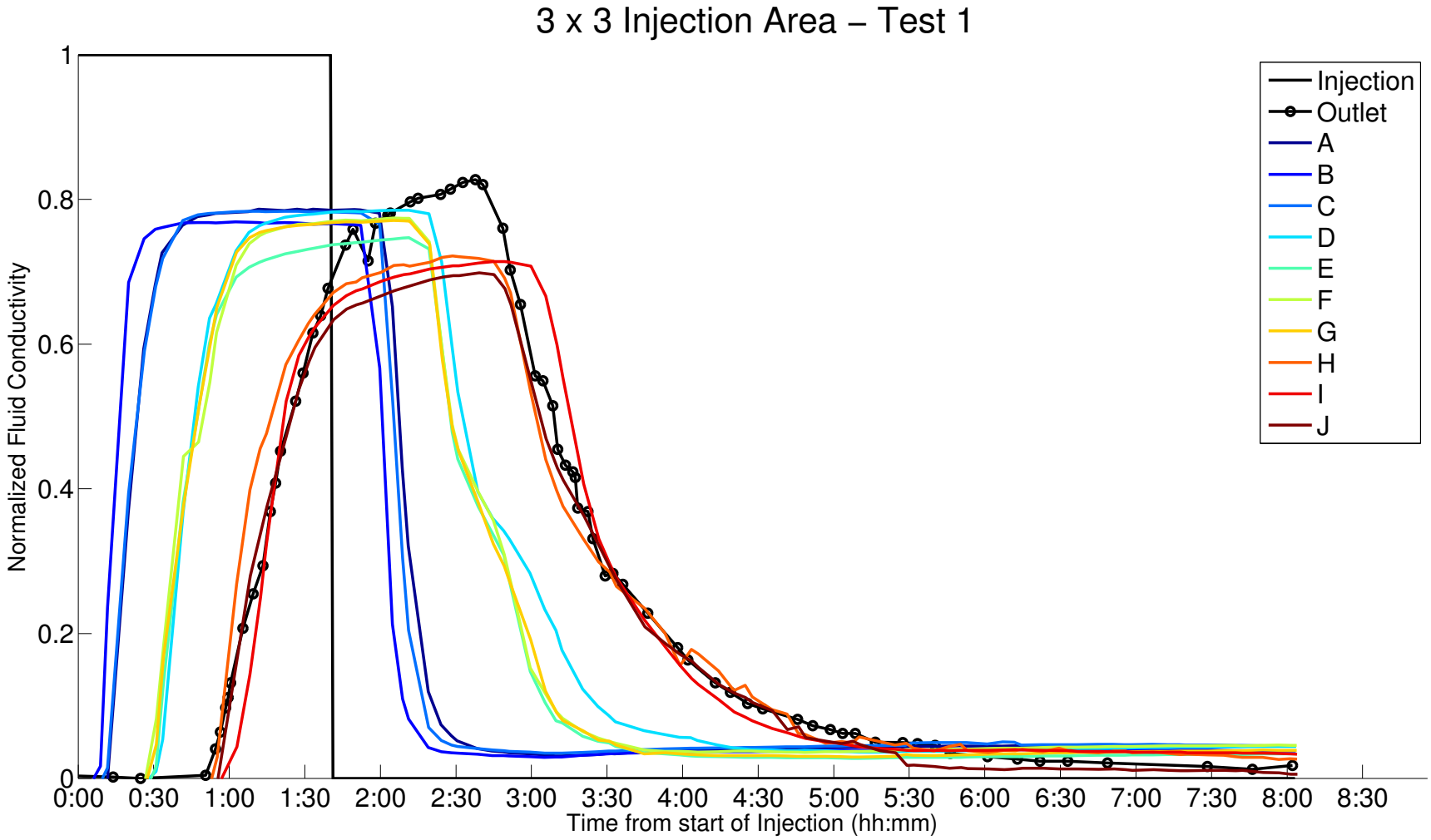

Figure B.32: Fluid Conductivity Measurements at all Wells for 0.55 g/L, Mid-Range Frequency Geophysical Measurements, 9 Injection Ports (Test06)

Well	**Mean Arrival Time (s)**	**Variance (s^2)**	**Skew**	**Kurtosis**	**Semi-invariant m3**	**Semi-invariant m2**	**Semi-invariant m1**	**Semi-invariant m0**
A	7310	6470	1.94	1.47	9.19E+12	4.85E+08	3.72E+04	5.09
B	7010	6630	2	1.7	9.02E+12	4.67E+08	3.52E+04	5.02
C	7370	6600	1.94	1.42	9.45E+12	4.93E+08	3.71E+04	5.04
D	8400	5520	1.66	0.41	9.07E+12	5.44E+08	4.52E+04	5.39
E	8410	5790	1.69	0.52	9.18E+12	5.30E+08	4.28E+04	5.09
F	8380	5810	1.71	0.57	9.36E+12	5.38E+08	4.33E+04	5.17
G	8290	5700	1.71	0.59	8.95E+12	5.22E+08	4.28E+04	5.16
H	10430	5490	1.41	-0.65	1.32E+13	7.94E+08	5.96E+04	5.72
I	10500	5080	1.37	-0.74	1.16E+13	7.24E+08	5.59E+04	5.32
J	10400	5090	1.37	-0.77	1.15E+13	7.24E+08	5.62E+04	5.4

Table B.16: Temporal Moments - 0.55 g/L, Mid-Range Frequency Geophysical Measurements, 9 Injection Ports - (Test06)

B.8.2 Test 2

Experimental values include: 0.55 g/L, Mid-Range Frequency Geophysical Measurements, 9 Injection Ports, this test is labeled Test07 in the data folder. Results for bulk conductivity are displayed in B.33, fluid conductivity in B.34, and temporal moments in B.17.

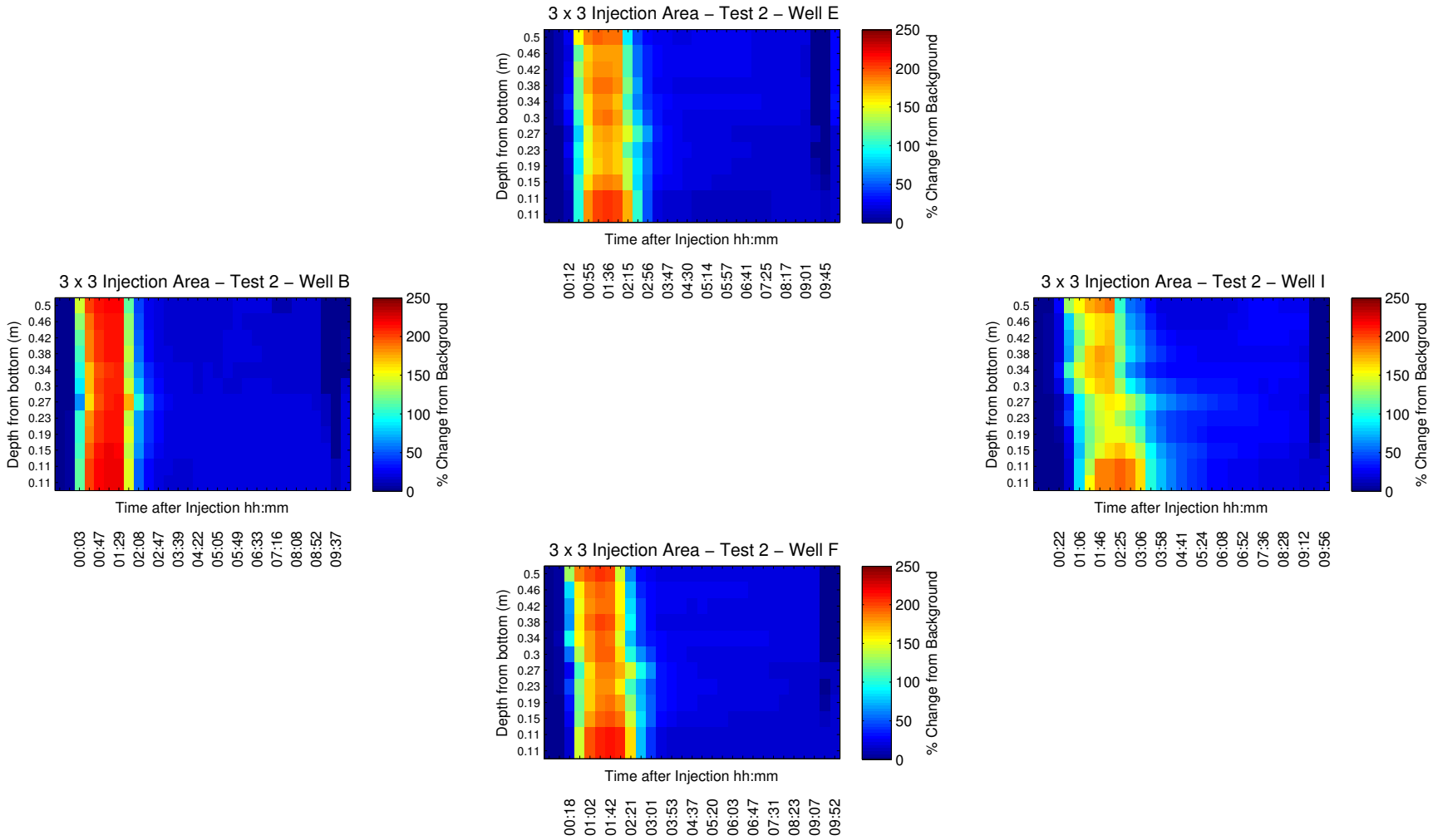

Figure B.33: Downwell Bulk Conductivity Measurements for 0.55 g/L, Mid-Range Frequency Geophysical Measurements, 9 Injection Ports (Test07)

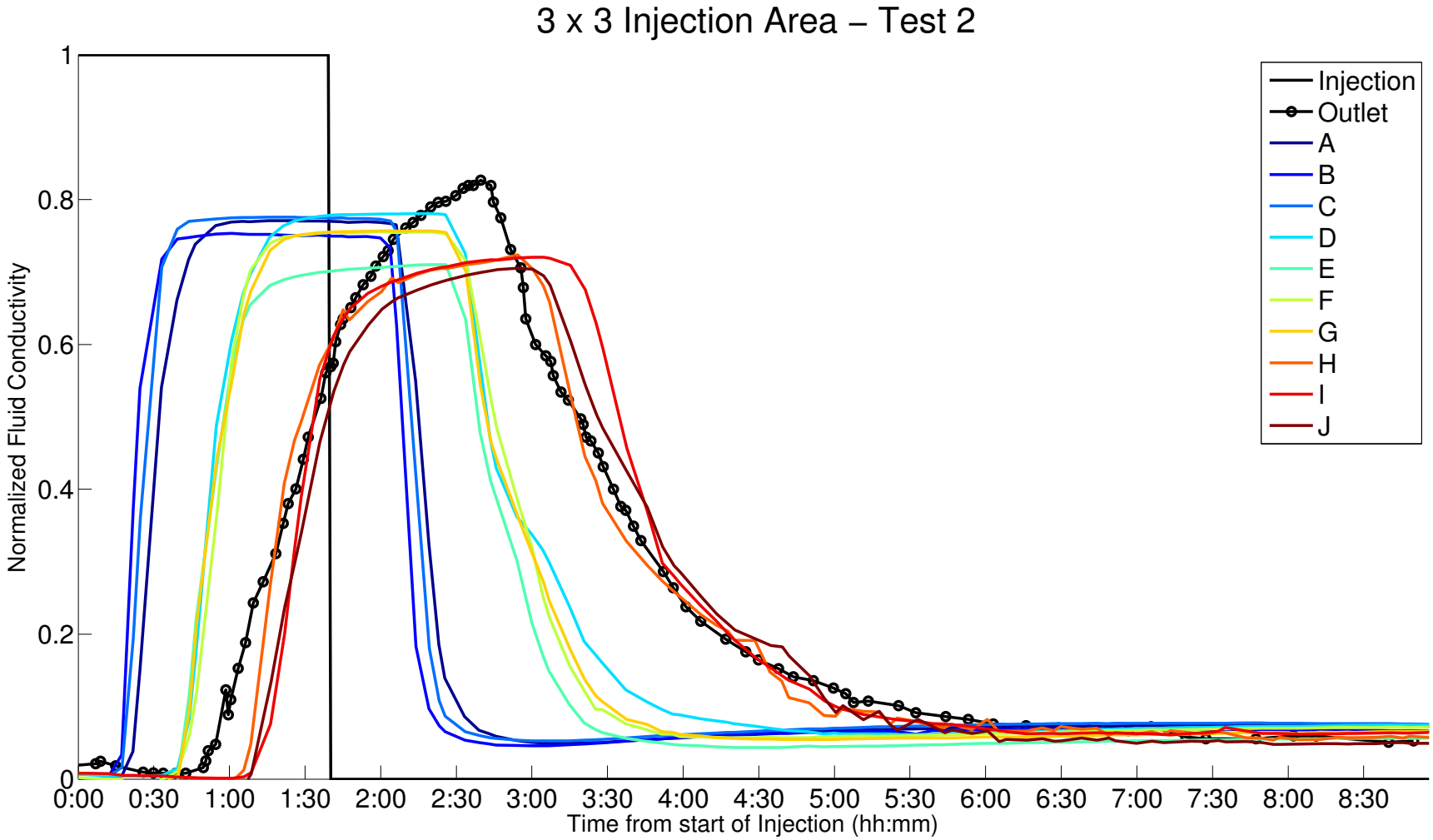

Figure B.34: Fluid Conductivity Measurements at all Wells for 0.55 g/L, Mid-Range Frequency Geophysical Measurements, 9 Injection Ports (Test07)

Well	**Mean Arrival Time (s)**	**Variance (s^2)**	**Skew**	**Kurtosis**	**Semi-invariant m3**	**Semi-invariant m2**	**Semi-invariant m1**	**Semi-invariant m0**
A	11380	10400	1.79	0.56	4.01E+13	1.46E+09	6.97E+04	6.12
B	10350	10040	1.89	0.98	3.14E+13	1.16E+09	5.75E+04	5.56
C	11130	10370	1.8	0.62	3.95E+13	1.44E+09	6.93E+04	6.23
D	11610	9040	1.73	0.49	3.47E+13	1.36E+09	7.29E+04	6.28
E	15860	11560	1.46	-0.7	1.74E+14	6.10E+09	2.51E+05	15.83
F	11530	9010	1.75	0.58	3.15E+13	1.23E+09	6.62E+04	5.74
G	15670	11420	1.46	-0.67	1.74E+14	6.13E+09	2.56E+05	16.3
H	16300	10970	1.42	-0.79	1.80E+14	6.46E+09	2.73E+05	16.73
I	13570	8370	1.53	-0.21	3.93E+13	1.61E+09	8.58E+04	6.32
J	21180	12540	1.29	-1.24	4.21E+14	1.32E+10	4.62E+05	21.82

Table B.17: Temporal Moments - 0.55 g/L, Mid-Range Frequency Geophysical Measurements, 9 Injection Ports - (Test07)

B.8.3 Test 3

Experimental values include: 0.55 g/L, Mid-Range Frequency Geophysical Measurements, 9 Injection Ports, this test is labeled Test08 in the data folder. Results for bulk conductivity are displayed in B.35, fluid conductivity in B.36, and temporal moments in B.18.

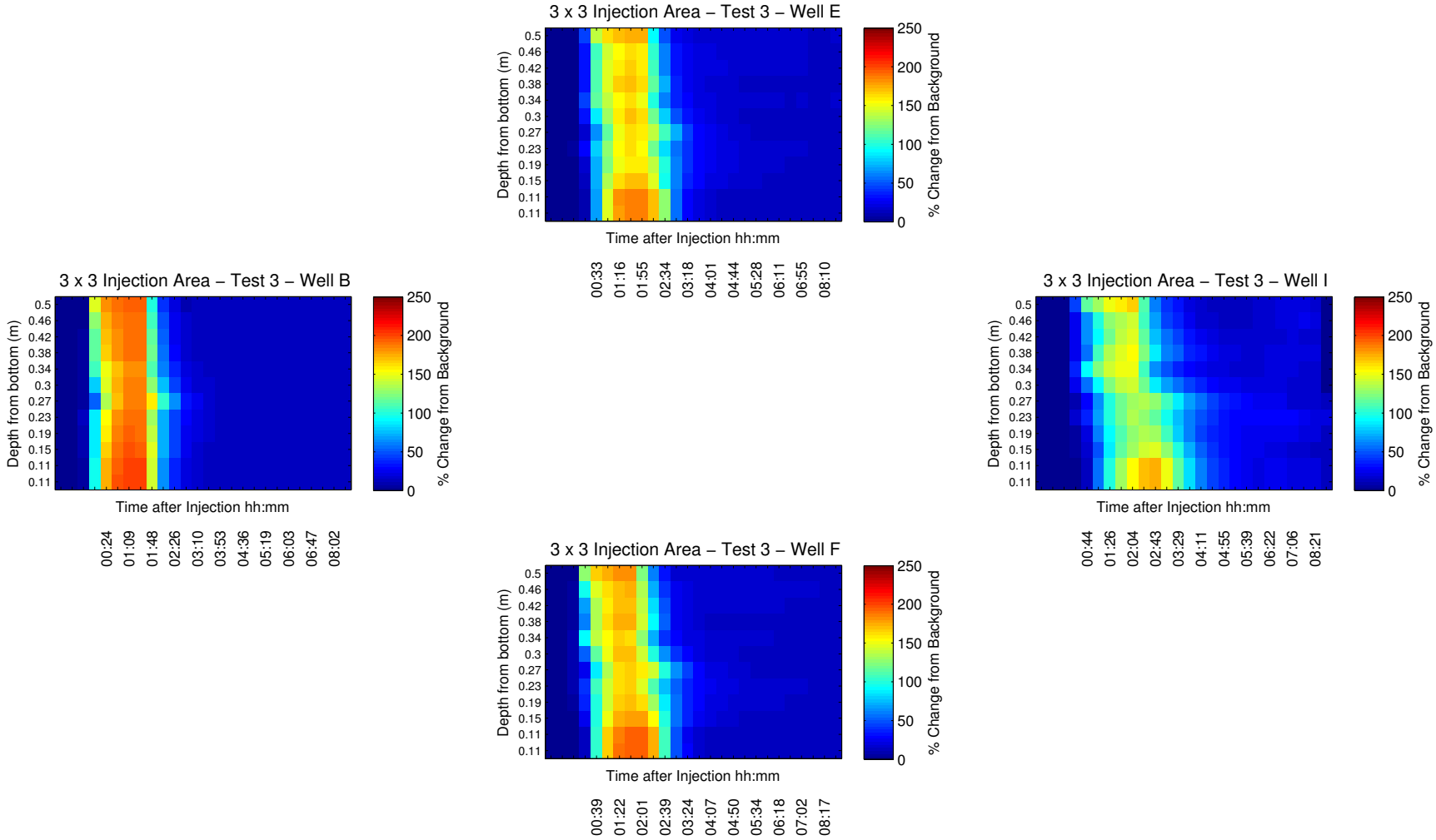

Figure B.35: Downwell Bulk Conductivity Measurements for 0.55 g/L, Mid-Range Frequency Geophysical Measurements, 9 Injection Ports (Test08)

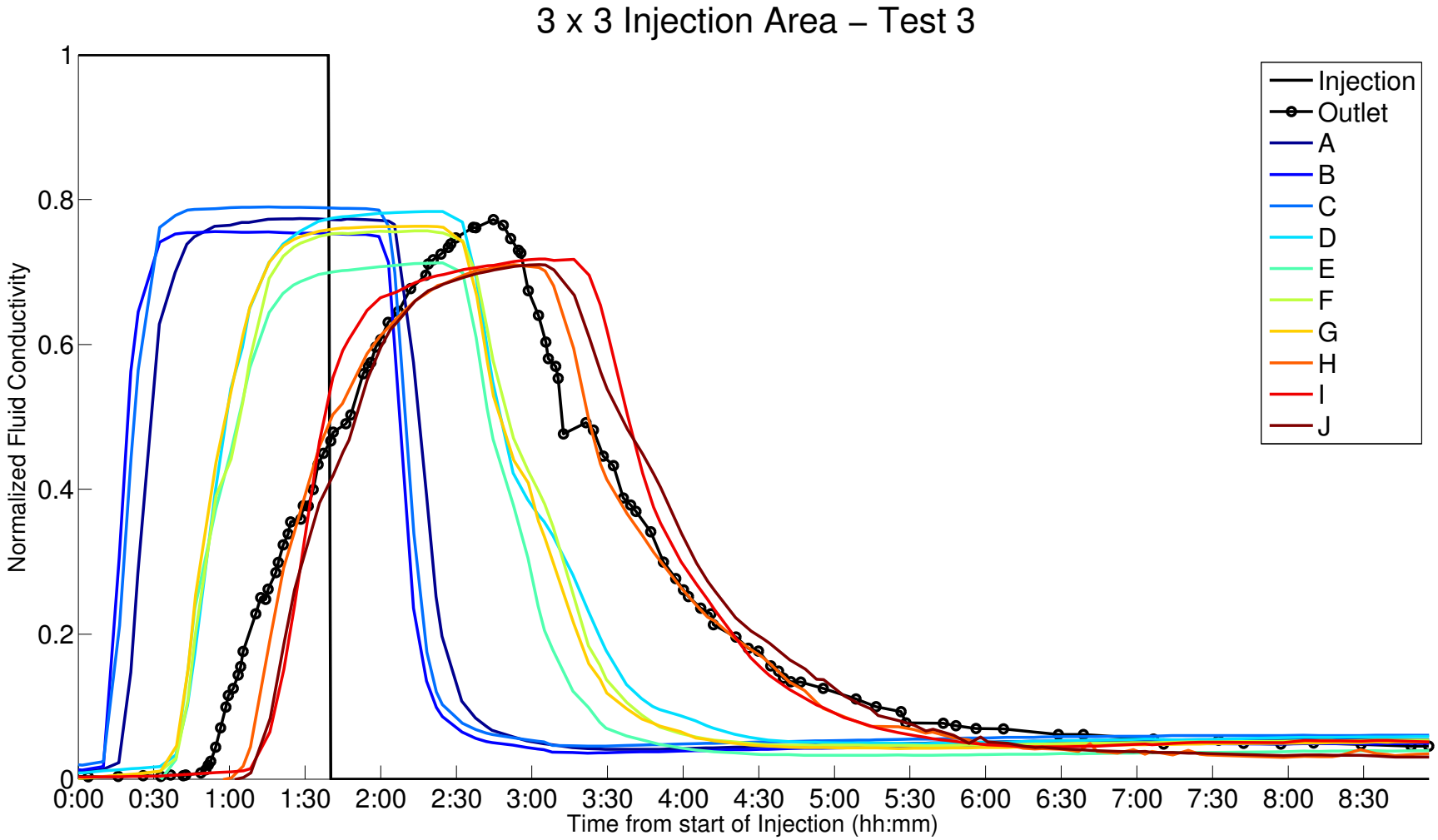

Figure B.36: Fluid Conductivity Measurements at all Wells for 0.55 g/L, Mid-Range Frequency Geophysical Measurements, 9 Injection Ports (Test08)

Well	**Mean Arrival Time (s)**	**Variance (s^2)**	**Skew**	**Kurtosis**	**Semi-invariant m3**	**Semi-invariant m2**	**Semi-invariant m1**	**Semi-invariant m0**
A	12730	10400	1.51	-0.54	1.04E+14	4.19E+09	1.98E+05	15.53
B	7920	7750	2.03	1.78	1.41E+13	6.29E+08	4.06E+04	5.12
C	8100	7770	2	1.65	1.50E+13	6.65E+08	4.28E+04	5.28
D	9760	6640	1.67	0.42	1.53E+13	7.77E+08	5.44E+04	5.58
E	9840	7000	1.7	0.5	1.53E+13	7.43E+08	5.01E+04	5.09
F	13200	9940	1.47	-0.63	1.05E+14	4.33E+09	2.09E+05	15.84
G	13100	9950	1.48	-0.61	1.04E+14	4.28E+09	2.07E+05	15.8
H	13830	9580	1.41	-0.8	1.06E+14	4.44E+09	2.17E+05	15.7
I	12420	6880	1.42	-0.6	2.61E+13	1.29E+09	7.94E+04	6.39
J	13930	9450	1.4	-0.83	1.06E+14	4.47E+09	2.20E+05	15.78

Table B.18: Temporal Moments - 0.55 g/L, Mid-Range Frequency Geophysical Measurements, 9 Injection Ports - (Test08)

Appendix C

Model Construction

C.1 ModelMuse

For ease of editing Modflow and MT3DMS files, ModelMuse [30] was used for a GUI. See `http://water.usgs.gov/nrp/gwsoftware/ModelMuse/ModelMuse.html` for further information and support for the program.

C.2 MODFLOW File Appendix

The following Modflow files in Table C.1 were used to generate model input/output. See [19] for file structure.

C.3 MT3DMS File Appendix

The following MT3DMS files in Table C.2 were used to generate model input/output. See [20] for file structure.

Table C.1: Modflow Input/Output

Input	
File Extension	Description
.BAS	Basic - describes the active cells and initial conditions for flow
.BCF	Block centered flow package
.CBC	Cell by cell flow output (Binary)
.DIS	Discretization - describes grid and time stepping
.HFB	Horizontal Flow Barrier - creates additional no-flow boundaries in tank
.LMT	Modflow/MT3DMS Linking File
.NAM	Modflow name file - used as a model driver
.OC	Output control - Used to print desired output
.SIP	Strongly Implicit Solver Package
.WEL	Well - describes flowrate at given locations (inlet outlet ports) (Pumping rate of 8e-7 m^3 is used for inlet ports, and -4e-6 m^3 for outlet ports)
Output	
File Extension	Description
.FDN	Results - Drawdown
.FHD	Results - Head Data
.LST	Listing file for Modflow output
.BAK	Backup file
.CNF	Model grid configuration file
.FTL	Flow Transport Link (Binary)

Table C.2: MT3DMS Input/Output

Input	
File Extension	Description
.ADV	Advective transport package - Modified method of characteristics (MMOC) solves this problem
.BTN	Basic Transport - Contains (1) Problem Definition, (2) Boundary Definition, (3) Initial Conditions, (4) Stepsize Determination, (5) Mass Balance Information, and (6) Simulation Printout
.DSP	Dispersive transport package
.GCG	Generalized conjugate gradient solver
.MT-NAM	MT3DMS Name file - used as model driver
.RCT	Chemical Reaction package - used for Dual Domain Mass Transfer (DDMT) Problem
.SSM	Sink and source mixing package
Output	
File Extension	Description
.MLS	MT3DMS list file
.UCN	Concentration values
.-MAS	Mass balance information

Appendix D

Scripts to Process Raw Data

D.1 Added Scripts/Files Required for Plotting

- Colormap and Colorbar Utilities - `http://www.mathworks.com/matlabcentral/fileexchange/24371-colormap-and-colorbar-utilities-sep-2009` (Used to display two different colormaps on the same figure)

  cbfit.m - Draws a colorbar with specific color bands between its ticks.

  cbfreeze.m - Freezes the colormap of a colorbar.

  cbhandle.m - Handle of current colorbar axes.

  cblabel.m - Adds a label to the colorbar.

  cbunits.m - Adds units to the colorbar ticklabels.

  cmapping.m - Colormap linear mapping/interpolation

  cmfit.m - Sets the COLORMAP and CAXIS to specific color bands.

  cmjoin.m - Joins colormaps at certain levels.

  cmlines.m - Change the color of plotted lines using the colormap.

  Contents.m - Describes the contents of Colormap and Colorbar utilities

- **freezeColors.m** - Lock colors of plot, enabling multiple colormaps per figure. `http://www.mathworks.com/matlabcentral/fileexchange/24371`

- **unfreezeColors.m** - `http://www.mathworks.com/matlabcentral/fileexchange/24371`

- **IDW.m** - Inverse Distance Weighting script, required to calculate spatial moments from fluid conductivity data. `http://www.mathworks.com/matlabcentral/fileexchange/24477-inverse-distance-weight`
- **nanmean.m** - Mean of a dataset excluding NaN values
- **nanstd.m** - Std Dev of a dataset excluding NaN values
- **rotateticklabel.m** - Required as function for downwell-imagesc.m, `http://www.mathworks.com/matlabcentral/fileexchange/8722-rotate-tick-label`
- **round2.m** - Rounds number to user-selected value of precision

D.2 Geometric Factors and Quadripole Sequences

- **geom-dist.m** - Loop to give all possible configurations of wells and deletes configurations with high geometric factors. Requires input files distance.txt and electrodes.txt. Creates workspace variables sequence-long and sequence-short
- **four-well-sequence.m** - Uses input sequence to expand borehole to borehole sequence into six borehole to borehole sequences

D.3 Fluid Conductivity

- **PlotAll.m** - Used for both Figure 2 and Table 1 in the GRL paper, as well as the Appendix B fluid figures. Requires TestXX.mat input as well as model input files after process-model.m has been run. Will additionally plot each of the different test types against each other (currently commented out). Calculates RMSE and Nash Sutcliffe values, along with model/observation error values (based on normalized concentration), calculates empirical CDF, KS density values, and Kruskal-Wallis test of statistical significance.

D.4 Bulk Conductivity

- **bulk-unique.m** - Used to find bulk quadripoles that appear in all three sequence lengths (Short - High Frequency Measurements, Med - Mid-range Frequency Measurements, Long - Low Frequency Measurements). Requires Three Input Files (Pro-long-sequence2.txt, Pro-medium-sequence2.txt, Pro-short-sequence2.txt) Output - C-all-seq (bulk quadripoles in all three sequences)

- **downwell-imagesc.m** - Provides imagesc plots of downwell bulk conductivity data at wells B,E,F,I. Conductivity is plotted as percent change from background (Non-inverted apparent resistivity values are used) Requires TestXX.mat input files

- **downwell-comb.m** - Creates images from 2011 AGU Poster (Uses flow tests that have since been discarded Tests 01, and Test 04) Requires flow-test1.mat, flow-test4.mat, flow-test5.mat and flow-test6.mat for plotting. (Input data for other plotting files have since been reorganized into TestXX.mat file format

- **downwell-offset.m** - Shows conductivity vs. time plots of bulk geophysical probes. Color corresponds to depth value in tank. Requires TestXX.mat input files

- **rho-solve.m** - Used in rhobulk to estimate apparent resistivity value, using voltage (V), current(I) and geometric factor(K)

- **plot-config.m** - Used in rhobulk.m as a built in function to find geometric factors

- **sequence-expand.m** - Expands a borehole to borehole sequence into six borehole to borehole sequences (six planes between four wells).

- **downwell.m** - Legacy plot to look at downwell data (now replaced by downwell-imagesc.m)

- **rhobulk.m** - used for bulk geometric factors

D.5 Moments

- **moment-specs.m** - Creates image of temporal moment data for each well.
- **tmoments.m** - Calculates temporal moments for data.
- **moment-comparison-well.m** Plots moments of different models against each other. Requires model input values (model-moments-well-disp.mat, model-moments-well-no-disp.mat, model-moments-well-dual-domain.mat). Shows range of calculations, debatable if these moment calculations make sense. (Requires IDW as input for fluid conductivity values)
- **plotmoments.m** - Plots the ranges of temporal moment values across each of the ten fluid conductivity measurements (A-J) and compares it to the modeled temporal moment data.
- **plot-variation.m** - Simple plot to look at the variation of moments across tests. Requires "TestXX.mat" input

D.6 2D Interpolation

- **IDW-Moments.m** - Calculates spatial moments based on the inverse distance weighting of the fluid conductivity data. Requires TestXX.mat for input.
- **IDW-Interp.m** - Uses IDW.m to interpolate fluid conductivity data at each time step. Requires TestXX.mat for input. Writes IDW data to txt files for plotting in VisIt. Can also create animations of conductivity through time.

D.7 3D VisIt Files

- **Downwell-Range.m** - Prints bulk conductivity data to VTK files for plotting in VisIt. Requires TestXX.mat input files
- **write-vtk.m** - writes 3D VTK files for visualizations in VisIt

D.8 Legacy Scripts and Files

- **depth-inv-wells.m** - Legacy plot for resistivity vs. depth
- **depth-v-rho.m** - Legacy plot for resistivity vs. depth
- **fluid-cond-comb.m** - Legacy plotting tool to create fluid conductivity images from 2011 AGU Poster. (Uses flow tests that have since been discarded Tests 01, and Test 04) Requires flow-test1.mat, flow-test4.mat, flow-test5.mat and flow-test6.mat for plotting. (Input data for other plotting files have since been reorganized into TestXX.mat file format
- **go-prosys-col-RU.m** - Legacy file to the StructureData.m (with SaveTest.m function). Used to transform raw data to apparent resistivity values. StructureData.m and SaveTest.m are the preferred file types now
- **porosity.m** - Legacy plot using Archies law to estimate in-situ porosity.
- **Kriging-Files.m** - Creates files to perform 2D kriging of fluid conductivity data. Precursor plot to IDW method of interpolation. IDW is preferred method of interpolation. Requires TestXX.mat for input.
- **plane-vis.m** - requires image-unique creates plot of quadripole locations (based on average distance)

D.9 Miscellaneous

- **time-plot.m** - A simple plot for illustrative purposes showing how quickly geophysical measurements are collected. Differences in slope indicate a different frequency in collection of data.
- **source-receive.m** - Largely unused, but creates source (SRC) and receiver (REC) files for RESINVM3D
- **test-length-calc.m** - Simple calculation to calculate the length of a test from when Injection is started until the IRIS machine stops collecting data

D.10 StructureTest.m/SaveTest.m Input Parameters

- **StructureData.m** - The file where the input values to SaveTest are placed, includes change directory (cd) commands so input files remain in separate directories. Structure Data creates "TestXX.mat" output file
- **SaveTest.m** - Takes the raw data and processes it. Requires a number of known variables from experiment. This is used as a built in function within StructureData.m. Once data is processed through SaveTest.m, a Matlab structure variable can be saved and loaded to plot and analyze various aspects of the data set.

Table D.1 details the required input parameters to process data results using StructureData.m/SaveTest.m

Table D.1: Input Parameters for SaveTest.m

Input	**Description**
Testname	TestXX
Filename	Prosys File Name (Electrical resistivity output filename .txt)
Quads	Number of quadripoles in sequence
NumCol	Number of columns in Prosys output file
Header	Number of header lines in sequence-name file
Sequence-Name	File to use for sequence and location of quadripole data (low, mid-range, high frequency values)
Sequence-Cols	Number of columns in sequence-name.txt
Sequence-Rows	Number of rows in sequence-name.txt

K-values	Geometric vaues to use for resistivity calculations. (K-BEFI-new.mat) saved in workspace
BTC-file	Breakthrough curve at tank outlet. BTCtestXX.txt
BTC-min	Minimum conductivity value (background conductivity of tap water)
BTC-max	Maximum conductivity value (Max conductivity once solution is mixed)
BTC-bulk-min	Not used - minimum value of bulk conductivity
BTC-bulk-max	Not used - maximum value of bulk conductivity
Inj-conc	Injected concentration in g/L
Iris-correction	Correcting for time error between clock and IRIS machine time
Inj-time	A time vector of (1) Test Start, (2) Injection start 1 minute, (3) Injection start, (4) Injection end, (5) Injection end + 1 minute, (6) Test End
Inj-val	Normalized step-pulse injection values to correspond to injection time [0;0;1;1;0;0]
xTitle	Plot title
xXlabel	X label
xYlabel	Y label
Condfig	Name to save fluid conductivity figure as
DWfig	Name to save downwell bulk conductivity figure as
res-time	Time vector for calculated residence time: res-time=[0 0 0 1h 45m 12s];

reshape-flag	Reshape flag based on if a test uses high (2), mid-range(1), or low frequency(0) geophysical collection

D.11 StructureTest.m/SaveTest.m Output

Table D.2 provides a detailed description of the output from the StructureData.m/SaveTest.m scripts

Table D.2: SaveTest.m Output

Input	**Description**
TestXX.filename	IRIS output file (.txt)
TestXX.quads	number of quadripoles
TestXX.numcol	number of columns in IRIS output file
TestXX.header	number of header lines in IRIS output file
TestXX.sequence-name	IRIS sequence name used to create IRIS output file
TestXX.sequence-cols	number of columns in the sequence file
TestXX.sequence-rows	number of rows in the sequence file
TestXX.K-values	geometric factor values used for the given sequence (quadripoles and their corresponding geometric factor values are stored here)
TestXX.BTC-file	concentration value at outlet of tank vs. time
TestXX.BTC-min	minimum concentration value for a test
TestXX.BTC-max	maximum concentration value for a test
TestXX.BTC-bulk-min	(not used, may not be correct) minimum bulk conductivity value for a test
TestXX.BTC-bulk-max	(not used, may not be correct) maximum bulk conductivity value for a test

TestXX.Iris-correction	IRIS clock time sometimes differs from correct clock time (in BTC-file), this corrects the IRIS data so they plot on the same time scale as the BTC-file data
TestXX.Inj-val	Used to create step-pulse shape on graphs for injection
TestXX.xTitle	Name of Test
TestXX.xXlabel	X label for fluid conductivity plot
TestXX.xYlabel	Y label for fluid conductivity plot
TestXX.Condfig	filename to save fluid conductivity plot
TestXX.DWfig	filename for downwell conductivity plot
TestXX.res-time	residence time for each test
TestXX.BTC-cond	BTC conductivity values read from BTC-file
TestXX.BTC-text	BTC time values read from BTC-file, converted to time values in the next step
TestXX.BTC-date	BTC time values read from BTC-file (in MATLAB time format)
TestXX.Inj-time	Vector of time values including (1) Test State, (2) Injection start minus 1 minute, (3) Injection start, (4) Injection end, (5) Injection end plus 1 minute, (6) Test End
TestXX.full-sequence	matrix of quadripole numbers, test quadripoles (#-#-#-#), vector of zeros, geometric factors, and time a measurement was taken (in MATLAB format)
TestXX.rhoIRIS	apparent resistivity reading from IRIS (not used)

TestXX.dev	standard deviation (quality factor, in %) from IRIS
TestXX.Sp	spontaneous polarization (mV)
TestXX.V	measured voltages from IRIS
TestXX.I	current injected from IRIS
TestXX.rscheck	resistance check for a quadripole
TestXX.txbat	transmitter battery voltages
TestXX.rxbat	receiver battery voltages
TestXX.date	vector of dates from IRIS file
TestXX.time	vector of time from IRIS file (hh:mm)
TestXX.AM-PM	vector of AM/PM values that correspond to time from IRIS file
TestXX.R	calculated resistance based on IRIS voltage and current
TestXX.rho-calc	calculated rho based on experimental geometric values
TestXX.unique-quads	used to store quadripole values for in-well fluid conductivity measurements
TestXX.date-time-AM-vec	vector of test times in (mm/dd/yyyy hh:mm:ss AM/PM) format
TestXX.Well-Cond	matrix of well conductivity values
TestXX.Well-Time	matrix of times when conductivity measurements were taken for each well
TestXX.(A-J)Cond	single vector of conductivity measurements for one well (A & J)
TestXX.(A-J)Time	single vector of time of conductivity measurements for one well (A & J)
TestXX.BTC-date-s	BTC time file converted to seconds (with t = 0 s is test start time)
TestXX.BTC-conc-vec	Used to read in BTC concentration data separate from BTC time data

TestXX.OutletMeanArrival	Temporal moment mean arrival time (MAT) calculated at outlet
TestXX.OutletVariance	Temporal moment variance (VAR) calculated at outlet
TestXX.OutletSkew	Temporal moment skew (SKEW) calculated at outlet
TestXX.OutletKurtosis	Temporal moment kurtosis (KURT) calculated at outlet
TestXX.Outletm3	Semi-invariant m3 calculated at outlet
TestXX.Outletm2	Semi-invariant m2 calculated at outlet
TestXX.Outletm1	Semi-invariant m1 calculated at outlet
TestXX.Outletm0	Semi-invariant m0 calculated at outlet
The previous eight calculations are also repeated for the inlet (based on the step-pulse injection timing)	
TestXX.MassRecovery	Mass recovery in grams
TestXX.Well-Time-Matt	Converts time to seconds and is used to calculate temporal moments for each well
TestXX.mat	placeholder value that gets rewritten with different values for MAT
TestXX.var	placeholder value that gets rewritten with different values for VAR
TestXX.skew	placeholder value that gets rewritten with different values for SKEW
TestXX.kurt	placeholder value that gets rewritten with different values for KURT
TestXX.m3	placeholder value that gets rewritten with different values for m3
TestXX.m2	placeholder value that gets rewritten with different values for m2
TestXX.m1	placeholder value that gets rewritten with different values for m1

TestXX.m0	placeholder value that gets rewritten with different values for m0
TestXX.mat-tail	calculation without tail (doesnt get used in current data)
TestXX.var-tail	calculation without tail (doesnt get used in current data)
TestXX.skew-tail	calculation without tail (doesnt get used in current data)
TestXX.kurt-tail	calculation without tail (doesnt get used in current data)
TestXX.m3-tail	calculation without tail (doesnt get used in current data)
TestXX.m2-tail	calculation without tail (doesnt get used in current data)
TestXX.m1-tail	calculation without tail (doesnt get used in current data)
TestXX.m0-tail	calculation without tail (doesnt get used in current data)
TestXX.Mass-Percent	Mass recovery scale of 0 - 1
TestXX.unique-bulk	unique bulk quadripoles
TestXX.Bulk-XXXX-X-X-X-X	conductivity, time, and temporal moments for bulk quadripoles
TestXX.bulk-seq	sequence file with bulk quadripoles only
TestXX.restart-bulk	Quadripoles where bulk probes start over for a sequence
TestXX.Loc-MatB	Matrix with quadripole numbers, quadripoles, average quadripole depth, resistivity measurement, time of measurement for well B
TestXX.Loc-MatE	“ for well E
TestXX.Loc-MatF	“ for well F
TestXX.Loc-MatI	“ for well I

TestXX.Loc-Bulk	“ for all bulk quadripoles
TestXX.restartB	Quadripole numbers where well B quadripoles restart
TestXX.restartE	“ well E “
TestXX.restartF	“ well F “
TestXX.restartI	“ well I “
TestXX.K-est-tank	K estimate calculation (not used)
TestXX.K-est-wells	K estimate calculation (not used)

Bibliography

[1] Emsellem, Y. and G. d. Marsily (1971) "An automatic solution for the inverse problem," *Water Resoruces Research*, **7**(5), pp. 1264 – 1283.

[2] Neuman, S. P. (1973) "Calibration of distributed parameter groundwater flow models viewed as a multiple-objective decision process under uncertainty," *Water Resources Research*, **9**(4), p. 10061021.
URL `http://onlinelibrary.wiley.com/doi/10.1029/WR009i004p01006/abstract`

[3] Carrera, J., A. Alcolea, A. Medina, J. Hidalgo, and L. Slooten (2005) "Inverse problem in hydrogeology," *Hydrogeology Journal*, **13**, pp. 206–222.

[4] Berkowitz, B., S. Emmanuel, and H. Scher (2008) "Non-Fickian transport and multiple rate mass transfer in porous media," *Water Resources Research*, **44**(W03402).

[5] Berkowitz, B. and H. Scher (2008) "Exploring the nature of non-Fickian transport in laboratory experiments," *Advances in Water Resources*, **32**(5), pp. 750 – 755.

[6] Zheng, C., M. Bianchi, and S. M. Gorelick (2011) "Lessons learned from 25 years of research at the MADE site," *Ground water*, **49**(5), pp. 649–662, PMID: 20860688.

[7] VanGenuchten, M. and P. Wierenga (1976) "Mass transfer studies in sorbing porous media: I. Analytical solutions," *Soil Science Society of America Journal*, **40**(4), pp. 473 – 480.

[8] ——— (1977) "Mass transfer studies in sorbing porous media: II. Experimental evaluation with tritium (3H2O)," *Soil Science Society of America Journal*, **41**(2), p. 272278.

[9] Haggerty, R. and S. Gorelick (1995) "Multiple-rate mass transfer for modeling diffusion and surface reactions in media with pore-scale heterogeneity," *Water Resources Research*, **31**(10), pp. 2383 – 2400.

[10] Benson, D., S. Wheatcraft, and M. Meerschaert (2000) "Application of a fractional advectiondispersion equation," *Water Resources Research*, **36**(6), pp. 1403 – 1412.

[11] Benson, D., S. Wheatcraft, and M. M. Meerschaert (2000) "The fractional-order governing equation of Lvy motion," *Water Resources Research*, **36**(6), pp. 1413 – 1423.

[12] Berkowitz, B., A. Cortis, M. Dentz, and H. Scher (2006) "Geological formations as a continuous time random walk," *Reviews of Geophysics*, **44**(RG2003).

[13] Molz, F. J., C. Zheng, S. M. Gorelick, and C. F. Harvey (2006) "Comment on Investigating the Macrodispersion Experiment (MADE) site in Columbus, Mississippi, using a three-dimensional inverse flow and transport model by Heidi Christiansen Barlebo, Mary C. Hill, and Dan Rosbjerg," *Water Resources Research*, **42**(6), p. n/an/a.
URL http://onlinelibrary.wiley.com/doi/10.1029/2005WR004265/abstract

[14] Hill, M. C., H. C. Barlebo, and D. Rosbjerg (2006) "Reply to comment by F. Molz et al. on Investigating the Macrodispersion Experiment (MADE) site in Columbus, Mississippi, using a three-dimensional inverse flow and transport model," *Water Resources Research*, **42**(6), p. n/an/a.
URL http://onlinelibrary.wiley.com/doi/10.1029/2005WR004624/abstract

[15] Major, E., D. A. Benson, J. Revielle, H. Ibrahim, A. Dean, R. M. Maxwell, E. Poeter, and M. Dogan (2011) "Comparison of Fickian and temporally nonlocal transport theories over many scales in an exhaustively sampled sandstone slab," *Water Resources Research*, **47**(10), p. n/an/a.
URL http://onlinelibrary.wiley.com/doi/10.1029/2011WR010857/abstract

[16] Fiori, A., G. Dagan, and I. Jankovic (2012) "Comment on Comparison of Fickian and temporally nonlocal transport theories over many scales in an exhaustively sampled sandstone slab by Elizabeth Major et al." *Water Resources Research*, **48**(7), p. n/an/a.
URL http://onlinelibrary.wiley.com/doi/10.1029/2011WR011706/abstract

[17] Archie, G. E. (1942) "The electrical resistivity log as an aid in determining some reservoir characteristics," *Transactions of the American Institute of Mining, Metallurgical and Petroleum Engineers*, **146**, pp. 54–62.

[18] Carman, P. C. (1956) *Flow of gases through porous media*, Butterworths Scientific Publications, London, UK.

[19] Harbaugh, A. W. (2005) *MODFLOW-2005, The U.S. Geological Survey Modular Ground-Water Modelthe Ground-Water Flow Process*, *Tech. Rep. Techniques and Methods 6-A16*, U.S. Geological Survey.

[20] Zheng, C. and P. P. Wang (1999) *MT3DMS: A modular three-dimensional multispecies model for simulation of advection, dispersion and chemical reactions of contaminants in groundwater systems: documentation and user's guide*, U.S. Army Engineer Research and Development Center, Contract Report SERDP-99-1. Vicksburg, Mississippi.

[21] Gelhar, L. W., A. L. Gutjahr, and R. L. Naff (1979) "Stochastic analysis of macrodispersion in a stratified aquifer," *Water Resources Research*, **15**(6), p. 13871397.
URL http://onlinelibrary.wiley.com/doi/10.1029/WR015i006p01387/abstract

[22] Swanson, R. D., K. Singha, F. D. Day-Lewis, A. Binley, K. Keating, and R. Haggerty (2012) "Direct geoelectrical evidence of mass transfer at the laboratory scale," *Water Resources Research*, **48**(10), p. n/an/a.
URL http://onlinelibrary.wiley.com/doi/10.1029/2012WR012431/abstract

[23] Nash, J. and J. Sutcliffe (1970) "River flow forecasting through conceptual models part I A discussion of principles," *Journal of Hydrology*, **10**(3), pp. 282–290.
URL http://www.sciencedirect.com/science/article/pii/0022169470902556

[24] Cortis, A. and B. Berkowitz (2004) "Anomalous Transport in Classical Soil and Sand Columns," *Soil Science Society of America Journal*, **68**(5), p. 1539.
URL https://www.soils.org/publications/sssaj/abstracts/68/5/1539

[25] National Research Council, . (2009) *Informing Decisions in a Changing Climate*, The National Academies Press.
URL http://www.nap.edu/openbook.php?record_id=12626

[26] ——— (2012) *Challenges and Opportunities in the Hydrologic Sciences*, The National Academies Press, Washington, D.C.

[27] ——— (2012) *Science for Environmental Protection: The Road Ahead*, The National Academies Press, Washington, D.C.

[28] Urban, R. L., K. Singha, and P. Reed (2011) "Exploring the worth of geophysical data for characterizing three-dimensional transport and heterogeneity in laboratory aquifer experiment." in *American Geophysical Union Fall 2011 Meeting*, American Geophysical Union, pp. H43E–1261.

[29] Luo, J., O. A. Cirpka, and P. K. Kitanidis (2006) "Temporal-moment matching for truncated breakthrough curves for step or step-pulse injection," *Advances in Water Resources*, **29**(9), pp. 1306–1313.
URL http://www.sciencedirect.com/science/article/pii/S0309170805002496

[30] Winston, R. (2009) *ModelMuseA graphical user interface for MODFLOW2005 and PHAST*, *Tech. Rep. U.S.G.S. Techniques and Methods 6A29*, U.S. Geological Survey.
URL http://pubs.usgs.gov/tm/tm6A29

Vita

Rachel Lorah Urban

Education

- M.S. in Civil Engineering, Penn State University, May 2013

  Advisers: Patrick Reed and Kamini Singha

  Thesis Title: Pandora's box: Can we distinguish groundwater transport hypotheses given observational uncertainties?.

  Cumulative GPA: 3.92

- B.S. in Civil Engineering with Honors, Penn State University, May 2010

  Adviser: Patrick Reed

  Thesis Title: Is Simpler Better? A Visualization-based Exploration of How Parametric Screening Influences Problem Difficulty and Equifinality in Multiobjective Calibration

  Cumulative GPA: 3.91

  In-Major GPA: 3.97

Publications

- Urban, R. L., Singha K., Reed, P. Big trouble in a little box: Can we distinguish groundwater transport hypotheses given observational uncertainties?. Geophysical Research Letters, (In-Preparation).

Presentations

- Urban, R. L., Singha K., Reed, P. Big trouble in a little box: Can we distinguish groundwater transport hypotheses given observational uncertainties?. American Geophysical Union Fall 2012 Meeting, December 3 - 7, 2012 - San Francisco, CA., Eos Trans. AGU Fall Meet. Suppl., Abstract H33D-1362.

- Urban, R. L., Singha K., Reed, P. Exploring the worth of geophysical data for characterizing three-dimensional transport and heterogeneity in laboratory aquifer experiment. American Geophysical Union Fall 2011 Meeting, December 5 - 9, 2011 - San Francisco, CA., Eos Trans. AGU Fall Meet. Suppl., Abstract H43E-1261.

- Urban, R. L., Reed, P. M., van Werkhoven, K. L., Wagener, T. *Is Simpler Better? A Visualization-based Exploration of How Parametric Screening Influences Problem Difficulty and Equifinality in Multiobjective Calibration.* American Geophysical Union Fall 2009 Meeting, December 14 - 18, 2009 - San Francisco, CA., Eos Trans. AGU Fall Meet. Suppl., Abstract H33F-0951.